



Effect of community agroforestry on vegetation resilience to drought in Kenya

Thesis, MSc Global Sustainability Solutions

Madeleine Henderson
September 2023
Global Systems Institute, University of Exeter

I certify that this dissertation is entirely my own work and no part of it has been submitted for a degree or other qualification in this or another institution. I also certify that I have not collected data nor shared data with another candidate at Exeter University or elsewhere without specific authorization.

Maddie Henderson

Acknowledgements

I am very grateful to my supervisor, Dr. Josh Buxton, for his excellent support throughout the project, as well as Mark, who very graciously served as my personal IT consultant.

Contents

Acknowledgements.....	1
Table of Figures	3
List of Tables.....	4
Abstract.....	5
1. Introduction	6
2. Literature Review	7
Kenya and drought.....	7
Agroforestry.....	9
Tipping points and resilience	10
The theory behind recovery rate and resilience.....	12
Remote monitoring of ecosystem resilience	13
Global decline of resilience.....	15
Resilience and human land management.....	15
3. Research Questions	16
4. Methodology	17
Study area, timeframe, and drought indicators	17
Data acquisition	20
Data preprocessing	21
Recovery rate estimation.....	24
Comparisons	25
5. Results.....	26
RQ1: Can resilience be estimated using recovery rates?.....	26
RQ2: Effect of TIST on recovery rates	30
RQ3: Recovery from subsequent droughts.....	31
RQ4: TIST spillover effects	33
6. Discussion.....	34
RQ1: Can resilience be estimated using recovery rates?.....	34
RQ2: Effect of TIST on recovery rates	35
RQ3: Recovery from subsequent droughts.....	38
RQ4: TIST spillover effects	38
Limitations and Future Work	39

7.	Conclusion.....	42
8.	Code Availability.....	43
9.	Appendix.....	44
10.	References.....	56

Table of Figures

Figure 1: A system diagram of the interaction of agroforestry with drought in Kenya.....	10
Figure 2: Resilience as a swifter recovery from perturbations	11
Figure 3: System $U(x)$	12
Figure 4: Approximation of $U(x)$ around x^* as a quadratic.....	13
Figure 5: An approximation of $x(t)$ after a perturbation at $t = 0$ as an exponential recovery with rate λ ..	13
Figure 6: (Left) Relevant counties and TIST groves (in purple) within those counties. (Top right)	17
Figure 7: Ecoregions (right) and landcover (left) of the study area.....	18
Figure 8 : Example drought classification	19
Figure 9: A subset of the drought categorizations.....	20
Figure 10: Data preparation process.	21
Figure 11: The percentage of months missing for each pixel in the study area.....	22
Figure 12: Example of gap filling.....	23
Figure 13: Example of STL decomposition.....	23
Figure 14: Recovery rate calculation process.	24
Figure 15: Example fitted recovery rate.	25
Figure 16 : Recovery rates for the recovery at month 59 across the four counties.	27
Figure 17 – Recovery rates for the recovery at month 77 across the four counties.	28
Figure 18a: Meru County at boxed location.	29
Figure 19a: Tharaka County at triangle location.....	29
Figure 20 : Spearman's rho for recovery rates and other characteristics in Tharaka. All $p < 0.001$	30
Figure 21: Spatially plotted results for the percent change in resilience over time.....	32
Figure 22: Median recovery rates from 59 vs. distance from TIST.	33
Figure 23: Median recovery rates from recovery 77 for each county vs. distance to nearest TIST pixel... Figure 24: Percent change in recovery rate from recovery 59 to 77, median over distance from nearest TIST grove.....	33
Figure 25: Distribution of estimated recovery rates for recovery 77.	34
Figure 26: These example pixels from Nyeri County show some seasonal cycle still present within the residual.....	36
Figure 27: Characteristics associated with improved recovery rates and recovery rates plotted vs. distance from closest TIST plot.....	39
Figure 28: Sensitivity to missing data.	40
Figure 29: Example of attempted gap filling with Savitzky-Golay reconstruction	46

Figure 30: The R ² value for the recovery rates vs. the difference between the local minimum and the (mean – one standard deviation).....	46
Figure 31: The R ² value for the recovery rates vs. the difference between the local minimum and the (mean – two standard deviations).....	46
Figure 32: Histograms of fitted recovery rate for a sample of data (n = 5000, Tharaka county) for different initial guesses of a, r, and c.....	47
Figure 33: Distance from TIST groves in meters.	48
Figure 34: Recovery rates and R-squared values for Recovery 59.....	50
Figure 35: Recovery rates and R-squared values for Recovery 77.....	50
Figure 36: Mean NDVI in each county for TIST, neighbors, and other pixels.	51
Figure 37: Spearman's rank correlations for recoveries and other characteristics across counties.	52
Figure 38a: Recovery rates for 59 by landcover type.	52
Figure 39a: Recovery rates for 59 by ecoregion.	53
Figure 40 : Characteristics of each landcover type with medians marked.	54

List of Tables

Table 1: Median recovery rates compared by county, recovery and landcover classification.	31
Table 2: Median percent change in recovery rate from Recovery 59 to Recovery 77,	32
Table 3: Drought classifications from the NDMA.	44
Table 4: Recovery calculation success rates.	49
Table 5: Sample size corresponding to recovery rates compared by county, recovery and landcover classification.	54
Table 6: Sample size for percent change in recovery rate from Recovery 59 to Recovery 77,	55

Abstract

Resilience, or the ability to quickly recover from shocks, is a critical quality for natural and social systems in the face of climate change which is increasing the frequency and severity of natural disturbances such as drought. Smallholder farmers are particularly exposed to the risks of climate change. Thus, identifying resilience-building practices and quantifying their effects can guide management in agro-ecological systems. Community-driven tree planting for carbon credits is a growing program in the Mount Kenya region of Kenya. Tree planting and agroforestry are known to have ecological benefits that improve soil quality, microclimate, and water retention, as well as economic benefits to farmers. To evaluate the benefits of these practices on resilience to drought, remotely sensed vegetation greenness (NDVI) was used to assess the state of the agro-ecological systems around Mt. Kenya during and after droughts within the last decade. Droughts were identified by the Kenyan government based on surveys of community members and remotely sensed data. Resilience was estimated using the rate term of a fit exponential curve to the vegetation recovery after a drought. The resilience estimation method was successful and found proven patterns of resilience with precipitation and landcover. Planted tree groves and immediate neighboring pixels have higher resilience to drought events than comparable pixels in the area, and they see less decrease in resilience to subsequent drought events than other pixels. Agroforestry programs are thus an important tool for building resilience to drought for smallholder farmers in Kenya who are increasingly threatened by climate change.

1. Introduction

Agriculture is a major driver of the environmental crisis on multiple planetary boundaries (Beare *et al.*, 2017), but it is also one of the sectors critical to human survival that is most impacted by climate change, especially in Africa. Warming is already reducing crop yields and productivity on the continent, which will worsen with further warming (Trisos *et al.*, 2023). Smallholder farmers are vulnerable to climate change as they are dependent on weather conditions to feed and support themselves (Mendelsohn, 2009; Lasco *et al.*, 2014) especially in Africa which depends largely on rain-fed agriculture (Ochieng *et al.*, 2016). Natural disasters, especially drought, can push people further into poverty (Sherwood, 2013), but climate change adaptation can both reduce poverty and vulnerability to climate change (Eriksen and O'Brien, 2007). Smallholder farmers can make adaptation decisions such as what to grow and how to grow it (Mendelsohn, 2009). Farming techniques that decrease environmental degradation and increase resilience to climate change are thus key to mitigation and adaptation, especially for smallholder farmers in developing countries.

The International Small Group and Tree Planting Program (TIST) is a program that works towards both mitigation and adaptation in an effort to sequester carbon, improve agricultural resilience, and improve the livelihoods of smallholder farmers through tree planting and agroforestry in Kenya, India, Tanzania, and Uganda (TIST, 2023). Agroforestry is the integration of trees or shrubs with crops or livestock as windbreaks, buffers to water, hedges, or interspersal with crops or pasture (Pantera *et al.*, 2021). TIST is locally driven: farmers determine how, where, and what types of trees to plant, though the trees are usually planted on degraded or unused land. Farmers are organized into small groups of 6-12 and clusters of 200-400 which create local leadership development opportunities, educate participants on conservation farming techniques, and mutually support members (Oppenheimer, 2011; Masiga *et al.*, 2012; TIST, 2023). Farmers have a contract to maintain the groves for 30 years in order to receive payments from the sale of credits on the voluntary carbon market. TIST facilitates verification and sale of the high-quality carbon credits, and 70% of profits are returned to the farmers. TIST, operating since 1999, now involves more than 180,000 farmers and 23 million trees planted (Masiga *et al.*, 2012; TIST, 2023). Besides providing additional income, the groves benefit the farmers via fuelwood, livestock fodder, fruit, windbreaks, improved soil quality, and erosion control, increasing their farm's resilience to the changing climate (Jose, 2009; Oppenheimer, 2011; Lasco *et al.*, 2014).

TIST exhibits characteristics of a potential social positive tipping point (Marshall, 2022); however, effects on the ecosystem are mostly unquantified. There is some evidence that TIST improves the ecosystem beyond the boundaries of its farms (Buxton *et al.*, 2021), even though in the last 40 years agriculture has rapidly expanded and intensified in Kenya, leading to land degradation (Eckert *et al.*, 2017). While local farmers already perceive that agroforestry is a beneficial practice for drought resilience (Quandt *et al.*, 2017), this has not been quantified. As precipitation extremes (both drought and floods) impact food and economic security in Kenya and are already worsening with climate change (Kimutai *et al.*, 2023; Trisos *et al.*, 2023), further evidence of TIST's benefits may promote expansion and improve both farmer livelihoods and the local environment.

Tipping points exist in systems with non-linearity and strong reinforcing feedback loops where a small change can trigger a large shift in system state (Lenton, 2020), which are well established in several climate and ecological systems (Lenton *et al.*, 2008). Resilience is the ability of the system to return to its previous state after disturbances (Pimm, 1984). A more resilient system recovers more quickly from disruption due to strong stabilizing feedbacks, but as a system approaches a tipping point, it exhibits critical slowing down (CSD) and recovers more slowly (Wissel, 1984). Because resilience is difficult to quantify directly, the observed recovery rate from disturbances can be used to measure resilience (Van Nes and Scheffer, 2007).

Remote sensing has been used to monitor terrestrial ecosystem resilience via measures of vegetation productivity and biomass which approximate the health of the ecosystem (Verbesselt *et al.*, 2016; Boulton *et al.*, 2022; Lenton *et al.*, 2022). Resilience of natural ecosystems has been estimated using the recovery rate of vegetation productivity observed by satellites after disturbances (van Belzen *et al.*, 2017; Buxton *et al.*, 2022; Smith *et al.*, 2022). As ecosystems globally exhibit decreased resilience due to the cumulative impacts of human activity (Armstrong McKay *et al.*, 2022; Boulton *et al.*, 2022; Smith *et al.*, 2022), the ability to monitor “invisible” qualities like resilience and quickly determine intervention efficacy is critical, creating self-aware feedbacks to help maintain the biosphere (Lenton and Latour, 2018). Quantifying the effects of human land management on agro-ecological resilience with remote sensing is relatively novel, though there are some previous examples in the literature (McKenna *et al.*, 2018; K. J. Lees *et al.*, 2021; von Keyserlingk *et al.*, 2021; Jing *et al.*, 2023). The TIST agroforestry program may improve the ability of the agro-ecosystem to recover more quickly from droughts which have been severely affecting the region in recent years (Gebremeskel Haile *et al.*, 2019; Nash, 2022); examining the effects of human intervention on resilience in an agro-ecological system will contribute to this knowledge base.

Therefore, this study will use remotely sensed vegetation data (NDVI) from the last decade as a proxy for the health of agro-ecological systems around Mt. Kenya. By estimating the recovery rate after drought events, the resilience of TIST farms to drought will be measured, and TIST farms will be compared with similar areas. This will help quantify and potentially support the experiential understanding of local farmers of the TIST program’s practices as drought resilience tools. Section 2 reviews the relevant literature on resilience, remote sensing, drought, and agroforestry, leading to research questions in Section 3; Section 4 describes and rationalizes the methodology; Section 5 describes results; Section 6 discusses results, limitations, and potential for future study; and Section 7 provides conclusions.

2. Literature Review

Kenya and drought

Droughts are one of the most detrimental natural hazards today because of their large spatial and temporal impact; unlike storms or earthquakes, droughts are not constrained to physical destruction in a particular area. Instead, they affect agricultural lands and have very high economic and social costs

beyond the impacted drought area (Mishra and Singh, 2010; Sherwood, 2013). As summarized by Mishra and Singh (2010), droughts can be defined in different ways, which creates difficulty in locating the exact start and end points. A meteorological drought is measured by the lack of precipitation over time, which occurs in the short term. A hydrological drought is defined by the deficit of surface and subsurface water. Further, an agricultural drought is measured by the failure of crops which is influenced not only by precipitation and soil moisture but also temperature and the water needs of crops (Liu *et al.*, 2016). Finally, socio-economic droughts are a combination of all of the above as they are defined by the deficit of available water supply (influenced by meteorological and hydrological conditions) to the demand (controlled by social and agricultural use of water) (Hayes *et al.*, 2011). The temporal scale of droughts ranges from months to years (Mishra and Singh, 2010).

Vegetation responds to drought on different timescales depending on the biome; semi-arid biomes such as those found in northern Kenya generally respond slowly to water deficits potentially due to acclimation to highly variable water availability, while the more humid biomes such as the East African montane forests found around Mount Kenya respond more quickly to water deficit (Vicente-Serrano *et al.*, 2013). Plant species also have individually different responses to water stress. In the short term, they may minimize water loss and protect against dehydration, while in the long term they may shorten their lifecycle or optimize water use through acclimation responses (Chaves *et al.*, 2003). Vegetation also retains a water memory, where current productivity is influenced by the water availability of the past several months or years (Liu *et al.*, 2018; Gao *et al.*, 2020).

Kenya has bimodal rainfall seasons with short rains from October to December and long rains from March to May (NDMA, 2023). In the last century, droughts in East Africa resulting in food security problems have occurred nearly every decade with increasing frequency and severity (Nicholson, 2017; Gebremeskel Haile *et al.*, 2020). Droughts lead to increased migration, displacement, conflict, higher prices of necessities, famine, disease, and death (Von Uexkull *et al.*, 2016).

The current drought in northern Kenya since 2020 has put more than 4 million people into critical food insecurity (NDMA, 2022); this drought was made 100 times more likely by climate change (Kimutai *et al.*, 2023). The main causes of changing drought patterns are climate variabilities (such as sea surface temperatures, El Niño, and land-atmosphere feedbacks) and anthropogenic effects (such as climate warming, aerosol pollution, urbanization, deforestation, and water usage) (Uhe *et al.*, 2018; Gebremeskel Haile *et al.*, 2020). The current drought, beyond the lack of precipitation creating a meteorological drought, has more severe agricultural and socio-economic impacts because of higher temperatures caused by global warming (Kimutai *et al.*, 2023). Beyond climate change, humans can trigger droughts by interfering with the ability of the land to capture and hold water through over-exploitation of land like deforestation, extractive farming, excessive water withdrawal, or contributing to erosion (Mishra and Singh, 2010). Land use change can also lead to desertification which causes a destabilizing chain of feedbacks that reduce the water holding capacity of land and change the atmosphere-vegetation interactions, thereby potentially changing rainfall patterns (Miralles *et al.*, 2019). As the climate warms, East Africa will likely experience more frequent and intense precipitation events and droughts (Trisos *et al.*, 2023). Thus, drought is a highly relevant environmental perturbation to investigate the effects of and strategies to increase resilience to.

Agroforestry

Agriculture has been expanding and intensifying in the Mount Kenya region in the last thirty years. The area of natural land has decreased from 75% to 45% due to conversion to agriculture (Eckert *et al.*, 2017). Kenya experienced browning trends, or a general decrease in vegetation productivity, in 21% of the country and greening in only 9% of the country between 1992 and 2015 and a decrease in forest area (Gichenje and Godinho, 2018). The pressures of intensifying agriculture for livelihoods and a growing population are putting increased pressure on land and water resources, which increases the possibilities of droughts and contributes to climate change. Forest and bushland conversion to cropland in East Africa increases the land surface temperature significantly, as well as decreasing carbon stocks (Abera *et al.*, 2018, 2020; Pellikka *et al.*, 2018). This contributes to desertification feedbacks (Miralles *et al.*, 2019). Methods of farming that increase farmer resilience to drought while decreasing environmental impacts are necessary.

Agroforestry, the integration of trees into crop or livestock farming, is a nature-based solution that can help farmers both economically and environmentally. Smallholder farmers are very dependent on ecosystem conditions as their farm both feeds and supports them (Mendelsohn, 2009). Trees can diversify income, provide food sources such as fruit or nuts, wood for energy, and fodder for livestock (Lasco *et al.*, 2014). Environmentally, agroforestry can cool the farm's microclimate, provide protection from sun and wind, enhance water storage in the soil, improve soil productivity, improve nutrient availability, increase soil microbe resilience to water stress, and control erosion. These properties can both decrease the degradation of land by agriculture as well as improve agricultural productivity (Jose, 2009; Rivest *et al.*, 2013; Dollinger and Jose, 2018). The ecosystem services of agroforestry thus ameliorate some anthropogenic mechanisms of drought. Surveys and interviews with households in Kenya (Isiolo County) showed that agroforestry was perceived as both directly and indirectly building livelihood resilience to drought and floods. Fruits like bananas, mango, and papaya are common for food and income, and ecosystem services like shade and soil conservation are recognized as top benefits (Quandt *et al.*, 2017); indeed, the most common trees planted in TIST groves include avocado and mango (Masiga *et al.*, 2012). Studies in other African communities have also identified the practice as increasing farmers' resilience to climate change (Nyong *et al.*, 2020). TIST quantifies these additional benefits aside from carbon credit income as \$8 (USD) per tree (TIST, 2023). In total, agroforestry can be beneficial both directly to farmer quality of life as well as indirectly by improving the environment and potentially increasing resilience to impacts like drought and flood (Figure 1). Agroforestry is not a one-size-fits-all solution to environmental degradation and climate change: the benefits depend on how and where trees are planted and what the prior use of the land was along with stakeholder engagement (Holl and Brancalion, 2020); however, as the practices of TIST farmers are locally driven and determined via the small group structure (Masiga *et al.*, 2012), that prevents many of these issues.

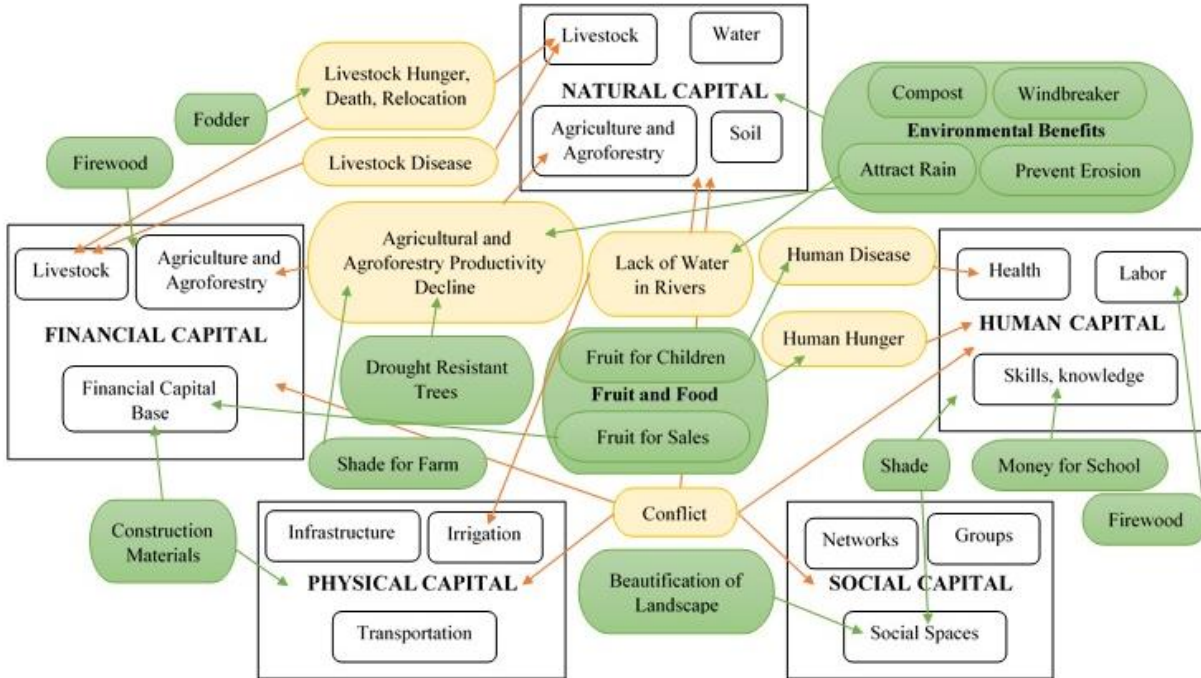


Figure 1: A system diagram of the interaction of agroforestry with drought in Kenya adapted from Quandt *et al.* (2017). Orange indicates a drought impact, while green indicates an agroforestry benefit. Agroforestry improves resilience to drought both environmentally and economically for smallholder farmers.

TIST agroforestry is quantifiably providing on-farm economic benefits as mentioned. There is some quantitative evidence as well that TIST influences the ecosystem beyond the farm: it greens the neighboring landscapes as well as the farm itself. Agroforestry has an observable effect that could be the result of tree microclimate, decreased pressure on local forests, or increased environmental awareness by farmers (Buxton *et al.*, 2021). Other ecological benefits of the program have yet to be quantified.

Tipping points and resilience

Tipping points are a sudden, nonlinear shift in the state of the system caused by only a small change in a system variable and accelerated by strong amplifying (positive) feedbacks (Lenton *et al.*, 2008). Tipping points have been shown to exist in many natural systems such as Amazon forest dieback, Arctic summer sea ice melt, populations of microbes, or human blood pressure (Lenton *et al.*, 2008; Scheffer *et al.*, 2018; Boulton *et al.*, 2022). Early warning signals (EWS) of tipping points are based on the detection of critical slowing down (CSD) of the system as a threshold is approached (Wissel, 1984). As a system is forced by external perturbations, the stabilizing feedback loops within the system act to return it to its stable state. If the feedbacks are strong, the system is quickly returned to its equilibrium state, but as the stabilizing feedbacks are weakened and the system approaches a tipping point, the system reacts more slowly to forcing, exhibiting CSD (Figure 2) (Van Nes and Scheffer, 2007). This ability of a system to recover more quickly from disturbance due to its strong stabilizing feedbacks is called resilience (Pimm, 1984).

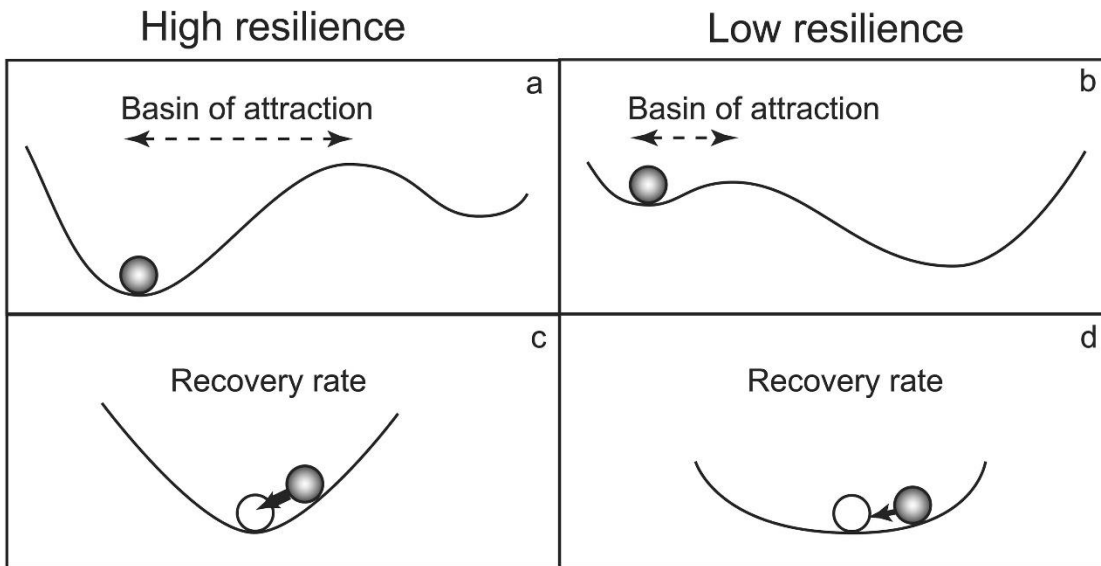


Figure 2: Resilience as a swifter recovery from perturbations (figure from Van Nes and Scheffer, 2007)

The term resilience is used colloquially and defined in multiple ways in the literature in relation to system dynamics and ecology (Hodgson *et al.*, 2015; Ingrisch and Bahn, 2018). Holling (1973) defined it as a measure of the persistence of systems, or how well they absorb change without changing the relationships and interactions within the system, which is sometimes called ecosystem resilience or resistance. Resilience, sometimes known as recovery (Hodgson *et al.*, 2015) or engineering resilience (Holling, 1996), is defined as the ability of the system to recover to its previous state after disturbances (Pimm, 1984). Here, the recovery definition will be used.

Resilience is difficult to measure in practice, but measuring the recovery rate from disturbances can represent the total system resilience and serve as EWS to tipping points (Van Nes and Scheffer, 2007). Systems will recover exponentially towards equilibrium after perturbation, and as systems lose resilience the recovery rate will tend to zero (Drake and Griffen, 2010). Recovery rates are best estimated by fitting an exponential curve to the recovery data and comparing the rate term (Lenton *et al.*, 2022). Their potential as an EWS was empirically shown by Veraart *et al.* (2011) in a controlled experiment on cyanobacteria where the recovery rate from regular perturbations was measured while increasing the stress on the system to the point of collapse. The recovery rate slowed as the bacteria colony approached its tipping point. Though the recovery rate estimation requires relatively high sampling frequency and a definition of the equilibrium state of the system, it is seen as a robust and direct method of measurement that is independent of the size of the perturbation up to a point (Lenton *et al.*, 2022). Some studies use the recovery time as a measure of resilience (Schwalm *et al.*, 2017; K.J. Lees *et al.*, 2021); however, this only is comparable between disturbances of similar magnitude, and in a real-world ecosystem, disturbances of the same severity may not occur frequently enough to be compared (Lenton *et al.*, 2022). The slope of the recovery has also been used, such as the ratio of the peak disturbance response to the recovery time (White *et al.*, 2020), but this ignores the exponential nature of the recovery and requires measuring the magnitude of the disturbance by the system response to it (Lenton *et al.*, 2022).

Autocorrelation with a time lag of one unit (AC1) is also widely used as a measure of system resilience and as an EWS because a system that recovers more slowly will have more influence of previous timesteps on the current timestep (Scheffer *et al.*, 2009). An advantage of AC1 is the equilibrium or recovered state of the system does not need to be defined, though it requires relatively long time series to generate (Lenton *et al.*, 2022); however, it measures the general state of resilience rather than the resilience or recovery from specific perturbations. As another option, the ecosystem state can be autoregressively modelled as a linear combination of factors such as environmental variables, noise, and the system state at a lagged timestep, where the coefficient of the lagged system state is used as a resilience measure (where higher coefficient means slower recovery) (De Keersmaecker *et al.*, 2015).

The theory behind recovery rate and resilience

The theory behind recovery rate, autocorrelation, and their relation to resilience is described in Scheffer *et al.* (2009) and Lenton *et al.* (2022). A dynamical system with a state variable x that tends to recover from perturbations may be in a basin of attraction at x^* (Figure 3).

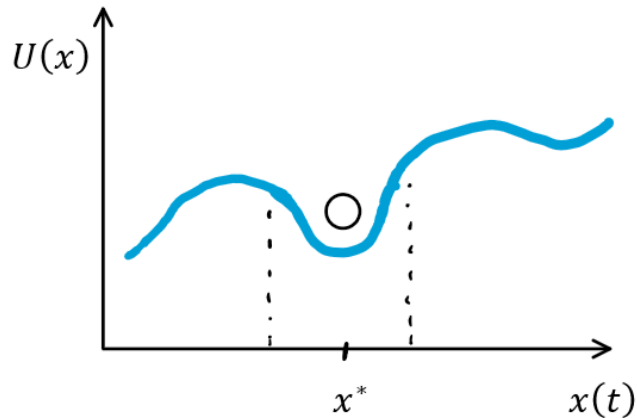


Figure 3: System $U(x)$

The system state can be described by a function $U(x)$ with, for simplicity, additive noise η with standard deviation σ . Thus, the dynamics over time of the system are represented by the derivative:

$$(Eq. 1) \quad \frac{dx(t)}{dt} = -U'(x(t)) + \eta(t)$$

Around the basin of attraction x^* , the function U can be approximated as a quadratic (Figure 4) such that for $\lambda < 0$ (Scheffer *et al.*, 2009):

$$(Eq. 2) \quad U(x) \sim -\frac{\lambda}{2}x^2$$

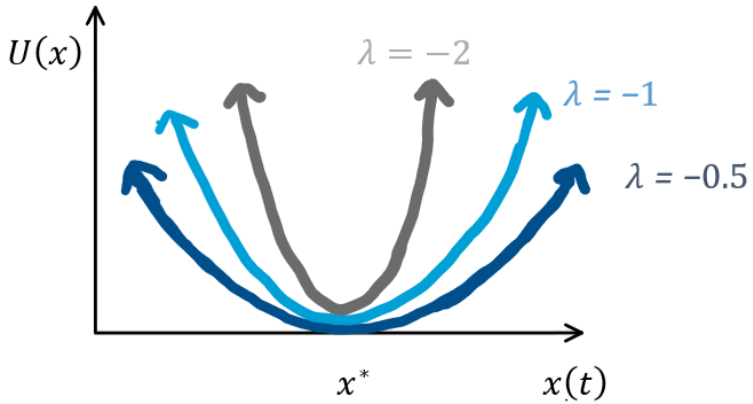


Figure 4: Approximation of $U(x)$ around x^* as a quadratic with various values of λ representing the steepness of the slope back to the bottom of the basin.

Therefore, the recovery rate of the system to x^* after a perturbation is λ , which provides a measure of the stabilizing negative feedback. The more negative λ is, the faster the system recovers and the more resilient it is. A recovery rate approaching 0 indicates a less resilient system (Scheffer *et al.*, 2009; Lenton *et al.*, 2022). The recovery over time after a perturbation to x_0 at $t=0$ (Figure 5) can be approximated as (Smith *et al.*, 2022):

$$(Eq. 3) \quad x(t) \sim x_0 e^{\lambda t}$$

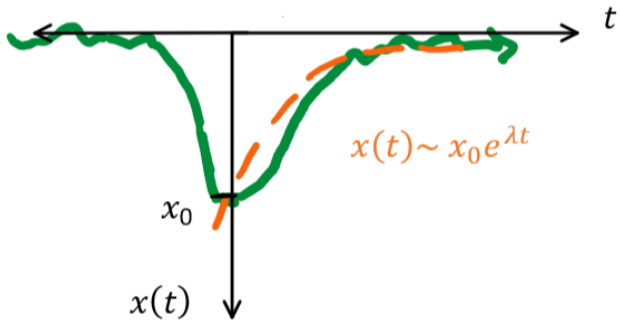


Figure 5: An approximation of $x(t)$ after a perturbation at $t = 0$ as an exponential recovery with rate λ .

This approximation can be used to determine λ by fitting an exponential curve to observed data.

Discretizing the dynamics of the system into timesteps allows the autocorrelation function α at lag n to be found analytically as:

$$(Eq. 4) \quad \alpha(n) = e^{n\lambda\Delta t}$$

When λ approaches zero as resilience decreases, $\alpha(1)$ (AC1) will increase towards 1.

Remote monitoring of ecosystem resilience

Remote monitoring has become an important tool for monitoring vegetation and ecosystems. Passive satellite sensors measure the intensity of electromagnetic waves that are reflected by the surface in different realms of the wavelength spectrum. Chlorophyll has a distinct spectral reflectance curve that

allows it to be easily quantified with measures of red and near infrared reflectance. High chlorophyll concentrations absorb more red wavelengths, and near infrared (NIR) wavelengths are reflected due to the structure of leaves (Petropoulos and Kalaitzidis, 2012). Thus, the difference between the red and NIR reflectance can be used as an index of the vegetation presence and productivity in a region (Myneni *et al.*, 1995; Silleos *et al.*, 2006). One of the most commonly used indices is Normalized Difference Vegetation Index (NDVI), which is defined as $NDVI = (NIR - Red) / (NIR + Red)$ reflectance (Petropoulos and Kalaitzidis, 2012). NDVI has been proven to strongly correlate with biomass, vegetation productivity, and vegetation response to precipitation and drought (Liu *et al.*, 1994; Wang *et al.*, 2004; Wessels *et al.*, 2006); thus it can be used as a proxy measurement for the overall vegetation health. It is not without limitations: NDVI is distorted by clouds, water, and bare soil (Huang *et al.*, 2021; Zeng *et al.*, 2022). It is also affected by sub-pixel mixing (Pettorelli *et al.*, 2005), saturation at high greenness such as dense forests (Huang *et al.*, 2021), and will be dominated by the tallest and most abundant species in the community (Cavender-Bares *et al.*, 2022). Most importantly, a single measurement via satellite is not a comprehensive measure of the health of an ecosystem and cannot completely replace ground observations (Cavender-Bares *et al.*, 2022). Nevertheless, measurements of vegetation health via remote sensing have allowed relatively inexpensive and widespread data collection through time and space of terrestrial ecosystems that represent the health of the ecosystem.

Remote monitoring of ecosystems has used vegetation indices through time and space to estimate resilience and look for EWS of tipping points. AC1 of NDVI and vegetation optical depth were used to examine tropical forest resilience against precipitation and temperature by comparing autocorrelations against annual precipitation and temperature. Evidence for a tipping point triggered by drought and heat was found by the rising AC1, indicating loss of resilience, against lower precipitation (Verbesselt *et al.*, 2016). Ground observations of forest mortality in the US were compared with AC1 and measures of drought, and AC1 of NDVI was the best indicator of real forest resilience (Tai *et al.*, 2023). Resilience via AC1 was shown to be an earlier warning signal of forest mortality than the decline of NDVI below a certain threshold (Liu *et al.*, 2019). Resilience estimation using vegetation indices from remote sensing is well established, especially using temporal autocorrelation.

There are studies using more linear methods of resilience measurement like the slope of recovery, or the ratio of disturbance magnitude to recovery time, such as quantifying the ecosystem stability of specific regions (e.g., Ireland by White *et al.* (2020), or Louisiana wetlands by Suir *et al.* (2020)). These studies are less relevant because the use of recovery time or slope ignores the exponential nature of recovery and thus can provide distorted analyses.

Few studies directly quantify the exponential recovery rate to look at vegetation resilience. Smith *et al.* (2022) analyzed resilience globally with NDVI and vegetation optical depth using both the recovery rate and AC1. They fit recovery rates using abrupt transitions in the data itself to identify perturbances such as drought or heatwaves. They also computed AC1 for the same data and found that the recovery rates had the expected exponential relationship to AC1, proving the theoretical expectation. On a local ecosystem level, van Belzen *et al.* (2017) analyzed aerial images of tidal marshes to determine their resilience to inundation time. By plotting the recovery times to regrow vegetation versus the local inundation time and then fitting an exponential model, they estimated the recovery rate for each site

and determined that longer tidal inundation caused decreased resilience, critical slowing down, and eventually a tipping point. While they also analyzed AC1 as a less data-intensive method, they found that direct measurement of the resilience via recovery rate was more effective. As a final example, Buxton *et al.* (2022) measured the rate of decay of NDVI from the “beneficial perturbation” of the rainy season in the arid Sahel as a resilience metric. Direct estimation of the resilience via recovery rate, as the most robust method of resilience measurement, will be utilized here. These examples of direct estimation of recovery rate will form the basis of the methodology explained in Section 4.

Global decline of resilience

The ability to remotely monitor resilience has shown that terrestrial ecosystems globally are exhibiting reduced resilience due to pressures such as climate change and deforestation. Forzieri *et al.* (2022) found that most forests are declining in resilience except for boreal forests, which are likely benefiting from warming and CO₂ fertilization. The Amazon rainforest has lost resilience in the last 20 years and is less resilient in areas that are closer to human activity. This is due to positive feedback from local fires amplifying drought and forest loss, as well as deforestation and degradation, which reduces the vegetation-atmosphere feedbacks that promote rainfall (Boulton *et al.*, 2022).

In particular, the effects of climate change on water availability are critical to vegetation and ecosystem resilience, and resilience to drought is commonly studied. Smith and Boers (2023) analyzed vegetation resilience across land cover types, using both directly estimated recovery rate and AC1 (using the same methodology as Smith *et al.* (2022)), and compared them with the aridity index of the region, the intra-year seasonality of precipitation, and the inter-year variability of precipitation. They found that landscapes with a water surplus rather than deficit had the fastest recovery rates. Additionally, high inter-annual variability, i.e., drought, was correlated with lower resilience across all land cover types (Smith and Boers, 2023). Multiple natural factors can modulate vegetation resilience to drought. As Anderegg *et al.* (2020) found, subsequent droughts are usually more detrimental to tree health than initial droughts, though it depends on the species and its ecosystem. Schwalm *et al.* (2017) analyzed global resilience to drought using recovery time rather than rate but did find that the post-drought precipitation and temperatures strongly affected recovery time. De Keersmaecker *et al.* (2015) analyzed global resilience to short-term climate anomalies by autoregressively modelling the current NDVI as a linear combination of the temperature anomaly, drought index, and the previous NDVI and using the coefficient of the previous NDVI as a measure of resilience. They found that semi-arid areas had low resilience to drought and that the amount of tree cover versus bare soil cover affected the resilience. As more variable precipitation and more frequent and intense droughts occur because of climate change (Trisos *et al.*, 2023), resilience of vegetation may further deteriorate globally. Measuring current ecosystem resilience and historical patterns to detect potential tipping points is critical for adaptation strategies and potential human management (or reduction thereof) of land (Dakos *et al.*, 2015).

Resilience and human land management

While resilience monitoring of natural ecosystems and remote monitoring of managed natural systems have recently become more common (Thackway *et al.*, 2013), the combination of remote sensing to monitor agro-ecological system resilience is relatively novel. von Keyserlingk *et al.* (2021) studied the

effect of grazing on Mediterranean rangeland using NDVI and the slope of the NDVI trend after a detected disturbance as a proxy for recovery rate. They found that areas with high grazing had a slower recovery after drought, suggesting that decreasing grazing intensity is a necessary intervention for drought resilience in the region. Lees *et al.* (2021) analyzed the recovery time of peatlands in the UK after management such as cutting or burning was performed using a metric derived from NDVI. The recovery times were affected not only by the management frequency but by other factors such as grazing, forestry, rewetting, and weather conditions. Remote monitoring of resilience to fire using the return rate has been studied in the Mediterranean for making forest management decisions after wildfires (Fernandez-Manso *et al.*, 2016). In Australia, the recovery of NDVI after experimental burns was examined in rehabilitated mine sites to determine whether the restored ecosystems were resilient to fire, providing potential evidence for improved restoration practices (McKenna *et al.*, 2018). In agriculture, New Zealand is considering the use of remote sensing to assess the effectiveness of regenerative agriculture on increasing resilience to drought and floods (Donovan *et al.*, 2021). Maize agriculture in China has also been assessed using NDVI for its resilience to drought with implications for more optimal and sustainable water use in agriculture (Jing *et al.*, 2023). Pastureland in the Netherlands and Uruguay have been assessed for resilience to drought and climate anomalies with remote sensing in order to determine more sustainable and optimal management practices (De Keersmaecker *et al.*, 2016; Tommasino *et al.*, 2023). To live and develop sustainably, social-ecological resilience is needed, thus determining the social-ecological feedbacks and practices that build resilience is necessary (Folke, 2006). Assessing resilience remotely can provide feedback on the effectiveness of management or agricultural practices and assist in decision making.

Quick monitoring and translation of information into decisions and actions are needed if humans are to contribute to the maintenance of a livable Earth (Lenton and Latour, 2018). Recovery rates can be used to compare over time and space and assess trends in resilience, provide maps of more vulnerable areas, and help assess the risk of approaching critical transitions (Dakos *et al.*, 2015). Knowing the areas of higher vulnerability, as well as the interventions or management strategies of places of higher resilience, can help speed the spread of effective resilience-building tools. Agroforestry is a proven tool for improving local soil, microclimates, and water management, as well as the economic resilience of smallholder farmers, and it is already used by Kenyan farmers as a tool to increase their farm resilience to water variability. Determining quantitatively whether agroforestry improves resilience on TIST farms and in the surrounding areas will provide more evidence for the adoption of locally driven agroforestry. Thus, my research questions are as follows.

3. Research Questions

RQ1: Can resilience to drought be estimated with vegetation recovery rate via remotely sensed data in Kenya?

RQ2: Do farms engaged in agroforestry with TIST exhibit greater resilience, as measured by recovery rate, to drought than non-TIST land?

RQ3: Does TIST membership affect the recovery from subsequent drought events?

RQ4: Are there any spillover effects from TIST groves into the surrounding areas?

This study will use remotely sensed data on vegetation health throughout the drought and recovery periods of recent years to assess resilience to drought using recovery rates. Farms involved in the TIST agroforestry program will be compared to surrounding areas to determine the effect of TIST on resilience to drought.

4. Methodology

Study area, timeframe, and drought indicators

The study area is Tharaka-Nithi, Meru, Embu, and Nyeri counties in Kenya, surrounding Mount Kenya (Figure 6). The study area was chosen to encompass arid and semi-arid lands (ASAL) counties, a large group of TIST farms, and comparable agricultural and semi-natural areas. Kirinyaga was excluded because it is not an ASAL county, and Laikipia was excluded as it is mainly dry rangeland with different

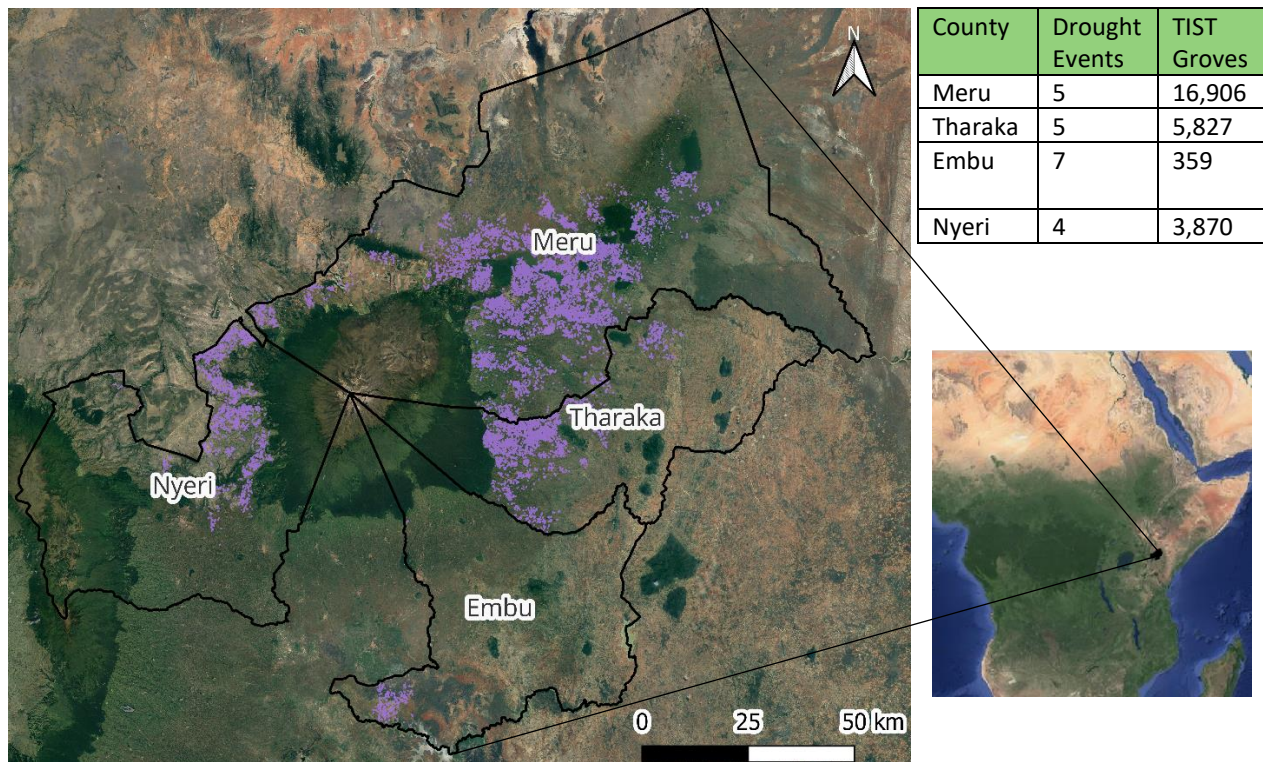


Figure 6: (Left) Relevant counties and TIST groves (in purple) within those counties. (Top right) Number of drought periods classified by the NDMA from its beginning in 2016 through May 2023. Number of TIST groves as verified between 2005-2018. (Bottom right) Location of study area within Africa. Figure created with QGIS. Background map data and imagery: ©2023 Landsat/Copernicus, TerraMetrics, Google

agro-ecological characteristics than the study counties (Recha, 2018). There are two major ecoregions represented. East African montane forest is a patchwork of evergreen tropical moist broadleaf forest and bamboo at middle altitudes that transitions to woodland and savannah at lower altitudes (Martin

and Burgess, 2023a). The ASALs moving away from the mountain are Acacia-Commiphora bushland and thicket, which are hotter and drier (Martin and Burgess, 2023b). Tharaka-Nithi, Embu, and Meru are classified as south-eastern marginal agriculture counties, and Nyeri is agro-pastoral (NDMA, 2023). The landscape within these counties is heterogenous (Figure 7). Agricultural practices vary between different agro-ecological zones which are delineated along altitude and corresponding precipitation and climate differences. Higher and wetter zones farm tea, coffee, maize, and sugarcane, while middle zones grow maize, beans, and sweet potato, and lower and drier zones transition to ranching, sorghum, and millet (Recha, 2018). There are more than 26,000 verified TIST groves in the region as of 2018, with a median of 84 trees and 0.279 hectares based on the data provided by TIST as collected through their carbon quantification process. The majority of TIST groves (16,906) are in Meru (Figure 6).

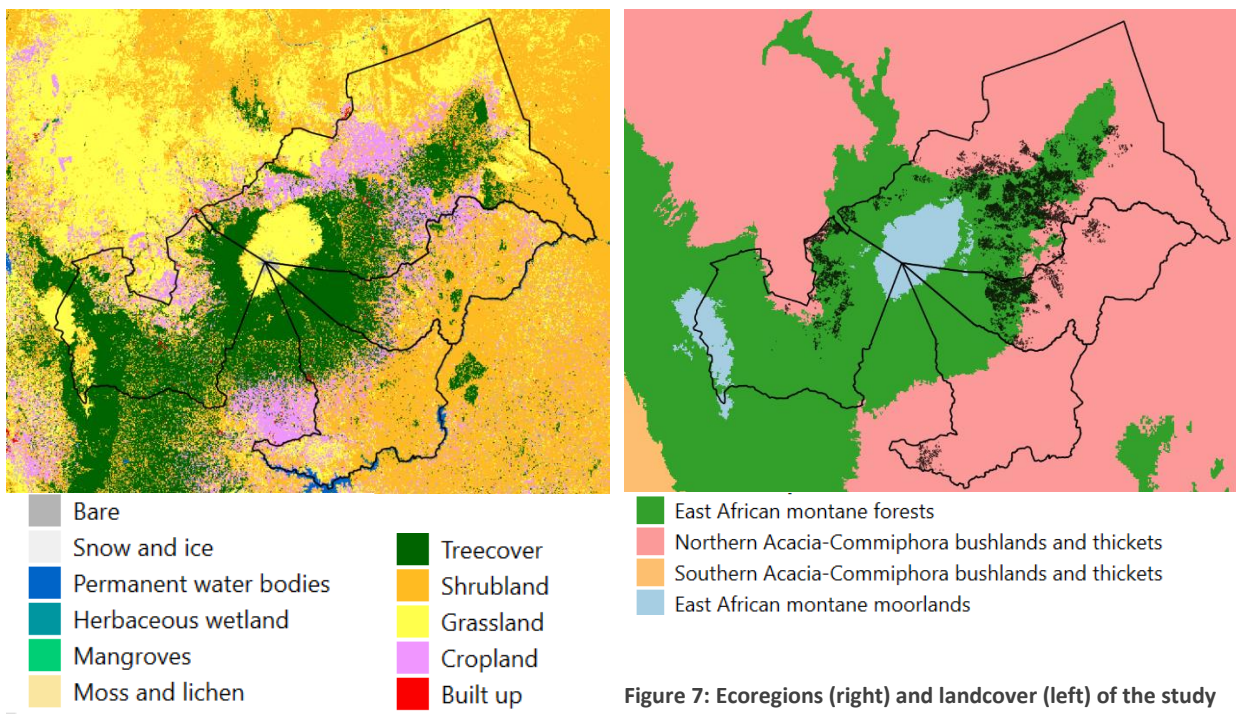


Figure 7: Ecoregions (right) and landcover (left) of the study area.

The timeframe of the study is between 2013-2023 due to the availability of Landsat-8 data and the recent droughts in Kenya (2016-18, 2020-present). To estimate the recovery rate, specific disturbances must be determined. Though some studies use the data itself to determine disturbances through abrupt shifts in the data (Smith *et al.*, 2022), that approach is more suited to large studies where disturbances cannot be readily identified for all pixels. In this geographically constrained study, disturbances are defined by the drought classifications issued by the Kenyan National Drought Management Authority (NDMA).

NDMA was established in 2016 and began issuing monthly drought severity classifications for each ASAL county as shown in Figure 8 (NDMA, n.d.). These publicly available bulletins are based on a combination of precipitation indices and surveys of residents to classify each month as Normal, in Recovery, Alert, or

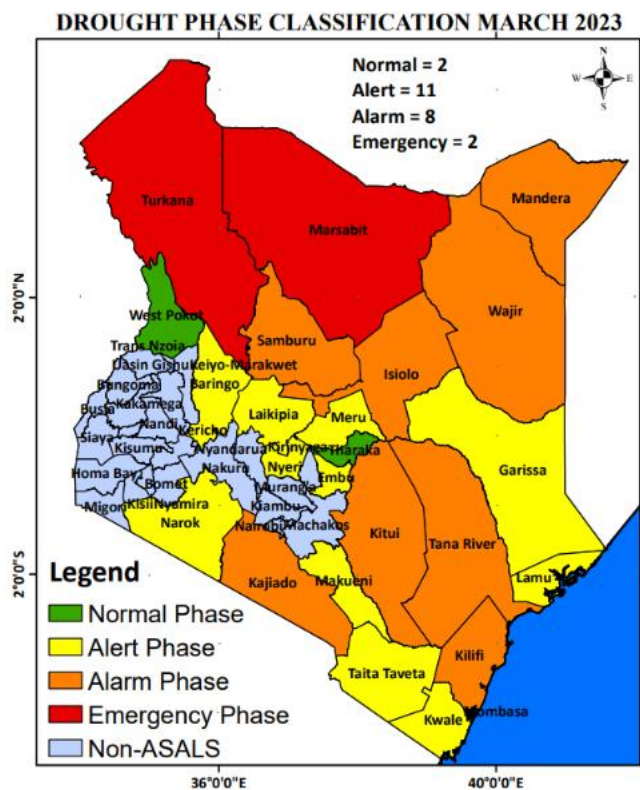


Figure 8 : Example drought classification by the National Drought Management Authority (NDMA, 2023).

multiple ways and is not exclusively a product of precipitation or temperature (Mishra and Singh, 2010), using a more holistic indicator of the drought state and its impacts as captured through the local surveys provides a more comprehensive picture, taking into account the socio-economic, agricultural, and hydrologic characteristics that are difficult to capture in another single metric. Though they are less geographically and temporally specific than available precipitation data such as CHIRPS, precipitation data spatial resolution is still large (e.g., CHIRPS at 5.5 km) and the tradeoff for spatial resolution in order to capture other aspects of drought was taken (Funk *et al.*, 2015). Nonetheless, it should be noted that each county is heterogenous, and the drought conditions may vary across the county despite the uniform classification. Thus, disturbance and recovery periods are based on the NDMA classifications; a disturbance is any month(s) classified as Alert or Alarm, and a recovery period is assessed for any transition to Recovery or Normal after a drought period that lasts more than one month. A subset of drought classifications and the major recovery periods according to the NDMA are shown in Figure 9. Because each county clearly has distinct histories and severities of droughts before any one recovery month, pixels from each county will be compared separately. The entire table can be found in the Appendix, Table 3.

Alarm phases. Surveys include questions about livestock forage quality, food scarcity, livestock body condition, water access, crop prices, and crop success (Bowell et al., 2021; NDMA, 2022). A separate study has shown that surveys of Kenyans' perception of the state of drought had a strong correlation with instrument measured rainfall and vegetation change, supporting the local knowledge basis of these classifications (Linke et al., 2020). A study of the NDMA classifications in comparison to standard drought indices such as the standard precipitation index, soil moisture, or vegetation condition index based on measured data like precipitation, temperature, or satellite observations found that the different indices correlated very differently with the NDMA classification for each county, potentially due to the very different human water withdrawal and geology of water reservoir buffers in the different counties (Bowell et al., 2021).

Additionally, because drought can be defined in

Figure 9: A subset of the drought categorizations from the start of the availability of the NDMA reports (Month 40, September 2016) until Month 80, January 2020. The highlighted months (54, 59, and 77) represent the start of recovery periods.

Data acquisition

Publicly available remotely sensed data was obtained from Google Earth Engine (GEE) (Gorelick *et al.*, 2017). Landsat-8 Operational Land Imager was chosen which has 30m resolution and a 16-day revisit period (NASA Landsat Science, n.d.). The surface reflectance dataset was used with data available beginning April 2013, including atmospheric correction and cloud masking. Sentinel-2 has higher spatial and temporal resolution at 10m and 5-day revisit period with two satellites; however, the first satellite did not collect images in the study area until December 2015, and the second satellite (along with cloud masking algorithms) are not available before April 2017 (ESA, 2023), well into the first drought period of interest. Landsat-8 has sufficient resolution to see important changes in vegetation and has comparable accuracy to Sentinel-2 for vegetation indices and analyses (Kennedy *et al.*, 2014; Arekhi *et al.*, 2019; Kowalski *et al.*, 2020).

Clouds, haze, or fog reduce the observed NDVI (Zeng *et al.*, 2022), therefore the atmospherically corrected data was masked using the Landsat quality pixels to remove these artefacts. Though differing angles of the sun to the sensor can cause the reflectance to vary (Sims *et al.*, 2006), the study area is on the equator, ensuring a more constant solar angle and also a constant time of day for the satellite crossing (approximately 10 am every day) (NASA Landsat Science, n.d.).

NDVI was chosen as the proxy measurement for the state of the vegetation system as it has been proven to reflect vegetation productivity and overall health, including in ASALs in Kenya (Shisanya *et al.*, 2011). It is correlated with precipitation and drought and has been used to monitor drought response (Liu *et al.*, 1994; Sims *et al.*, 2006). Though NDVI is strongly affected by bare soil which may occur around harvest times (Zeng *et al.*, 2022), NDVI has been used in this area effectively (Buxton *et al.*, 2021). Thus, NDVI was calculated in the study area between April 2013 and May 2023. GEE code is included in the repository in Section 8.

To classify pixels into counties, SHP files of county boundaries were obtained (RMCMRD Africa GeoPortal, 2020). Boundaries of TIST groves were provided by TIST. Though the outlines are intended to encompass only the grove, trees are not always planted in a contiguous grove and are sometimes planted along field borders in narrow strips; therefore, pixels with any part contained within the outlined grove were considered grove pixels. To classify neighbors, the Euclidean distance from the center of all non-TIST pixels was found to the center of the nearest TIST pixel. Any pixel with a distance

between 0 and 60m (exclusive) is considered a direct neighbor, i.e. any pixel bordering a TIST pixel (Appendix, Figure 33).

To consider other explanatory variables, several other datasets were downloaded from GEE. For relevant comparisons between similar land cover types and to remove built-up land, the ESA Worldcover v100 for 2020 was used which has 73.6% accuracy in Africa and is more accurate for higher resolution, heterogenous landcovers than other comparable datasets (Tsendbazar *et al.*, 2021; Zanaga *et al.*, 2021; Venter *et al.*, 2022). The landcover categories were reduced from 10m to 30m resolution using mode (Smith *et al.*, 2022). In the ten years of the study, land cover change is assumed to be minimal, as land converted from forest to farmland or vice versa will have a shift in NDVI pattern. To compare ecoregions, RESOLVE Ecoregions 2017 was used (Dinerstein *et al.*, 2017). To control for the effects of unmodified versus highly human modified land, the Global Human Modification Gradient was used, which compiles datasets of agriculture, human settlement, transportation, and energy production to produce an index of human modification at 1 km resolution circa 2016 (Kennedy *et al.*, 2019). Altitude was obtained from the NASA SRTM Digital Elevation at 30m resolution (Farr *et al.*, 2007). The yearly average precipitation over the study period was derived from CHIRPS (5.5 km resolution) (Funk *et al.*, 2015). Finally, the mean and standard deviation of the monthly NDVI over the study period was calculated after the filtering described below.

Data preprocessing

Preprocessing was performed as shown in Figure 10. First, the data was temporally reduced to monthly resolution using a maximum composite to minimize missing data from cloud masking; monthly resolution is sufficient because it is more frequent than the vegetation drought recovery being measured which is usually several months (Vicente-Serrano *et al.*, 2013). Maximum value compositing is effective for NDVI because errors tend to reduce NDVI, and it is computationally inexpensive (Pettorelli *et al.*, 2005).

Then the data was downloaded from GEE for local processing using Python 3.11. Pixels with landcover other than tree cover, cropland, shrubland, and grassland were removed, such as bare ground or built-up areas.

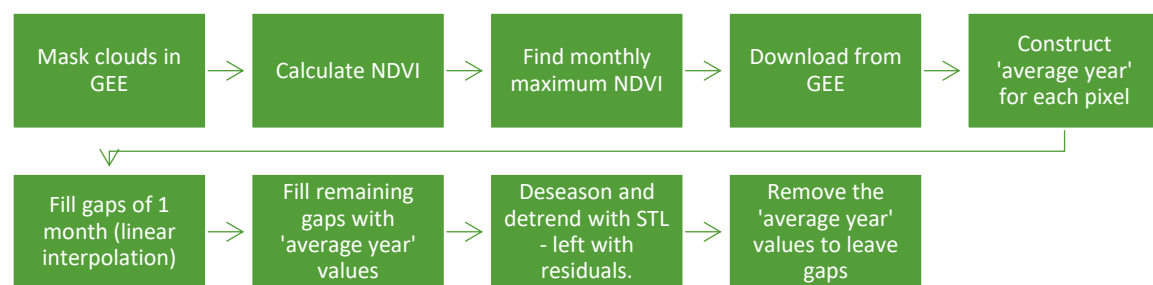


Figure 10: Data preparation process.

Despite the monthly maximum composite, most pixels still had months with no valid measurements taken, especially in forested and cloudier areas (Figure 11). There were not enough semi-continuous

observations to fit recovery rates well across the study area (e.g., fewer than half of pixels had 9/12 valid data points in recovery periods for Tharaka county; while 75-90% of pixels in each county had 6/12 valid data points in recovery periods, this was found to be insufficient for estimates). To proceed, several approaches were investigated to maximize data quantity and quality. There are many NDVI reconstruction algorithms available in the literature utilizing temporal or spatial gap-filling (Liu *et al.*, 2017; Cao *et al.*, 2018). Because there are two growing seasons in Kenya, each monthly observation is likely to experience a shift in direction from the previous month. This limits the use of common algorithms such as the Savitzky-Golay filter (Chen *et al.*, 2004) as used by Smith *et al.* (2022) which uses linear interpolation to fill gaps which are then smoothed. This is effective for a higher sampling frequency and short gaps, but linearly interpolating over long gaps eliminates the seasonal variation expected in the study area (Appendix, Figure 29), which is a recognized constraint of many reconstruction algorithms in cloudy tropical areas (Liu *et al.*, 2017). Algorithms that merge observations from other satellites such as MODIS to fill in gaps in the Landsat timeseries were also investigated (Chen *et al.*, 2021) but could not be implemented due to time and computing resource constraints.

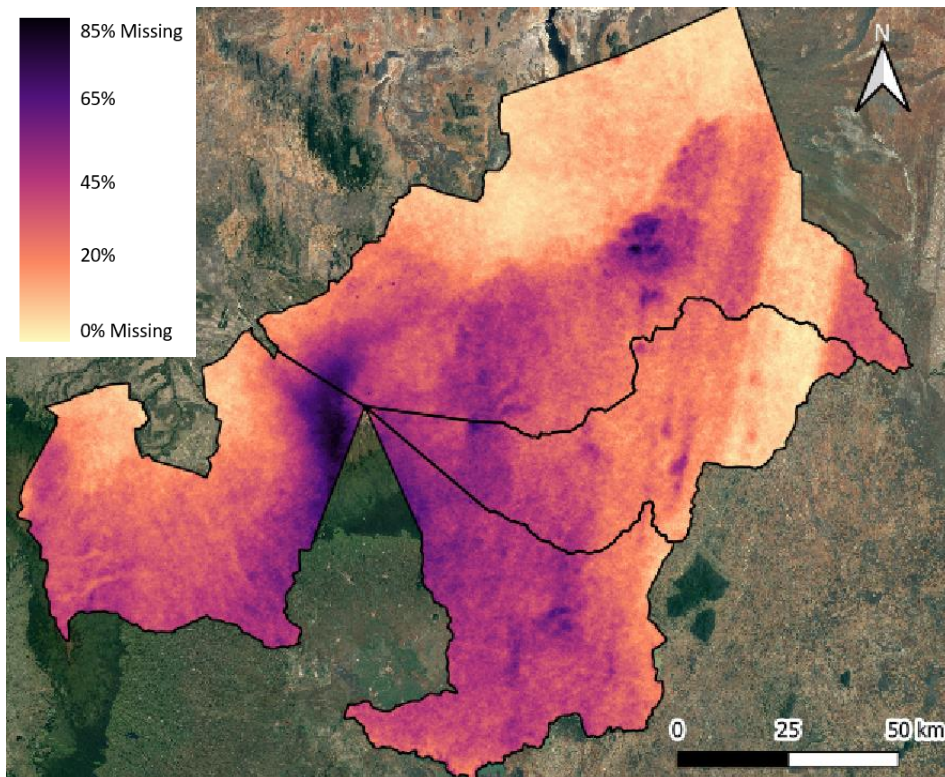


Figure 11: The percentage of months missing for each pixel in the study area. Forested areas around Mount Kenya are cloudier and missing more pixels, between 50-75% generally. The lighter vertical band is the area where Landsat-8 tiles overlap and thus have more opportunities for cloud-free observations each month. Cloudier areas have missing streaks up to 35 months long. Most pixels are missing 3-10 months in the longest missing streak. Figure created with QGIS. Background map: ©2023 Landsat/Copernicus, TerraMetrics, Google

Thus, gap filling and decomposition were performed as follows. First, the average NDVI for each month over the decade was found per pixel. Then, gaps of one month were filled per pixel with linear interpolation. No more than one month was filled because the seasons in Kenya are two to three months long (NDMA, 2022). After filling, any remaining empty pixels were replaced with the corresponding monthly average to create a continuous timeseries in approximately the correct seasonal shape for detrending (Figure 12). The replaced average pixels were removed after decomposition.

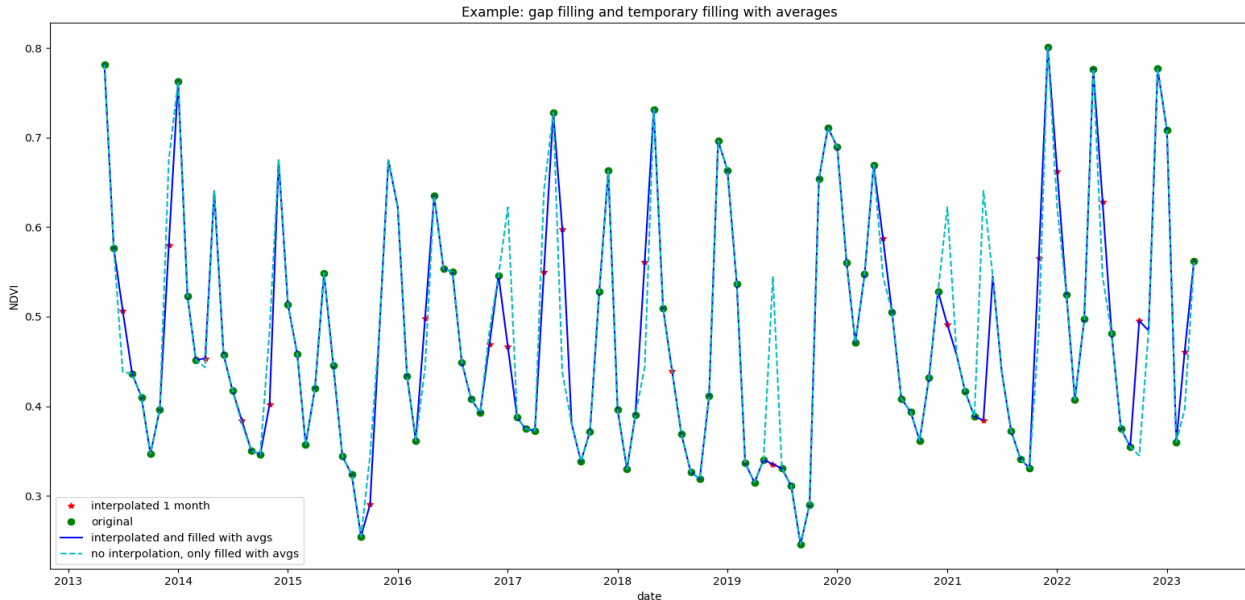


Figure 12: Example of gap filling. Green points are the original time series. Red stars show linear interpolation for gaps up to one month. The dark blue line shows the trend created with the original data, one month interpolation, and remaining gaps filled with averages. The cyan dotted line shows the trend if all gaps were filled with the monthly averages, indicating places where linear filling could cover up the seasonal shape. Filling one month was found to be the best compromise between maintaining enough data for recovery rate calculation while not overly smoothing the dataset.

To remove any non-stationarities in the greenness data, such as a gradual greening in agroforestry groves, and the typical yearly cycle of greenness from seasons, an additive model was assumed and seasonal trend decomposition by Loess (STL) was used (Cleveland *et al.*, 1990) as implemented for Python by Smith *et al.* (2022). This algorithm is commonly used, robust to outliers, and less computationally expensive than comparable algorithms (Verbesselt *et al.*, 2016; Ben Abbes *et al.*, 2018). The parameters were chosen as suggested by the authors (Cleveland *et al.*, 1990). A slow-changing seasonal window of 21 was selected because the normal cycles of seasons could be distorted by long droughts. The decomposition yields a residual, representing the base state of the system (Figure 13). After discarding the residuals obtained from the replaced average “observations,” the mean and standard deviation of each pixel’s residual was calculated and saved for the recovery rate estimation. Using the residuals also

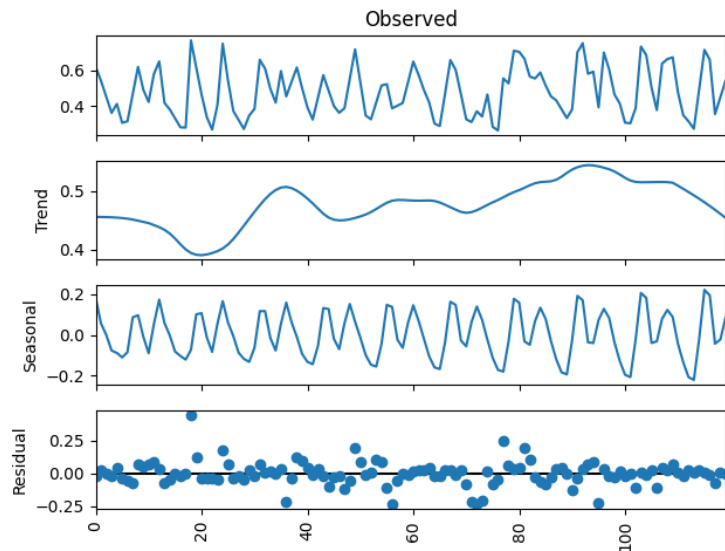


Figure 13: Example of STL decomposition. The top plot shows the input NDVI observations after linear interpolation and gap filling with monthly averages. The timeseries is then decomposed into its trend, seasonal, and residual components. The residual represents the base state of the system and is used for resilience analysis.

accounts for the differences in mean NDVI and seasonal cycles for different vegetation types, e.g., from consistently green trees to constantly cycling crops.

Recovery rate estimation

To estimate the recovery at each pixel (Figure 14), the recovery period was obtained for the 12 months centered around a recovery month. Recovery months are defined as months that transitioned from an Alert or Alarm phase into a Recovery or Normal phase for more than one month. A twelve month period was chosen because plants in tropical biomes tend to respond to drought conditions and recoveries within four to seven months (Vicente-Serrano *et al.*, 2013) while also minimizing the overlap with subsequent droughts and recoveries. Only pixels with at least 9/12 months with valid data during the recovery period were selected. Then, the local minimum of the residual was found within the 12 months (White *et al.*, 2020). The local minimum was required to be more than one standard deviation from the mean residual to indicate a true disturbance. This was supported by tests of recovery estimation from a sample of pixels ($n = 5000$) without any threshold; those with disturbances greater than one standard deviation away from the mean tended to have a better fit (measured by R^2) of the recovery (Appendix, Figure 30 - Figure 31). If the minimum was not lower than the threshold, the pixel was marked as no disturbance. After finding the local minimum, the remainder of the 12-month recovery period was included after it for the sample to be fit. Finally, to ensure that the fitted exponential was a reflection of a recovery to the equilibrium state (Lenton *et al.*, 2022), the mean of the pixel's residual was added as six additional datapoints to the recovery sample. Using the residual also prevented the equilibrium state from being influenced by any long-term trend in the data.

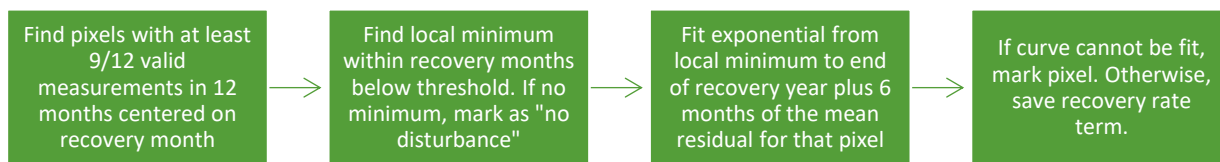


Figure 14: Recovery rate calculation process.

Then, an exponential of the form $x(t) = ae^{\lambda t} + c$ was fit using nonlinear least squares to the recovery sample (Figure 15) (Buxton *et al.*, 2022; Smith *et al.*, 2022). An initial guess was provided. After testing with sampled data ($n= 5000$) for optimal convergence and fit (measured by R^2), the initial guess was set to $a = -0.05$, $\lambda = -0.2$, and $c = 0.05$ (Appendix Figure 32). After fitting, the appended six months of the mean were removed, and R^2 was calculated. The pixel was marked as no valid calculation for four conditions: a) if the curve fitting could not converge; b) if the local minimum was more than four months after the recovery month, meaning less than three months of real data were available to fit to; c) if the R^2 value was outside the normal range of zero to one, indicating that the data was fit to a nonsensical model and did not demonstrate the exponential recovery; or d) if the determined a and c parameters were far outside the expected values (c outside of $[-1, 0.5]$ or $a > 0.1$), again indicating a nonsensical model fit.

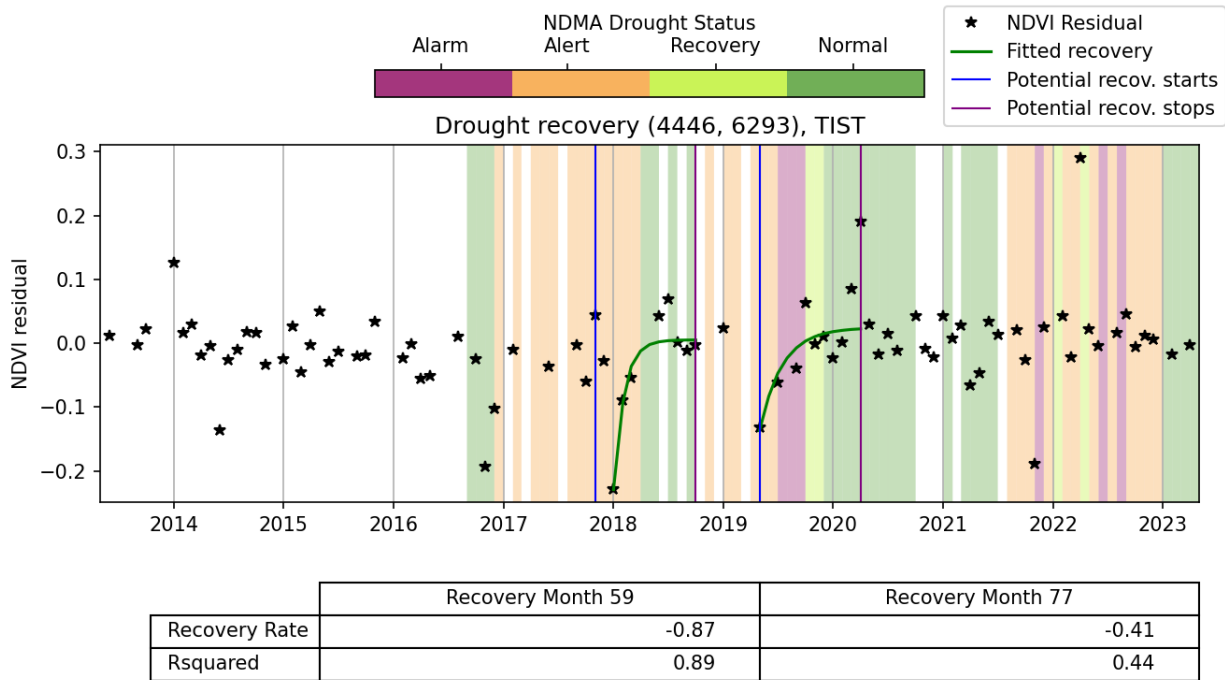


Figure 15: Example fitted recovery rate.

Comparisons

For all analysis, the absolute value of the recovery rate was used (higher rate indicates faster recovery). To compare how the recovery rate may have changed over time, the percent change between subsequent recoveries was calculated for any pixel that had a valid recovery rate calculation for both recovery periods. While this ignores any categorical changes between pixels that may not experience a disturbance in the first drought but did in the second, that would measure resistance more than resilience, which is outside of the scope of this study.

Spearman's rank correlation was used for non-parametric correlations (Tai *et al.*, 2023). The chi-square test for independence was used to compare effects of categorical variables on categorical outcomes (e.g., landcover type vs. disturbance or no disturbance detected) which is appropriate due to the large sample size (Franke *et al.*, 2012).

To test the difference between distributions of the continuous recovery rate results, the Kruskal-Wallis H test (KWH) was used with post-hoc Dunn (PHD) test for a non-parametric analysis of more than two groups (Campbell and Wang, 2020; Nolè *et al.*, 2022). While the original null hypothesis for the KWH is that the samples are from the same distribution, if the two distributions have similar shape and scale the test can be used to find difference in location (Kruskal and Wallis, 1952). The recovery rate results are left skewed with highest probabilities around 0.5-1.5 with long tails to the right, so this assumption was used (Appendix, Figure 34, Figure 35). Because of the long tail of the distribution, means are right skewed, so the median was used as the measure of central tendency. The Dunn post-hoc test compares the results pairwise after the KWH (Dunn, 1964). All comparisons were made only between pixels from

the same county for the same recovery period because each county has a different history of droughts and recoveries.

To fairly compare TIST groves, neighbors, and non-TIST pixels given the variable agro-ecological conditions across each county, the landcover categorization was used to compare like for like pixels, and the human modification gradient filtered out pixels with very few anthropogenic stressors (score < 0.1). The landcover classification algorithm is based on characteristics such as the ecoregion, altitude, spectral characteristics, and vegetation indices (Van De Kerchove *et al.*, 2020); each landcover type has a statistically significantly different profile in yearly precipitation, greenness, and altitude (Appendix Figure 40, KWH with PHD, $p < 0.001$). Comparing by landcover type is a concise method to generally control for these advantageous characteristics. This also somewhat controls for the different seasonal patterns of each landcover (e.g., planting-harvest cycle of cropland).

The management of TIST farms is assumed to be sufficiently similar to each other and different from non-TIST farms, due to the training and best practice knowledge dispersed through the TIST clusters and small groups, that the overall differences may be attributable to TIST membership between otherwise similar pixels.

To assess spillover effects, the distance to the nearest TIST pixel was used. Because the landcover types are somewhat mixed in space and each county is heterogenous, the landcover approach does not necessarily control for the way that a drought might have different severity across the county. The landcover types also might not be completely accurate as they were composited with mode, and a 30m Landsat pixel might contain crop areas, built up areas, and trees. Thus, to compare TIST only with pixels in its immediate area that would be experiencing very similar drought (meteorological, hydrological, agricultural, and socio-economic) conditions and to determine how far any benefits might reach, pixels were compared using the distance to the nearest TIST grove. Only pixels within 1km were considered to ensure that the comparison pixels were experiencing sufficiently similar agro-ecological conditions because the climate and meteorological conditions are highly spatially variable (Fischer *et al.*, 2013; Camberlin *et al.*, 2014). Additionally, TIST groves have been shown to have a greening effect only up to 390m away (Buxton *et al.*, 2021). Human modification filtering was not necessary because there are no areas with a modification score less than 0.1 within one kilometer of TIST groves.

5. Results

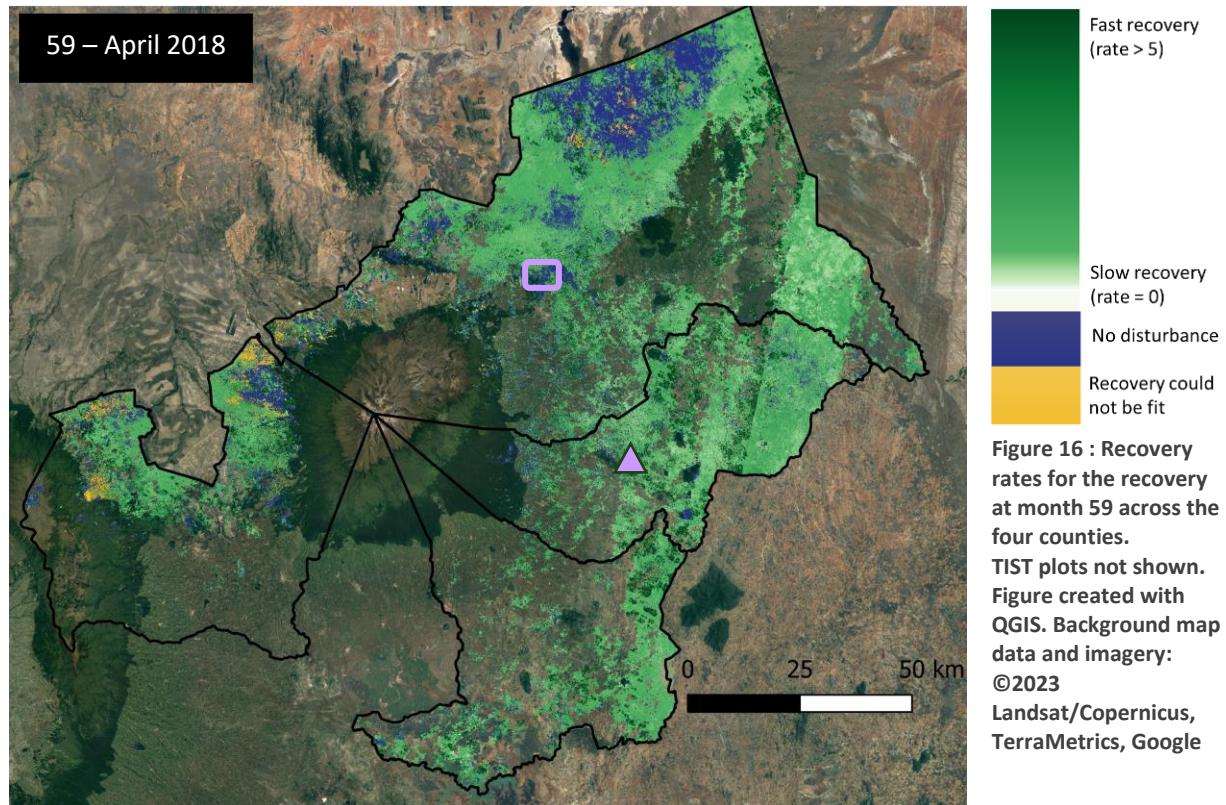
RQ1: Can resilience be estimated using recovery rates?

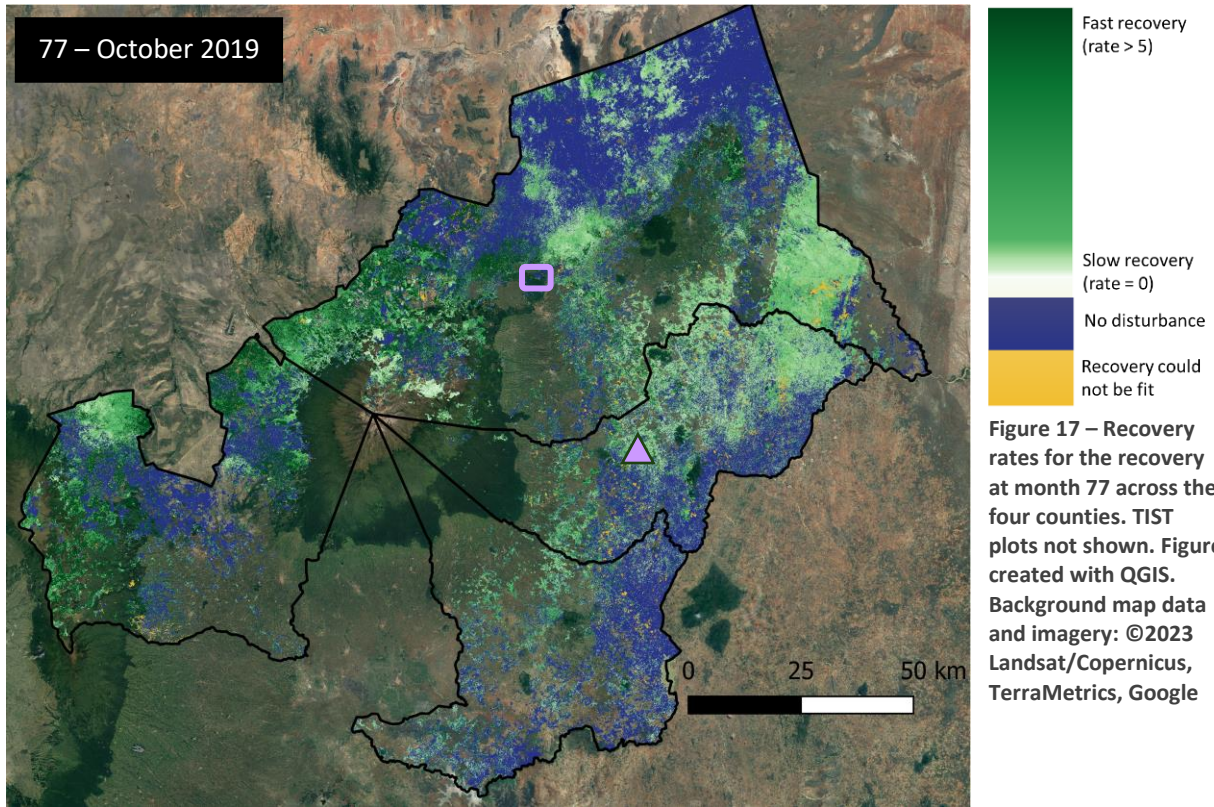
While recoveries were calculated for the relevant counties for months 54, 59, 77, 104, 114, and 116, only results from 59 (April 2018) and 77 (October 2019) will be discussed. Recoveries 104 and 114 were highly contaminated by clouds, resulting in only 2% and 18% of pixels attempted. Recovery 116 was too close to the end of the timeseries for the return to equilibrium to be observed effectively. Finally, Recovery 54 significantly overlapped with Recovery 59, causing the recovery associated with month 59 to be detected at the end of the Recovery 54 period. Thus, the rates calculated for Recovery 54 are

highly correlated with 59 and cannot be attributed to Recovery 54 without individual analysis of each timeseries, and it will not be considered further here.

Meru and Tharaka had proportionally the most pixels with sufficiently complete timeseries to be attempted for Recoveries 59 and 77 (56%-70%), resulting in pixels with disturbances detected and rates estimated out of all pixels at 44% and 55% respectively for Recovery 59 and 36% and 37% for Recovery 77. Embu and Nyeri were less successful mainly because of less complete timeseries due to clouds (29%-42% pixels attempted, between 14% and 28% successfully calculated). Over all counties, there were relatively few pixels where a disturbance was detected but a curve could not be fit (between 1%-4% of attempted pixels for all counties except Nyeri in Recovery 59 at 10%). The pixels where no curve could be fit tend to be in wetter (higher yearly precipitation) and greener (higher mean NDVI) areas across counties and recoveries and have higher amounts of missing months. Recovery 77 has a higher proportion of pixels where no disturbance was detected (39-63% of attempted pixels by county) than Recovery 59 (6-20% of attempted pixels). The complete table is in the Appendix, Table 4.

A visual analysis of the results shows spatial trends (Figure 16, Figure 17). For example, the north of Meru transitions from montane forest to bushland, and generally pixels exhibit different resilience. In 77 the differences between shrubland and forest are especially noticeable, with bushlands farther away from Mt. Kenya showing more No Disturbance (shrubland pixels exhibited greater proportion of No Disturbance in all counties except Nyeri, chi-square test, $p < 0.001$). The maps also demonstrate that





calculated pixels skew towards drier areas as those areas have less cloud contamination and fewer missing pixels. Zooming in, denser vegetation can often be seen reflected in the recovery rates as areas with higher recovery rates or no disturbance shown (Figure 19, Figure 18). These spatial trends provide validation that the calculated recovery rates are reflecting real vegetation recoveries. Distributions of recovery rates across counties and recoveries are similar (Appendix Figure 34, Figure 35). Most recovery rates are estimated between zero and two, with some extreme values clustered at 10 and 20, and a small number of outliers estimated as high as 60; however, Nyeri in Recovery 77 has a much higher proportion of high rates estimated (Discussion, Figure 25).

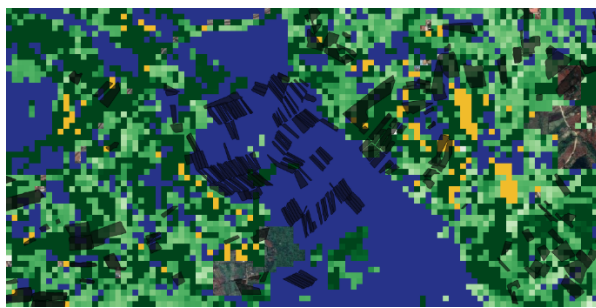
Factors besides TIST membership have relationships with resilience. Of the considered other variables, most have some relationship with recovery rates and are often interrelated. Mean NDVI is weakly positively correlated with faster recovery (Spearman's ρ -0.06-0.37, $p < 0.001$) depending on the county and recovery. Precipitation (-0.02-0.22, $p < 0.001$), altitude (-0.05-0.37, $p < 0.001$), and percent missing months (-0.07-0.23, $p < 0.001$) are also weakly correlated with faster recovery rates (see Appendix Figure 37 for complete matrices). These beneficial characteristics are interrelated. Mean NDVI is moderately positively correlated with yearly average precipitation (0.46-0.71, $p < 0.001$), altitude, and missing pixels (see example correlation plot, Figure 20). The proportion of missing months and precipitation are moderately correlated (0.21-0.79, $p < 0.001$), and altitude and yearly average precipitation have a variable positive relationship depending on the county (0.18-0.92, $p < 0.001$). Each of these beneficial characteristics was weakly negatively correlated with the standard deviation of NDVI, indicating that drier, lower, and less green areas generally had more variable greenness. Additionally,



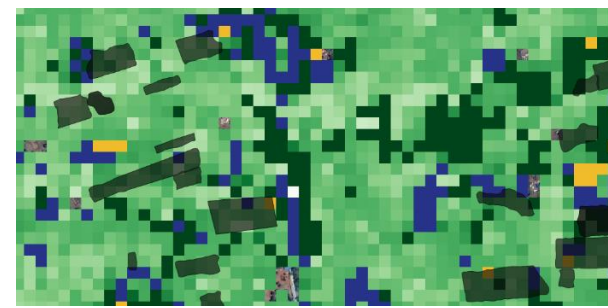
Figure 18a: Meru County at boxed location.
TIST grove outlines in black. Figure created with QGIS.
Background map data and imagery: ©2023
Landsat/Copernicus, TerraMetrics, Google.
Scale: 1 recovery pixel : 30m



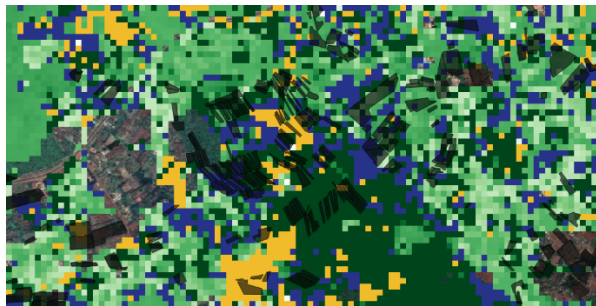
Figure 19a: Tharaka County at triangle location.
TIST grove outlines in black. Figure created with QGIS.
Background map data and imagery: ©2023
Landsat/Copernicus, TerraMetrics, Google
Scale: 1 recovery pixel : 30m



18b: Recovery 59 – Denser vegetation shows no disturbance.



19b: Recovery 59 – Waterway and vegetation visible in stronger recoveries or no disturbance shown



18c: Recovery 77 – Denser vegetation has faster recovery than surrounding areas.



19c: Recovery 77 - Waterway is still visible, and areas closer to it show either no disturbance or slightly stronger recoveries. Generally, recovery is slower after this drought.

landcover types and ecoregions have significantly different recovery rates across counties and recoveries (KWH test, $p < 0.001$ for all ecoregions and landcovers). Pixels classified as tree cover have the fastest median recovery rates (Appendix, Figure 38). By ecoregion, montane forests have higher median recovery rates than bushlands (Appendix, Figure 39).

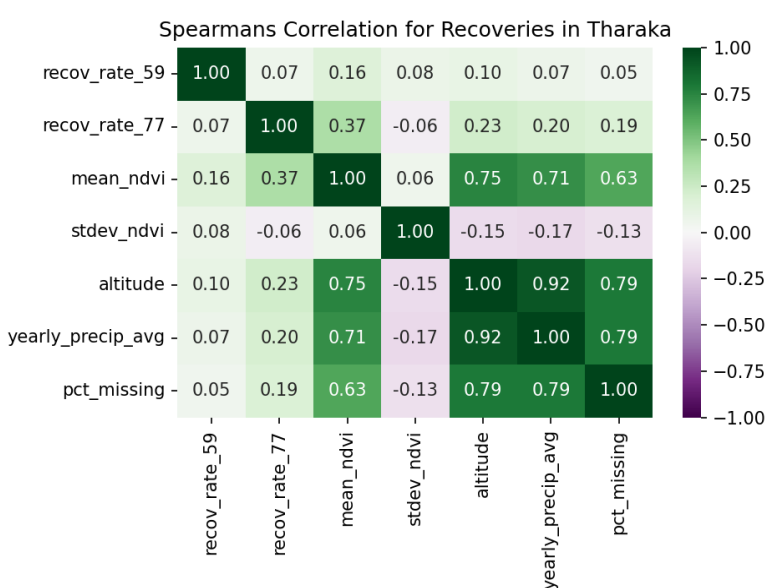


Figure 20 : Spearman's rho for recovery rates and other characteristics in Tharaka. All $p < 0.001$.

The correlations of estimated rates with the extracted residuals were assessed to check that the method did not impart some sort of bias. The mean and standard deviation of the residual were weakly negatively correlated with recovery (Spearman's ρ , $-0.30-0.01$ for mean residual, $-0.26-0.05$ for standard deviation, $p < 0.001$). The mean residual was negatively correlated with mean NDVI (-0.69 to -0.28 , $p < 0.001$), meaning a greener area had a lower residual after decomposition; the correlation of mean residual with slower recovery is likely due to this association.

RQ2: Effect of TIST on recovery rates

Categorizing all calculated pixels by recovery period, county, and belonging to a TIST grove, immediate neighbor, or non-TIST, TIST appears to have a significant beneficial effect on recovery rates. However, there are other explanatory variables that also have a statistically significant effect as described above such as mean greenness, precipitation, landcover type, and ecoregion. TIST groves tend to have more of these beneficial characteristics: TIST and Neighbors tend to be in montane forest regions, have landcover classified as trees or crops, have a higher mean NDVI, higher altitude, and higher yearly precipitation (significantly different distributions, chi-square test for landcover and ecoregion, all $p < 0.001$, KWH test for all others, all $p < 0.001$, Appendix Figure 36). However, the relative characteristics of TIST pixels do differ by county (see Discussion, Section 6).

Comparing by landcover to control for these characteristics as discussed in the Methods, TIST pixels demonstrate some benefit but not universally (Table 1). In Tharaka, TIST and/or Neighbors have significantly different median recovery rates to Other pixels in every land cover ($p < 0.001$). TIST and/or Neighbors have higher median recovery rates across land cover types. In Meru, TIST and/or Neighbors are significantly different ($p < 0.001$) than Other for all categories except Recovery 59 in shrubland, where Neighbors are significantly different and TIST and Other pixels are not. TIST and Neighbors have higher medians for grassland, cropland, and shrubland (only in Recovery 77), while Other pixels have higher recovery rates in tree cover. In Nyeri, TIST and Neighbors were significantly different to Other pixels ($p < 0.001$). Other pixels had faster recoveries in 59, while TIST had faster recoveries in 77. The overall magnitude of median recovery rates is much higher in Nyeri. Embu had mixed results, and some recoveries had no significant differences; note that Embu has the smallest sample size by orders of magnitude (Appendix, Table 5).

Table 1: Median recovery rates compared by county, recovery and landcover classification. (No marking indicates $p < 0.05$ after KWH and pairwise PHD; * indicates no significant difference in pairwise PHD). Grouping with the highest median recovery rate highlighted; if pairwise differences were not significant between the fastest rates, both groups are highlighted. The sample size for each group can be found in the Appendix, Table 5.

Landcover class		Tree cover		Shrubland		Grassland		Cropland	
Recovery Period		59	77	59	77	59	77	59	77
Tharaka	TIST	1.61	1.68*	1.21	0.97	1.06	0.70	1.17	0.72
	Neighbor	1.72	1.71*	1.25	1.03	1.10	0.65	1.14	0.74
	Other	1.34	1.38	1.20	0.69	1.04	0.62	1.13	0.61
<hr/>									
Meru	TIST	1.38	1.87*	1.16*	2.14	1.18*	2.76*	1.14*	1.68
	Neighbor	1.42	1.94*	1.20	2.23	1.22*	2.88*	1.13*	1.75
	Other	1.50	2.45	1.22*	0.94	1.14	0.83	1.13	0.98
<hr/>									
Nyeri	TIST	1.63*	10.99*	1.30*	16.86	1.25	20.70*	1.29*	17.49*
	Neighbor	1.82*	11.13*	1.29*	12.55	1.29	20.74*	1.32*	13.59*
	Other	2.44	2.44	1.37	2.54	1.33	4.31	1.35	9.83
<hr/>									
Embu	TIST	1.33*	10.79	1.29*	0.58*	1.32*	0.84*	1.37	0.65*
	Neighbor	1.31*	2.63*	1.31*	0.63*	1.34*	0.95	1.33	0.65*
	Other	1.54*	1.31*	1.33*	0.90	1.23	0.75*	1.24	0.74

RQ3: Recovery from subsequent droughts

The percent change in recovery rate from Recovery 59 to Recovery 77 was compared by county and landcover or distance from TIST. As can be seen in Figure 21, there are very few pixels where both recoveries were available so that the change could be calculated. There were no calculated change pixels with a modification score less than 0.1.

When comparing by landcover, TIST and Neighbors often experienced less decline in recovery rates than Other pixels during the second drought (KWH test with pairwise PHD). In Tharaka, TIST and Neighbors were significantly different ($p < 0.001$ unless otherwise noted in Table 2) from Other in all categories except grassland. In Tharaka, in each category there was a median decrease in recovery rate, but TIST and Neighbors decreased less than Other. In Meru, all landcover categories showed significant differences between TIST/Neighbor and Other pixels ($p < 0.001$). Except for tree cover, TIST pixels increased recovery rate while Other pixels decreased recovery rate. Other pixels in tree cover increased rate more than TIST or Neighbor pixels. In Nyeri, extremely high percent changes were observed, but TIST/Neighbors were significantly different ($p < 0.001$) in all landcover types and had higher increases in rate. Results in Embu, as for the recovery rates themselves, were mixed and not always significantly different; the sample size was also orders of magnitude lower than other counties (Appendix, Table 6).

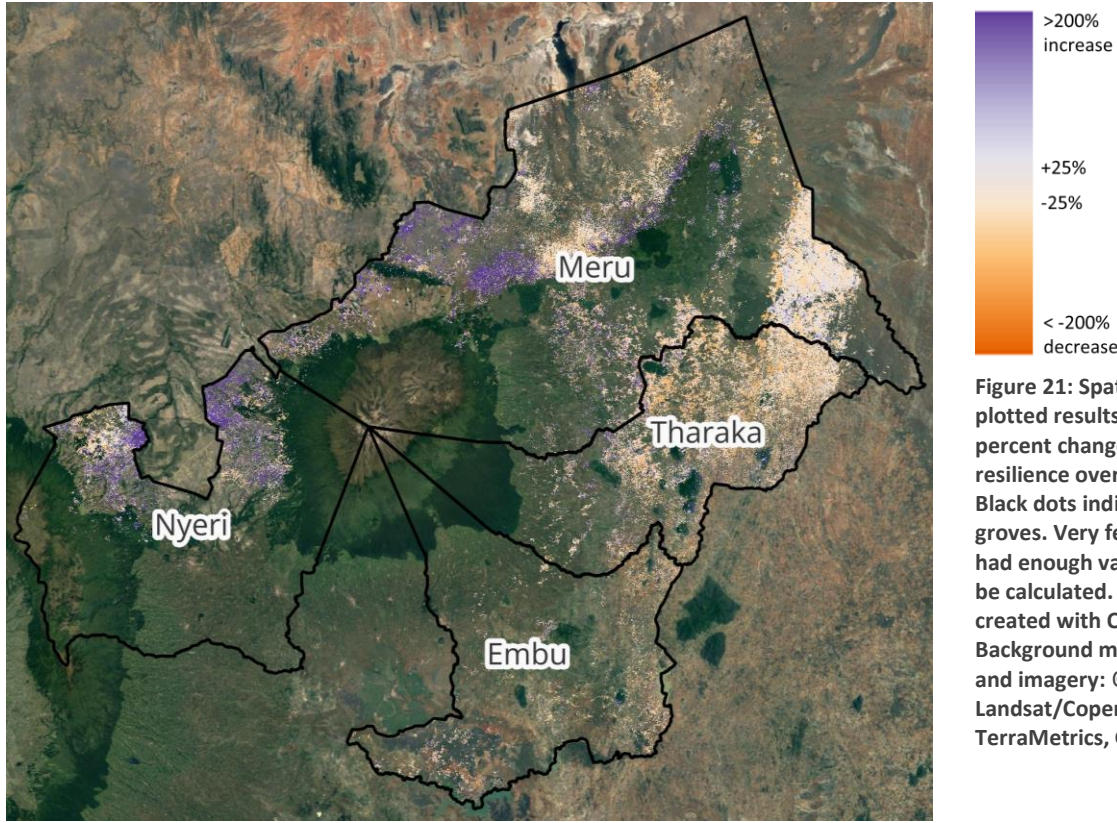


Figure 21: Spatially plotted results for the percent change in resilience over time. Black dots indicate TIST groves. Very few pixels had enough valid data to be calculated. Figure created with QGIS. Background map data and imagery: ©2023 Landsat/Copernicus, TerraMetrics, Google

Table 2: Median percent change in recovery rate from Recovery 59 to Recovery 77, compared by landcover. (No marking indicates $p < 0.05$ after KWH and pairwise PHD; * indicates no significant difference in pairwise PHD). Grouping with the highest median recovery rate highlighted; if pairwise differences were not significant between the fastest rates, both groups are highlighted. The sample sizes are shown in Appendix, Table 6.

Pct. change in recovery rate (median)		Tree cover	Shrubland	Grassland	Cropland
Tharaka	TIST	-2% *	-29% *	-39% *	-40% *
	Neighbor	-2% *	-26% *	-44% *	-39% *
	Other	-7%	-39%	-40% *	-47%
Meru	TIST	2% *	14% *	53%	8% *
	Neighbor	4% *	18% *	31%	14% *
	Other	13%	-21%	-26%	-20%
Nyeri	TIST	89% *	724%	1053% *	841%
	Neighbor	86% *	426%	994% *	591%
	Other	-3%	64%	117%	131%
Embu	TIST	363% *	-60% *	-47% *	-53% * †
	Neighbor	43% *	-62% *	-20%	-57% *
	Other	-16% *	-44%	-44% *	-48% *

[†] In this category, TIST pixels are not significantly different to either Neighbor or Other pixels, but Neighbors and Others are significantly different.

RQ4: TIST spillover effects

Controlling for distance from TIST showed a general decrease in median recovery rate farther away from TIST groves for some counties (Figure 22, Figure 23). Tharaka shows similar shallow declining trends for 59 and 77. In 77, Meru shows an increase in recovery rates up to about 250m away, and then declines with distance, but shows a steady decline with Recovery 59. Nyeri shows much steeper trends with higher general magnitude than the other counties but shows an increasing rate with distance for 59 but a decreasing rate for 77. Embu exhibits a very erratic trend; however, the sample size for Embu is far smaller than the other three counties (Appendix, Table 6).

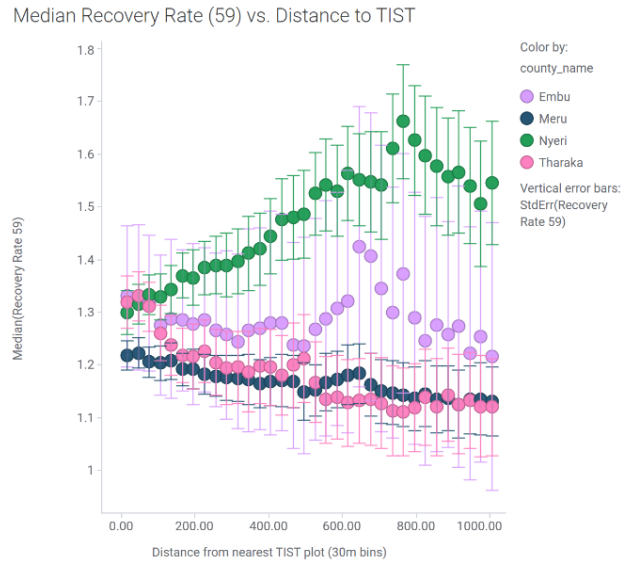


Figure 22: Median recovery rates from 59 vs. distance from TIST.

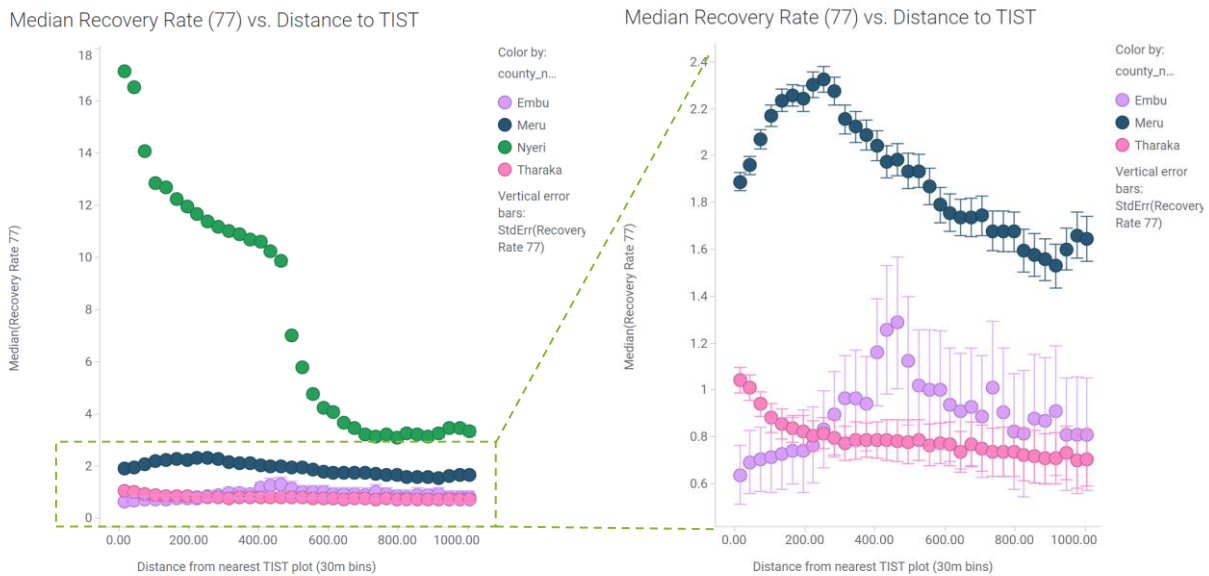


Figure 23: Median recovery rates from recovery 77 for each county vs. distance to nearest TIST pixel. At right, Nyeri has been removed from plot to show detail.

Looking at the change in resilience over time, trends emerge that echo the results for recovery rate versus distance. No completely unmodified land is included because it is not within one kilometer of any TIST groves. Embu has mixed results but a somewhat positive trend moving away from TIST. Nyeri has a strong decline in rate over time with increasing distance from TIST. Meru has an improving rate up to approximately 200m away from TIST plots and then declines. Tharaka shows a slight decline away from TIST plots. Nyeri shows a general increase in recovery rates between the two droughts and recoveries

over all distances, while Tharaka and Embu showed a general decrease in recovery rates over time over all distances. Meru shows an increase for pixels within about 500m of a TIST grove but declines below zero farther away.

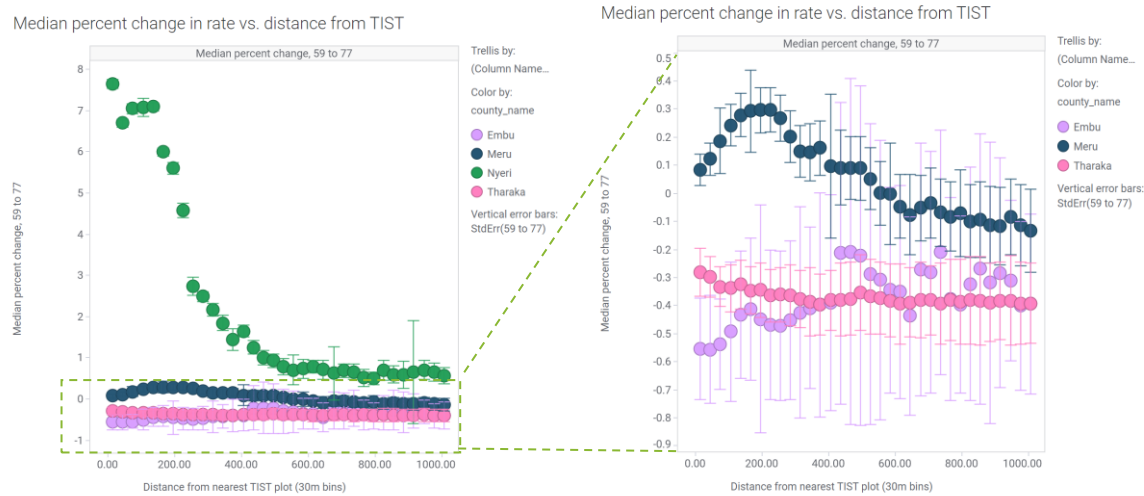


Figure 24: Percent change in recovery rate from recovery 59 to 77, median over distance from nearest TIST grove. Right graph is the same except Nyeri has been removed to show details.

6. Discussion

RQ1: Can resilience be estimated using recovery rates?

The results found here largely agree with existing resilience literature, though to the author's knowledge no localized study with the same methodology has been performed for a more direct comparison. The fitted recovery rates match in magnitude with those found by Smith *et al.* (2022). This increases confidence in the methodology and results.

The higher occurrence of no disturbance in drier shrubland areas is supported by existing literature. For example, in all counties, the bushland ecoregion is more likely to have no disturbance observed in Recovery 77 and for all counties except Nyeri shrubland or grassland landcovers are much more likely to have no disturbance observed in recovery 77. In Meru, only one month of drought preceded recovery 77, while other counties had much longer and more severe droughts. Different ecosystems respond on different timescales to drought; semi-arid ecosystems have longer response times to drought than completely arid or humid ecosystems, which is posited to be because they tolerate a wider variety of water availability. Humid regions may react quickly to a lack of water availability because of stress, and arid regions react quickly as a survival adaptation mechanism (Vicente-Serrano *et al.*, 2013; Liu *et al.*, 2018). Months of water stress may not have caused a detectable disturbance in the semi-arid shrublands because of their adaptations, while normally wetter ecoregions (montane forests) did experience a disturbance.

While these semi-arid areas might react more slowly to water stress, they also recover more slowly thus exhibiting lower resilience by this definition. The shrubland ecoregion and shrub, grass, and crop

landcovers have the lowest recovery rates across counties and recoveries (except Nyeri in 77). This relationship was also found by several previous studies (De Keersmaecker *et al.*, 2015; Liu *et al.*, 2019; Smith and Boers, 2023; Tai *et al.*, 2023). Tree cover and forest have been found to be generally the most resilient to water scarcity (De Keersmaecker *et al.*, 2015; Liu *et al.*, 2019; Miralles *et al.*, 2019). These results agree, with tree cover and montane forest having the fastest median recovery rates across counties and recoveries (except Nyeri in Recovery 77). The correlations between precipitation and mean NDVI with faster recovery also agree with the literature; resilience to drought is generally higher in wetter climates with a water surplus, and wetter areas generally have higher mean NDVI (Smith and Boers, 2023; Tai *et al.*, 2023). The positive association with altitude is also likely related to the changes in climate and precipitation with altitude (Camberlin *et al.*, 2014). The agreement of these general relationships validates the method of recovery rate estimation to measure resilience in this area.

RQ2: Effect of TIST on recovery rates

TIST and Neighbors demonstrating higher recovery rates without controlling for environmental factors echoes results in the literature that assess management of agro-ecological systems: a combination of management practices as well as environmental conditions are strong determinants of resilience (De Keersmaecker *et al.*, 2016; K. J. Lees *et al.*, 2021; von Keyserlingk *et al.*, 2021). Nonetheless, the effect of TIST is entangled with the background increased resilience from being situated in greener, wetter, and higher altitude areas than Other pixels. These beneficial background patterns are true for Tharaka and Meru. Nyeri and Embu show different patterns in these explanatory variables. Nyeri is on the leeward and drier side of Mt. Kenya and engaged primarily in agro-pastoralism rather than marginal agriculture (Camberlin *et al.*, 2014; NDMA, 2022). TIST groves in Nyeri tend to have a lower mean NDVI (mean precipitation, altitude) than other pixels in the county (Appendix, Figure 36) whereas Meru and Tharaka's TIST pixels tend to have higher NDVI (mean precipitation, altitude) than other pixels. In Embu, there is less distinction and TIST/Neighbor/Other pixels are more similar in all of these characteristics (though they are still statistically significantly different); the median NDVI, precipitation, and altitude of TIST pixels are also generally lower than the other counties. Embu also has the least TIST groves (only 359), which are clustered far away from Mt. Kenya, unlike the other counties. Nyeri and Embu have the fewest pixels with calculation attempted (29-42% of total over the two recoveries, Appendix Table 4), suggesting that cloud cover posed a larger problem than for Tharaka and Meru.

These differences appear to have affected the results from Nyeri and Embu. In Nyeri, Other pixels have faster recoveries for all of Recovery 59, but the opposite occurs in Recovery 77. The recovery rates for 77 are also much higher than those in other counties or even 59 in Nyeri (rates around 10-20 rather than 1-2, Figure 25). This may be in part due to cloud cover issues. As to be discussed in Limitations, pixels with only a single low month or highly erratic residuals often result in much higher recovery rates. Thus, if most pixels in the region are missing a month near the local minimum, this could result in many pixels with higher rates. Additionally, there appears to be some decomposition issues in Nyeri. A sampling of pixels' residuals showed that some seasonal cycle is still present, which alters the residual values (Figure

26). Because this happened more often in Nyeri than other counties, the validity of results in Nyeri may be questioned. The issue with decomposition may be because of the climatic and agricultural differences in the county to the others. Because the decomposition was trialed and optimized on a sampling of pixels in Tharaka, it is possible that different parameters should have been used for the STL decomposition in Nyeri due to its physical differences.

Histogram – Recovery Rate 77

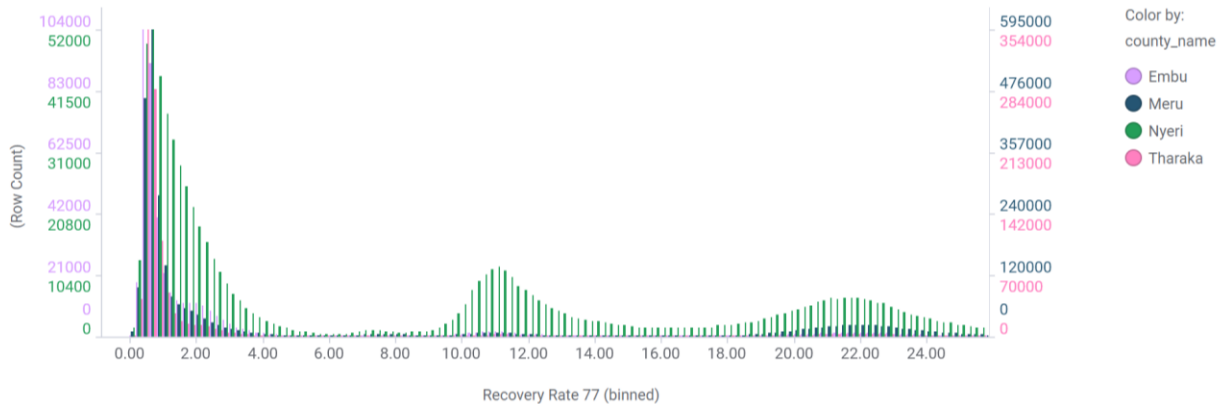


Figure 25: Distribution of estimated recovery rates for recovery 77. Note that Nyeri has a much higher proportion of pixels with very high rates.

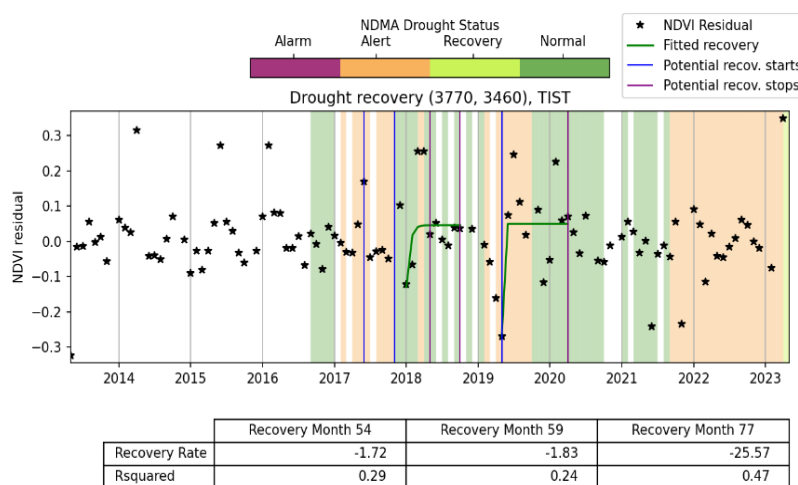


Figure 26: This example pixels from Nyeri County show some seasonal cycle still present within the residual, potentially leading to the very steep recovery rates estimated.

and Neighbor pixels generally recover faster than Other pixels across landcover types, except for tree cover in Meru. This may be due partly to the advantageous characteristics of higher altitude and precipitation for TIST pixels; however, the landcover classifications largely stratify the pixels, as tree cover occurs in the higher and wetter areas, and cropland, shrubland, and grassland are mostly in the lower and drier areas (Appendix, Figure 40). Thus, in Meru and Tharaka, TIST does appear to have a relationship with increased resilience to drought beyond its physical location.

In Embu, the limited number of TIST pixels and cloud contamination likely leads to very mixed results. Embu pixels (with calculation attempted) have a median 39% of months missing, while the other counties have medians between 20-23%. This sparsity of calculated pixels which is visible on the maps (Figure 16, Figure 17) likely contributes to the inconsistent results.

Considering the two remaining counties, Meru and Tharaka TIST

TIST pixels in Meru do not recover more quickly than Other tree cover pixels; this may be because more natural or unmodified woodlands are more resilient to drought (Zhong *et al.*, 2021). Indeed, the median human modification score for tree cover pixels in Meru is lower for both recoveries, indicating less human disturbance in areas of tree cover outside of TIST farms (e.g. Recovery 77: TIST = 0.71, Neighbors = 0.70, Other = 0.43, KWH with PHD indicates Other significantly different, $p < 0.001$). This is consistent with the case in Tharaka, where the median modification scores of tree cover pixels are higher for Other pixels, and the Other pixels had a slower recovery rate (e.g. Recovery 77, TIST=0.37, Neighbor = 0.36, Other = 0.41, KWH with PHD indicates Other significantly different $p < 0.001$). This supports previous findings that human disturbance decreases resilience of forests (Hishe *et al.*, 2021; Boulton *et al.*, 2022) and suggests that comparisons using anthropogenic stressors may be warranted in future work.

Though correlation does not prove causation, it is plausible that TIST membership contributes to the observed higher resilience because TIST practices have been previously shown to contribute to a healthier agro-ecosystem that would be more resilient to drought. The positive effect on resilience of TIST groves and farms may stem from the trees themselves, the practices of TIST farmers, or both. The tree groves improve the soil and water usage by preventing erosion, fixing nutrients, and reducing water runoff which increase resilience to water stress (Jose, 2009; Rivest *et al.*, 2013; Dollinger and Jose, 2018). Especially in semi-arid landscapes, patches of trees increase the amount of water stored in the soil by increasing the depth that water can infiltrate and obstructing the runoff of water over the surface (Ludwig *et al.*, 2005). Trees also can exploit water from deeper soil (Wallace, 2000). Intermittent tree cover has also been shown to be optimal in semi-arid zones for resilience (De Keersmaecker *et al.*, 2015) which TIST creates by planting amongst otherwise agricultural areas in bare or disused land (TIST, 2023). The increased resilience of TIST grove pixels even when controlling for landcover type is likely influenced by the trees.

The effect of trees can extend beyond the areas inside the groves due to the microclimate effects and provision of products from the groves. The shade of the trees reduces moisture evaporation from soil, increases evapotranspiration, and increases the surrounding humidity, creating a microclimate and cooling the area (Wallace, 2000; Ludwig *et al.*, 2005). This improves not only the conditions in the grove but also the surrounding areas on the farm. Nearby pixels may also be stands of semi-natural woodland. Buxton *et al.* (2021) hypothesized that the greening effect from TIST groves observed in neighboring areas may be a combination of microclimate effects from the trees as well as decreased pressure on local woodlands. With farmers able to take fuelwood from their own trees by thinning or pruning the groves (TIST, 2023), there is less need to harvest wood from nearby woodlands. These avenues suggest that tree groves do contribute to the increased resilience of the Neighbor pixels.

In both grove and neighbor pixels, the practices of farmers may increase resilience. The recovery rates of TIST and Neighbors were often statistically less significantly different than either group was to Other pixels and sometimes were not significantly different at all. This may be because pixels immediately surrounding the TIST groves are part of the TIST farm, and the techniques taught by TIST and used on the farm have a beneficial effect. Conservation agriculture and agroforestry are taught and emphasized in the small groups of TIST (TIST, n.d.; Oppenheimer, 2011; Masiga *et al.*, 2012). Conservation agriculture focuses on reducing soil disturbance, leaving crop residues on the field, and rotating crops. These

practices increase water infiltration, reduce evaporation, and improve water use efficiency by improving soil quality and reducing runoff (Micheni *et al.*, 2016; Boillat *et al.*, 2019). By improving soil quality and water retention, conservation agriculture helps resilience to drought. Conservation agriculture practices are likely part of the increased resilience of TIST and Neighbor areas to drought. In total, while higher resilience of TIST farms cannot be definitively or solely attributed to TIST membership, the practices of tree planting, agroforestry, and conservation agriculture likely contribute.

RQ3: Recovery from subsequent droughts

The effect of TIST groves on resilience to subsequent drought is positive; however, the number of pixels with valid data is very limited and is skewed towards areas with less cloud cover and the area where Landsat tiles overlap. Results from Embu and Nyeri will be ignored for the reasons discussed above.

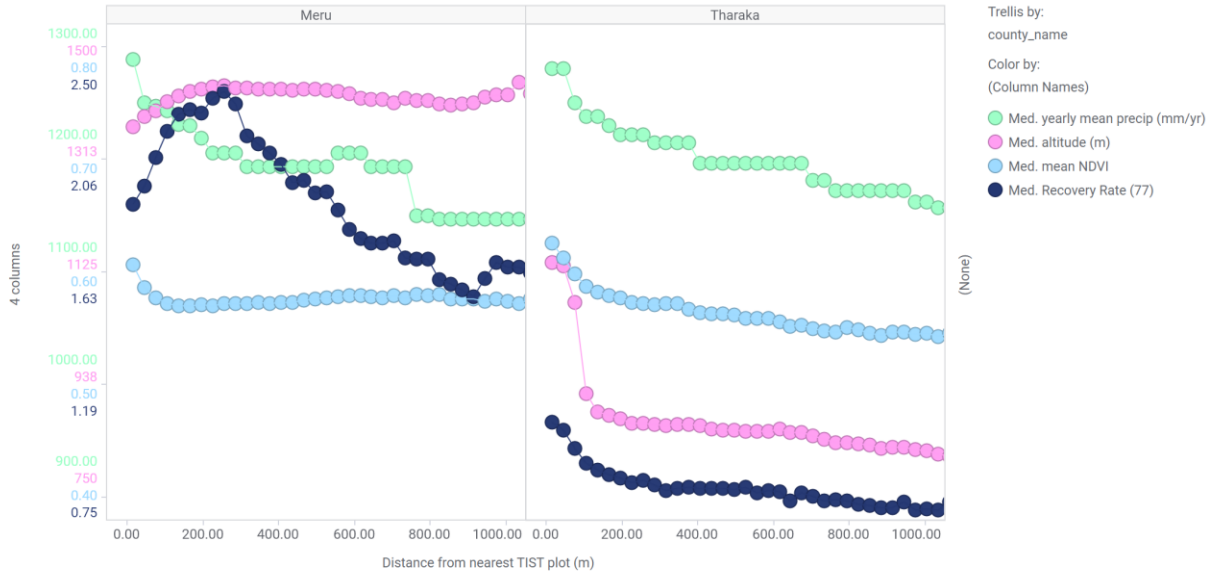
When considering the landcover comparison, the severity of the droughts is also apparent in the data; Meru generally showed less decrease in recovery rates from 59 to 77 because the drought prior to Recovery 77 was only one month long, while Tharaka showed decreased recovery rates because the prior drought was one year long and included months in the more severe Alarm phase. TIST had a significant effect; in Tharaka, the decreases were less severe, and in Meru, recovery rates even improved for TIST and Neighbors while Other declined. Subsequent droughts do generally have a more detrimental impact and can decrease resilience (Anderegg *et al.*, 2020). Treecover showed the least change in resilience overall, which is not surprising given the ability of trees to access deeper water sources and improve the soil and microclimate around them (Wallace, 2000; Ludwig *et al.*, 2005). There also may be an increasing benefit with time for TIST groves as the trees mature and land has been under conservation agriculture practices for longer, which tends to produce more benefits with time (Micheni *et al.*, 2016).

RQ4: TIST spillover effects

The assumption underpinning the comparison of pixels within 1km of TIST pixels was that these areas likely experienced similar agro-ecological conditions as well as drought severity, despite the highly varied landscape (Camberlin *et al.*, 2014; Recha, 2018). However, these assumptions may not hold across that of that distance, even excluding Nyeri and Embu for the reasons discussed above. When looking at the other measured beneficial characteristics (altitude, precipitation, and mean NDVI), there are clearly changes with distance from TIST plots (Figure 27). Tharaka shows a more consistent pattern of decreasing beneficial characteristics and recovery rates with distance from TIST. Meru shows a more mixed pattern. While the mean NDVI, precipitation, and recovery rates follow a similar downward trend for Recovery 59, the trends are much less consistent in Recovery 77, such as an increase in altitude farther from TIST sites. These differences probably influence some of the decline in recovery rates with distance from TIST. These results are also influenced by which pixels had calculated results, which can be seen in the differences in median characteristics with distance from TIST plots from one recovery to the next in the two counties. This does not mean that there is no TIST effect; TIST groves are greenest and recover fastest, followed by immediate neighbors; however, without further analysis, any spillover effect in resilience from TIST groves to farther neighboring areas is difficult to isolate.

Comparing the change in resilience over time with distance from TIST holds the same caveats as discussed above; while TIST and neighbors have an effect on the change in resilience, it is difficult to isolate any spillover effect from other factors at play within one kilometer of TIST pixels.

Recovery 77 vs. Distance to TIST



Recovery 59 vs. Distance to TIST

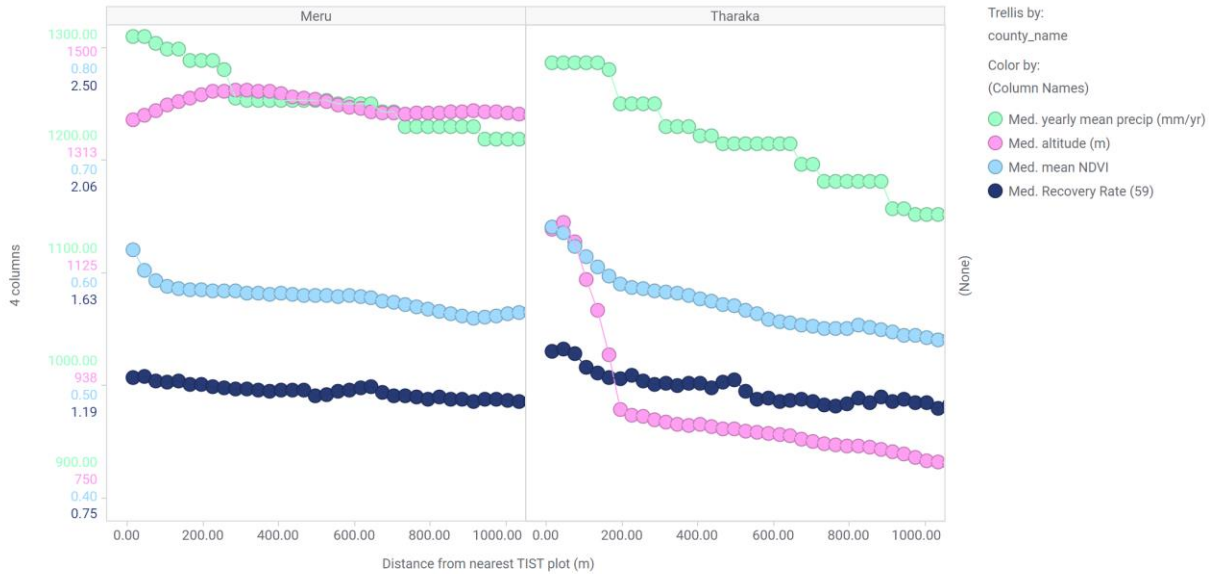


Figure 27: Characteristics associated with improved recovery rates and recovery rates plotted vs. distance from closest TIST plot. Note that the precipitation data is much lower spatial resolution (5.5 km rather than 30m) and has been resampled which is why it appears in steps. Bins are 30m wide, so first point is TIST plots and second point is immediate neighbors.

Limitations and Future Work

One limitation is that the recovery rates demonstrate some sensitivity to missing months during the recovery period. In instances where a disturbance was detected but no curve could be fit, there were

slightly more missing pixels. These missing pixels affected the ability to fit a curve. Even when a curve was able to be fit, the rate could be affected by a missing month. For example, the overlap of Landsat tiles at the eastern edge of Meru and Tharaka counties is visible in the recovery rates for 59. The pixels in the overlap area have much lower recovery rates than those directly next to them which are experiencing similar drought conditions. The difference is that pixels in the overlap area have a measurement for a month immediately after the local minimum of the disturbance (Figure 28) whereas the pixels directly west are missing that month due to cloud contamination. This results in a very steep recovery rate fit to the pixels with only one low month of residual. This limitation is due to the slow return time of Landsat. While this specific rate calculation issue could be ameliorated by requiring all 12 months of the recovery period to have valid measurements, that would have resulted in almost no pixels being calculated with the greatest reduction being on wetter and cloudier locations (which likely have higher recovery rates).

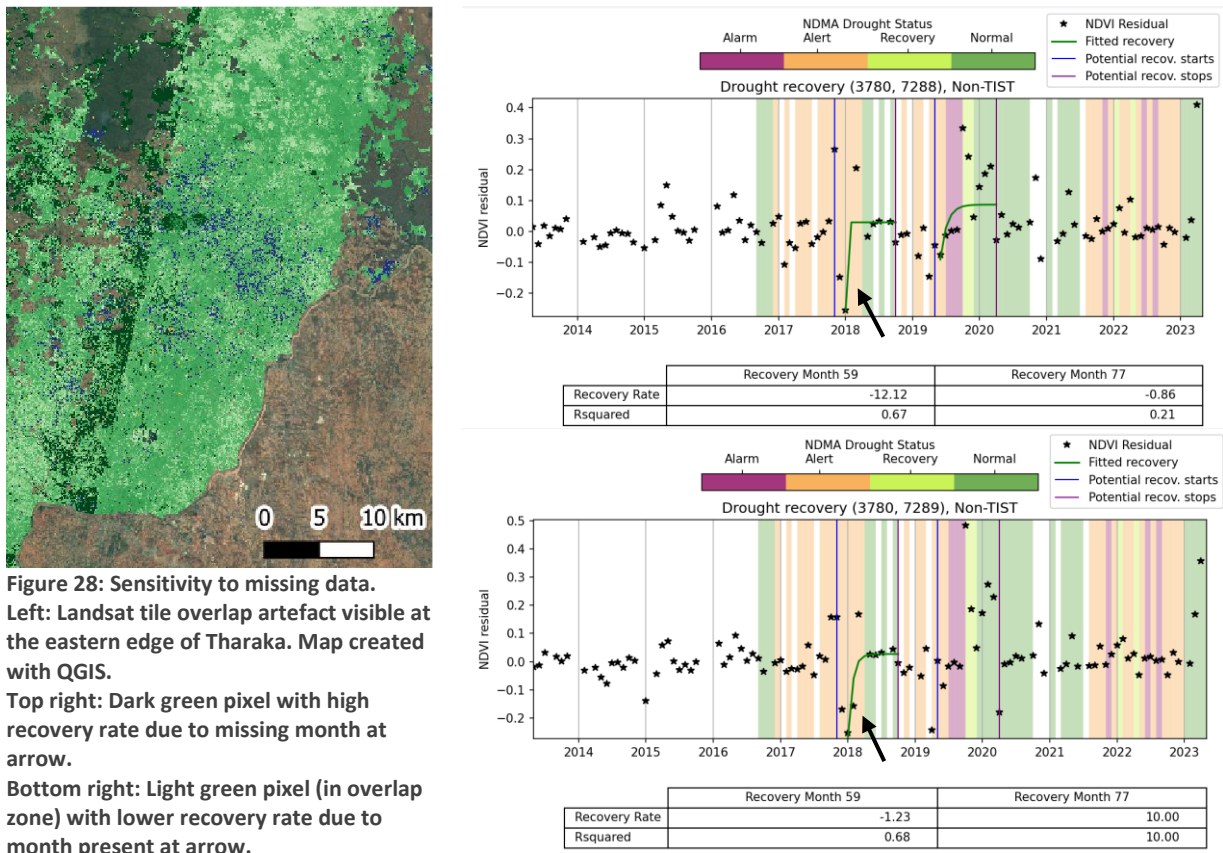


Figure 28: Sensitivity to missing data.
Left: Landsat tile overlap artefact visible at the eastern edge of Tharaka. Map created with QGIS.
Top right: Dark green pixel with high recovery rate due to missing month at arrow.
Bottom right: Light green pixel (in overlap zone) with lower recovery rate due to month present at arrow.

The sensitivity to missing pixels increases the impact of the inherent sampling bias towards drier pixels in this study. Pixels that are greener, wetter, and at higher altitude have a strong correlation with missing pixels (Appendix Figure 37), so the pixels that had sufficiently continuous timeseries to calculate a recovery rate tend to be in drier places, which tend to have lower recovery rates. As was shown above, timeseries with certain months missing can greatly change the calculated rate to be higher; thus, the trend of wetter pixels having stronger recoveries may be amplified by higher rates being calculated than would otherwise. Additionally, despite masking known cloudy pixels, there may still be cloudy or hazy

observations causing a decreased NDVI observation that has no relation to the true state of the agro-ecological system. This issue could be improved with an NDVI reconstruction algorithm utilizing another satellite such as MODIS (e.g., Chen, Y. et al., 2021) to spatially and temporally fill gaps as Sentinel-2 did not come online with both satellites until 2017 (ESA, 2023). Additionally, this analysis could also be attempted for the 2020-23 drought in Kenya using Sentinel-2's higher temporal and spatial resolution which could result in more continuous timeseries.

While this study focused on drought, there are other perturbances at play in the landscape during this time. For example, human-caused wildfires are not uncommon on Mt. Kenya (Henry *et al.*, 2019). All counties in the study area were affected by floods and landslides in 2017-19, including flooding specifically Tharaka and Meru in March-May 2018 (Recovery 59) (UNICEF, 2018; Muchui, 2019; Kenya Meteorological Department, 2020). There was also a 2019-20 locust infestation (USAID, 2020). These could both cause noise in the observations of NDVI and affect the actual resilience and recovery rate of the system. Narrowing the recovery estimation to specific time periods as determined by the NDMA county classifications likely reduced the probability of estimating recovery from other perturbances during the study period except for times of overlap such as Recovery 59; however, this also may have missed relevant drought recoveries in pixels with a local minimum outside the designated windows. Even though the county-wide classifications of drought were based on surveys of individuals around the county as well as measures such as precipitation and vegetation conditions, given the variability within agricultural practices and climate conditions, the droughts (and other disasters) no doubt had varying severities and different onset and cessation times across the county. If the system disturbances had been pinpointed with a generalized method such as using sudden shifts in the data itself as in the method used by Smith *et al.* (2022), disturbance detection would be more specific to each pixel in the heterogeneous landscape. The recoveries may have been able to be matched to specific drought events via the disturbance timestamp. This approach would also lose specificity to drought and detect disturbances from other events such as floods but might provide a more complete picture of the system's resilience.

Additionally, the parameters chosen throughout the methodology (STL decomposition, the threshold for valid measurements, the length to search for a minimum, and the initial guesses for curve fitting) have some effect on the final recovery rates (Lenton *et al.*, 2022). While all parameters in this study were chosen based on a balance of maximizing calculated pixels while minimizing erroneous estimations, this was based on testing on a subset of the data. Sensitivity testing with different window sizes and parameters would reveal the effect of methodological choices on the result. This is a necessary step to increase the robustness of the results.

Finally, the limitations of drawing conclusions about an area using only remotely sensed data should be noted. Remote sensing data cannot speak to several factors that are known to affect vegetation resilience, such as which species are present, functional biodiversity, or soil health (Hishe *et al.*, 2021; Cavender-Bares *et al.*, 2022). Additionally, the data about TIST farms is limited; there may be additional groves that are unmarked, or farms that are marked may no longer be participating. While some groves had information about the number of trees planted or the date of establishment, not all groves had that information, so it was not utilized. Moreover, the exact agricultural practices used in TIST farms and the

surrounding farms cannot be confirmed with NDVI or TIST membership only. Further, the vegetation resilience to drought might not reflect the outcomes experienced by the farmers in the study area or the resilience of other aspects of the agro-ecosystem. Pairing remote sensing with field measurements could improve understanding of the drought severity across the county, or additional data sources such as interviews could reveal of the intensity of TIST practices and more detail on resilience of farms and surrounding areas.

7. Conclusion

Resilience after drought disturbance was estimated for four counties surrounding Mt. Kenya based on drought categorizations by the Kenyan National Drought Management Authority. The recovery rates were estimated using an exponential fit on the NDVI residuals from Landsat-8 and used as a direct measure of resilience. The patterns of resilience matched with existing literature, including higher resilience in areas with more water availability and tree cover, and more instances of no disturbance observed in semi-arid zones that may be more tolerant of water stress. These results validate the method as a useful way to measure resilience to specific disturbances.

The resilience of TIST groves and neighboring pixels were compared to other pixels to assess whether the agroforestry and conservation agriculture practices of TIST participants affect resilience to drought. TIST groves and Neighbors generally exhibited faster recoveries than pixels of the same landcover type across counties and recoveries. TIST and Neighbors also showed less decrease in resilience to subsequent droughts than comparable Other pixels. It was difficult to isolate the spillover effects of TIST groves into further neighboring pixels due to the change in other favorable conditions such as precipitation, altitude, and general greenness within one kilometer of TIST groves which speaks to the heterogeneity of the study area.

Given the methodological limitations such as sensitivity to missing months and the lack of complete timeseries in greener and more tree-covered locations due to cloud contamination, this study could provide further conclusions with additional data sources such as combining satellite sources for more complete NDVI series, fieldwork to localize drought severity, or information on the extent of TIST practices.

Because of the warming climate and pressures on planetary boundaries, ecosystems globally are exhibiting lower resilience while simultaneously the frequency and intensity of disasters like drought are increasing. Smallholder farmers are particularly exposed to the risks of climate change. TIST, a community-driven tree planting program for carbon credits, economically and environmentally benefits participating farmers, and the practices of agroforestry and conservation agriculture have previously been found to increase their resilience to climate change. This study supports the TIST program by quantifying that participants exhibit higher resilience to drought than comparable areas, and it corroborates farmers' experiential understanding that agroforestry improves drought resilience. By assessing the resilience of agro-ecosystems such as the area surrounding Mt. Kenya and identifying resilience-increasing management methods such as TIST practices, this study contributes to the concept of resilience monitoring systems and supports the use of resilience-building agricultural techniques.

8. Code Availability

Python scripts and utilized packages are available at <https://github.com/ml-henderson/TIST>.

Google Earth Engine code for retrieving the landcover, ecoregion, human modification gradient, and altitude data is available at:

<https://code.earthengine.google.com/97419690785510dfa3e44271ae7dc88e>.

Map figures were created using QGIS 3.32.0 (QGIS.org, 2023). Recovery rates and correlation plots were created with Python. Other graphs were created using TIBCO Spotfire 12.5.0.

9. Appendix

Table 3: Drought classifications from the NDMA. Months with NA had no report available online (NDMA, 2017, 2023).

Month #	Date	Meru	Tharaka	Embu	Nyeri
119	Apr-23	Normal	Normal	Normal	Recovery
118	Mar-23	Alert	Normal	Alert	Alert
117	Feb-23	Alert	Normal	Alert	Alert
116	Jan-23	Alert	Normal	Alert	Alert
115	Dec-22	Alert	Alert	Normal	Alert
114	Nov-22	Alert	Alert	Normal	Alert
113	Oct-22	Alert	Alert	Alert	Alert
112	Sep-22	Alert	Alert	Alert	Alert
111	Aug-22	Alert	Alarm	Alert	Alert
110	Jul-22	Alert	Alert	Alert	Alert
109	Jun-22	Alert	Alarm	Alert	Alert
108	May-22	Alert	Alert	Alert	Alert
107	Apr-22	Alert	Recovery	Normal	Alert
106	Mar-22	Alert	Alert	Normal	Alert
105	Feb-22	Alert	Alert	Normal	Alert
104	Jan-22	Alert	Recovery	Normal	Alert
103	Dec-21	Alert	Alert	Alert	Alert
102	Nov-21	Alert	Alarm	Alert	Alert
101	Oct-21	Alert	Alert	Alert	Alert
100	Sep-21	Alert	Alert	Alert	Alert
99	Aug-21	Alert	Alert	Alert	Normal
98	Jul-21	NA	NA	NA	NA
97	Jun-21	Normal	Normal	Normal	Normal
96	May-21	Normal	Normal	Normal	Normal
95	Apr-21	Normal	Normal	Normal	Normal
94	Mar-21	Normal	Normal	Normal	Normal
93	Feb-21	NA	NA	NA	NA
92	Jan-21	Normal	Normal	Normal	Normal
91	Dec-20	NA	NA	NA	NA
90	Nov-20	NA	NA	NA	NA
89	Oct-20	NA	NA	NA	NA
88	Sep-20	Normal	Normal	Normal	Normal
87	Aug-20	Normal	Normal	Normal	Normal
86	Jul-20	Normal	Normal	Normal	Normal
85	Jun-20	Normal	Normal	Normal	Normal
84	May-20	Normal	Normal	Normal	Normal
83	Apr-20	Normal	Normal	Normal	Normal
82	Mar-20	Normal	Normal	Normal	Normal

81	Feb-20	Normal	Normal	Normal	Normal
80	Jan-20	Normal	Normal	Normal	Normal
79	Dec-19	Normal	Normal	Normal	Normal
78	Nov-19	Normal	Recovery	Normal	Normal
77	Oct-19	Normal	Recovery	Normal	Normal
76	Sep-19	Alert	Alarm	Alarm	Alert
75	Aug-19	Normal	Alarm	Alert	Alert
74	Jul-19	Normal	Alarm	Alert	Alert
73	Jun-19	Normal	Alert	Alert	Alert
72	May-19	Normal	Alert	Alert	Alert
71	Apr-19	Normal	Alert	Alert	Alert
70	Mar-19	NA	NA	NA	NA
69	Feb-19	Normal	Alert	Alert	Alert
68	Jan-19	Normal	Alert	Normal	Normal
67	Dec-18	NA	NA	NA	NA
66	Nov-18	Normal	Alert	Normal	Normal
65	Oct-18	NA	NA	NA	NA
64	Sep-18	Normal	Normal	Normal	Normal
63	Aug-18	NA	NA	NA	NA
62	Jul-18	Normal	Normal	Normal	Normal
61	Jun-18	NA	NA	NA	NA
60	May-18	Normal	Normal	Normal	Normal
59	Apr-18	Normal	Normal	Normal	Normal
58	Mar-18	Alert	Alert	Alert	Alert
57	Feb-18	Alert	Alert	Alert	Normal
56	Jan-18	Alert	Alert	Normal	Normal
55	Dec-17	Normal	Alert	Normal	Normal
54	Nov-17	Normal	Alert	Normal	Normal
53	Oct-17	Alert	Alert	Alert	Alert
52	Sep-17	Alert	Alert	Alert	Alert
51	Aug-17	Alert	Alert	Alert	Alert
50	Jul-17	Alert	Alert	Alert	Alert
49	Jun-17	Alert	Alert	Alert	Alert
48	May-17	Alert	Alert	Alert	Alert
47	Apr-17	Alert	Alert	Alert	Alert
46	Mar-17	NA	NA	NA	NA
45	Feb-17	Alert	Alert	Normal	Alert
44	Jan-17	NA	NA	NA	NA
43	Dec-16	Alert	Alert	Alert	Normal
42	Nov-16	Normal	Normal	Alert	Normal
41	Oct-16	Alert	Normal	Normal	Normal
40	Sep-16	Alert	Normal	Normal	Normal

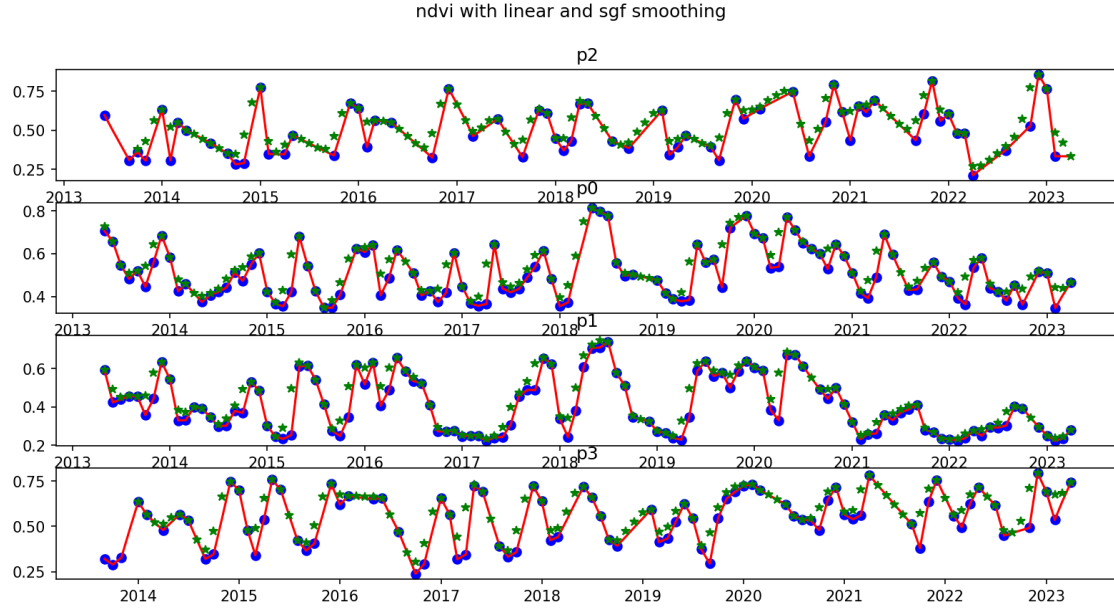


Figure 29: Example of attempted gap filling with Savitzky-Golay reconstruction on four pixels, which uses linear gap filling as the first step (Chen *et al.*, 2004). Blue points are original data. Red line is linear interpolation of all gaps (no size limit). Green stars are smoothed points. Filling gaps longer than seasons (2-3 months in Kenya) may not accurately reconstruct the NDVI timeseries, which can be seen by the long periods of reconstructed data with no fluctuations as might normally be expected.

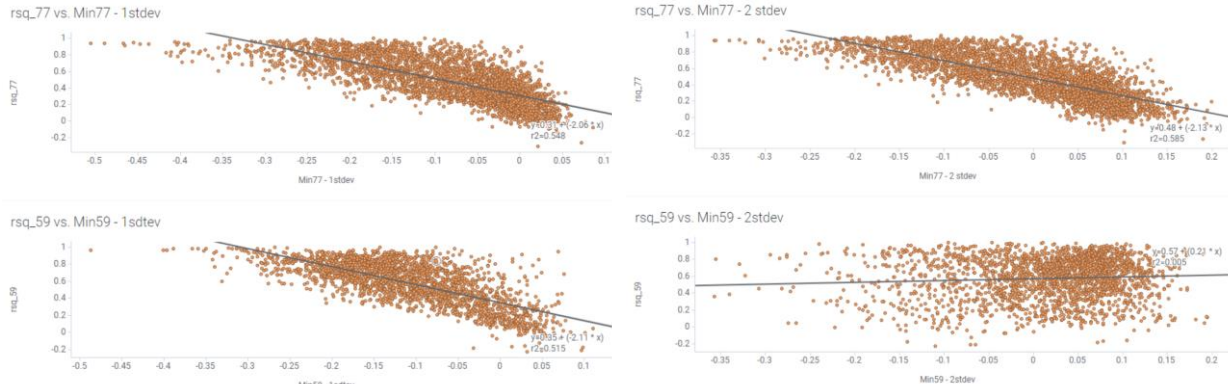


Figure 30: The R^2 value for the recovery rates vs. the difference between the local minimum and the (mean – one standard deviation). A positive difference indicates that the local minimum found was closer to the mean than one standard deviation, while a negative value indicates a local minimum farther from the mean than one standard deviation. Recovery fitted for 5000 pixels in Tharka county for two recoveries (59th month and 77th month). The overall trend shows that for pixels with a local minimum closer than one standard deviation to the mean, the overall fit of the equation is worse, and sometimes even less than zero, indicating a nonsensical result from an incorrect model fit. This led to the decision to require local minimums to be below one standard deviation from the mean.

Figure 31: The R^2 value for the recovery rates vs. the difference between the local minimum and the (mean – two standard deviations). A positive difference indicates that the local minimum found was closer to the mean than two standard deviations, while a negative value indicates a local minimum farther from the mean than two standard deviations. Recovery fitted for 5000 pixels in Tharka county for two recoveries (59th month and 77th month). The overall trend shows that for one recovery, a threshold below the second standard deviation led to better R^2 values, while the other recovery showed no trend. This led to the decision to require local minimums to be below one standard deviations from the mean.

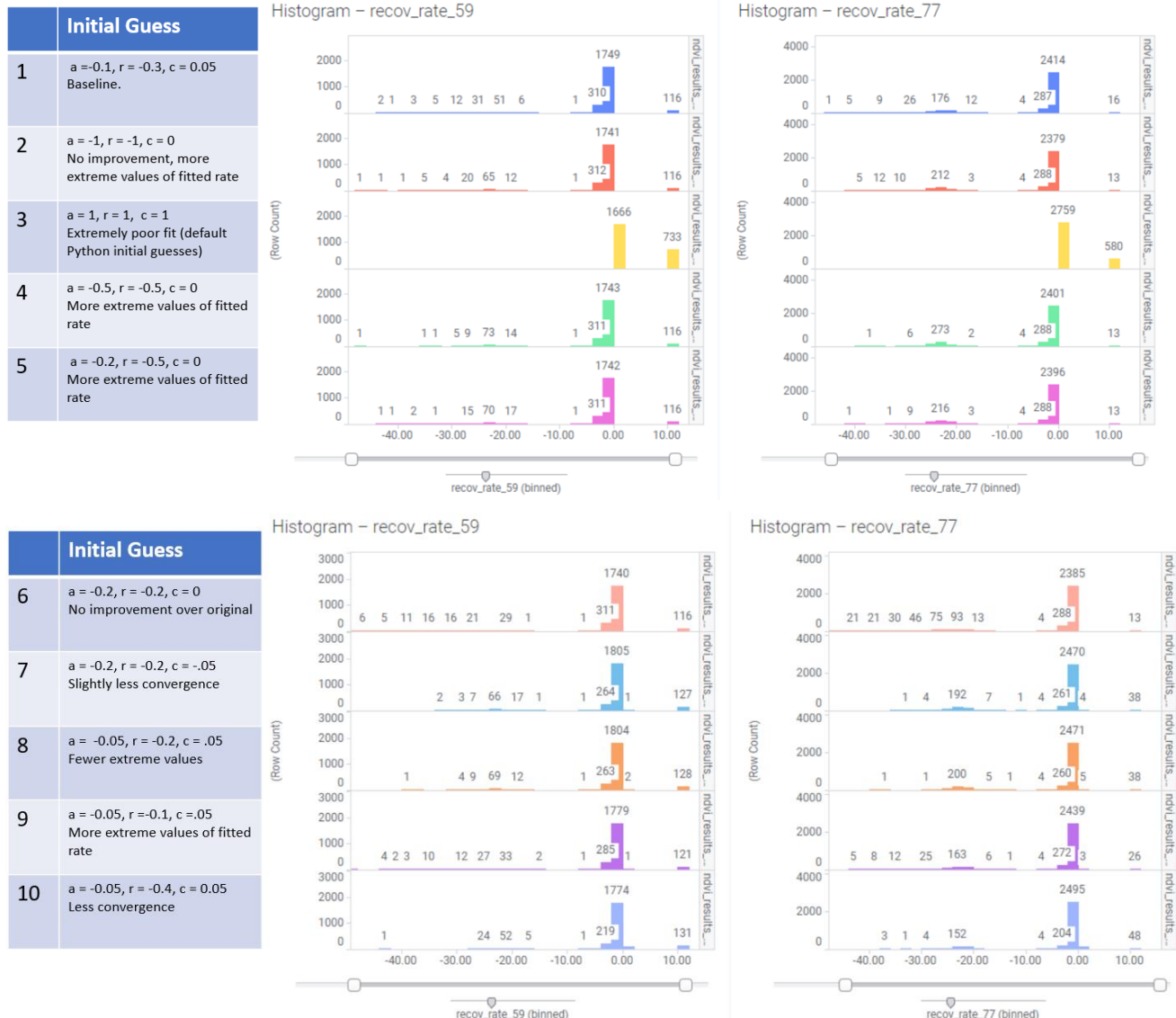


Figure 32: Histograms of fitted recovery rate for a sample of data ($n = 5000$, Tharaka county) for different initial guesses of a , r , and c . Recovery rate of 10 indicates no convergence. The results are only somewhat sensitive to these initial guesses. The eighth set of tested parameters was chosen as a sufficient starting guess for curve fitting.

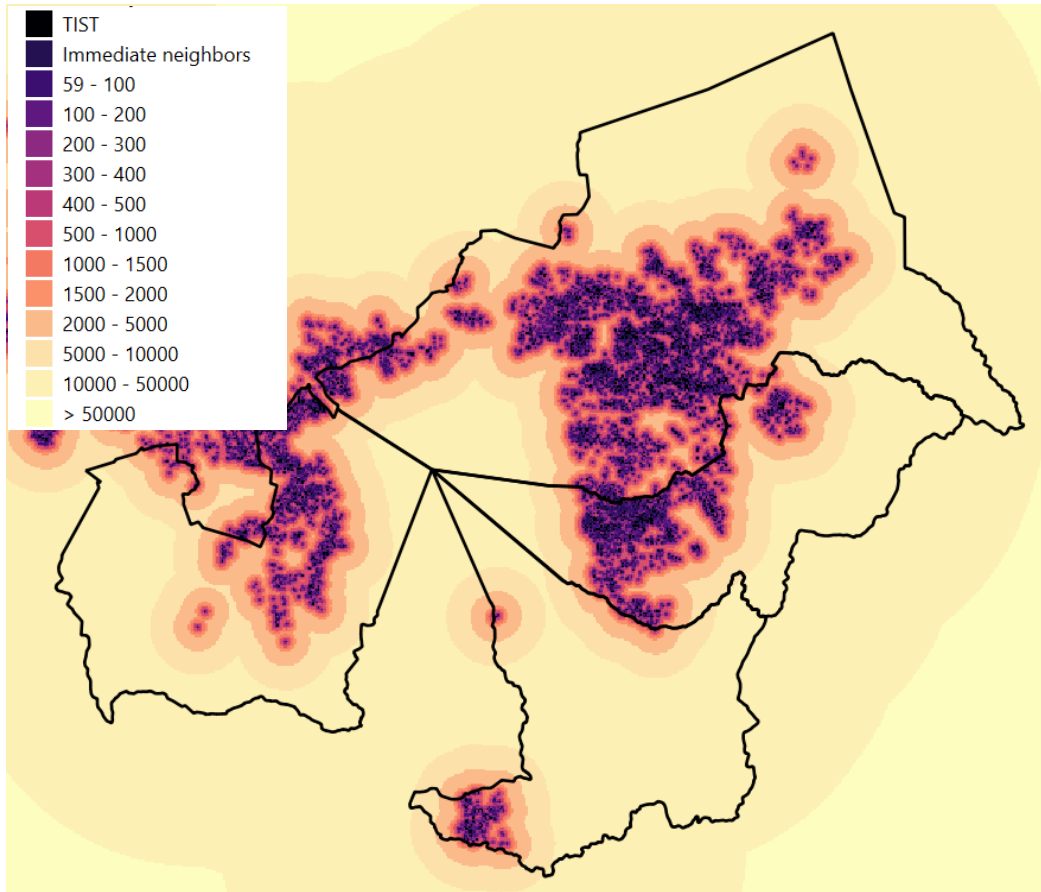


Figure 33: Distance from TIST groves in meters.

Table 4: Recovery calculation success rates.

	Number of pixels	Total pixels	Total attempted, 59	Disturbance detected, rate calculated, 59	No disturbance detected, 59	Disturbance detected, curve could not be fit, 59
Meru	7,720,270	4,355,850 (56%)	3,431,380 (44% of total, 79% of attempted)	843,196 (11% of total, 19% of attempted)	81,274 (1% of total, 2% of attempted)	
Tharaka	2,990,072	1,802,477 (60%)	1,659,332 (55% of total, 92% of attempted)	132,224 (4% of total, 7% of attempted)	10,921 (0.4% of total, 0.6% of attempted)	
Nyeri	3,733,796	1,072,462 (29%)	755,417 (20% of total, 70% of attempted)	210,178 (6% of total, 20% of attempted)	106,867 (3% of total, 10% of attempted)	
Embu	3,170,195	947,371 (30%)	888,370 (28% of total, 94% of attempted)	53,131 (2% of total, 6% of attempted)	5,870 (0.2% of total, 0.6% of attempted)	
	Total pixels	Total attempted, 77	Disturbance detected, rate calculated, 77	No disturbance detected, 77	Disturbance detected, curve could not be fit, 77	
Meru	7,720,270	5,413,373 (70%)	2,776,504 (36% of total, 51% of attempted)	2,477,926 (32% of total, 46% of attempted)	158,953 (2% of total, 3% of attempted)	
Tharaka	2,990,072	2,047,445 (68%)	1,099,377 (37% of total, 54% of attempted)	870,388 (29% of total, 43% of attempted)	77,680 (3% of total, 4% of attempted)	
Nyeri	3,733,796	1,338,556 (36%)	790,413 (21% of total, 59% of attempted)	520,975 (14% of total, 39% of attempted)	27,168 (1% of total, 2% of attempted)	
Embu	3,170,195	1,326,543 (42%)	453,140 (14% of total, 34% of attempted)	830,522 (26% of total, 63% of attempted)	42,881 (1% of total, 3% of attempted)	

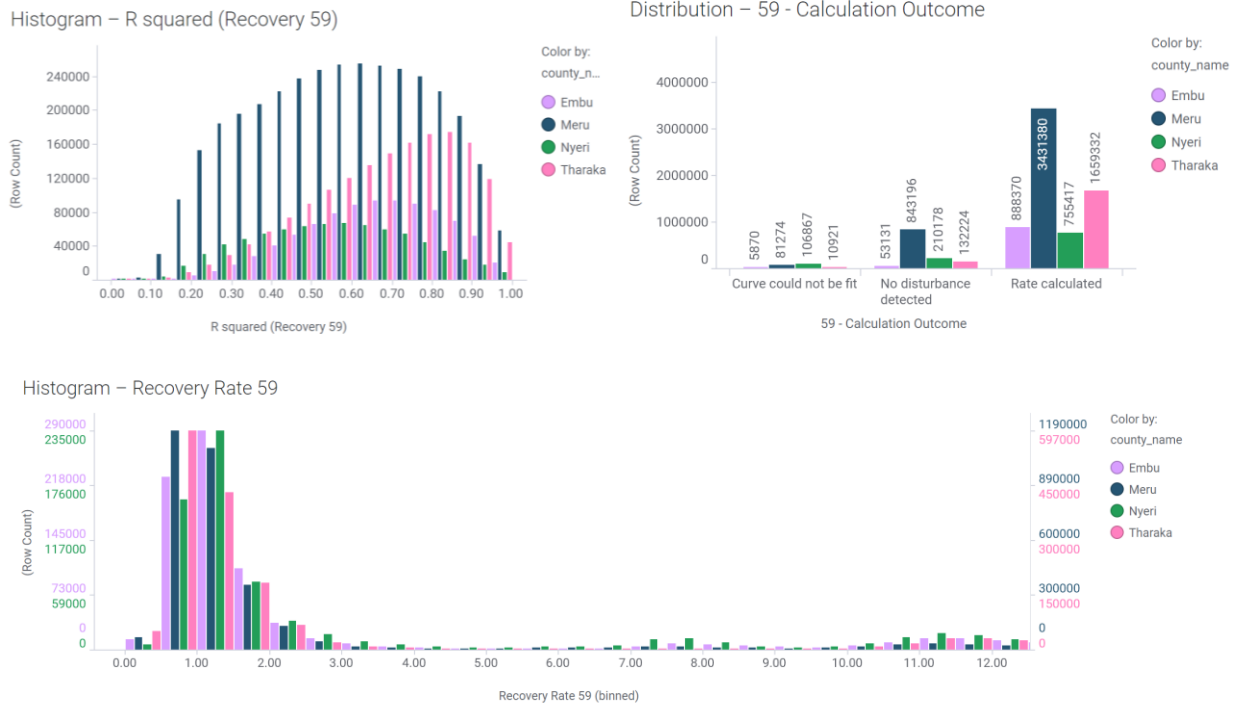


Figure 34: Recovery rates and R-squared values for Recovery 59. Bottom histogram of recovery rates has zoomed x-axis to show detail; outliers persist up to a rate of approximately 60.

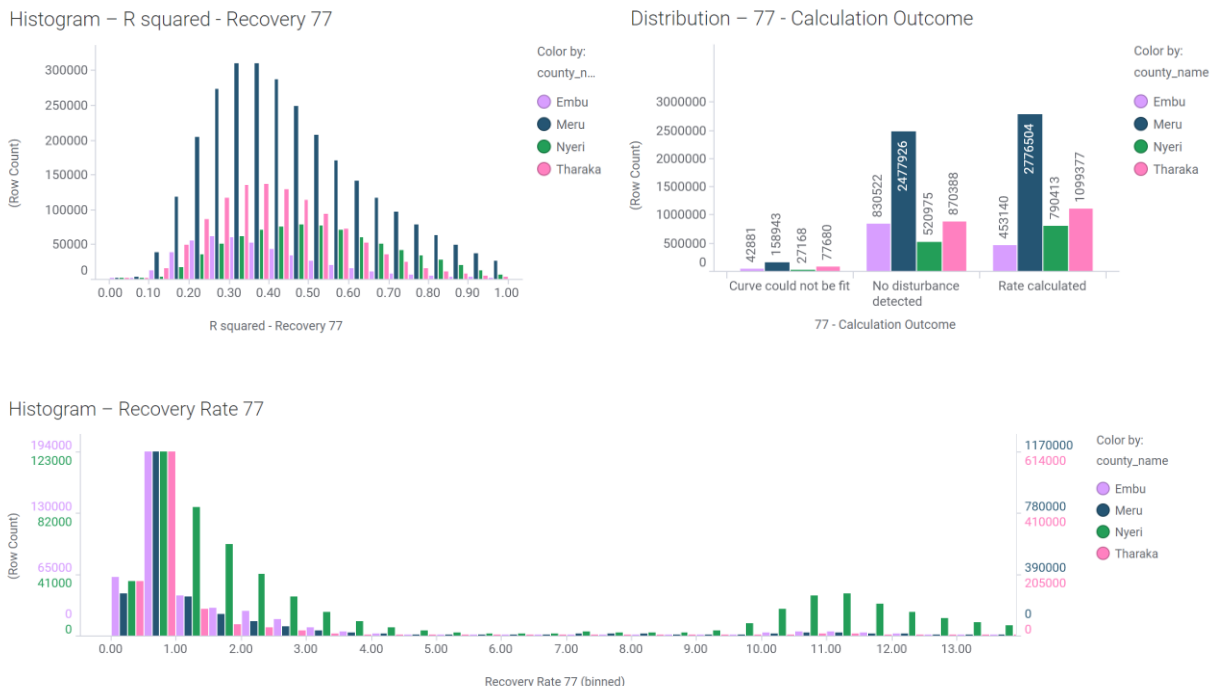


Figure 35: Recovery rates and R-squared values for Recovery 77. Bottom histogram of recovery rates has zoomed x-axis to show detail; outliers persist up to a rate of approximately 60.

Histogram – Mean NDVI

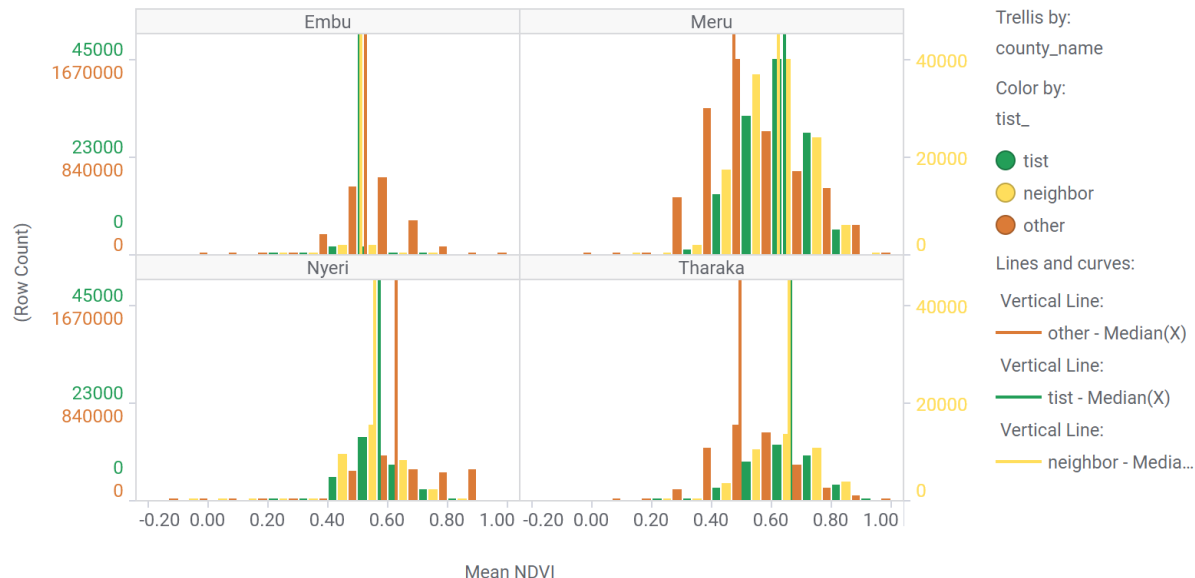


Figure 36: Mean NDVI in each county for TIST, neighbors, and other pixels. Meru and Tharaka have very similar patterns that TIST and neighbors tend to be wetter, greener, and at higher altitude, while Embu has less differences between the groups. Nyeri has the opposite trends: TIST and neighbors tend to be drier, less green, and at lower altitudes. Similar distributions are seen in yearly average precipitation and altitude.

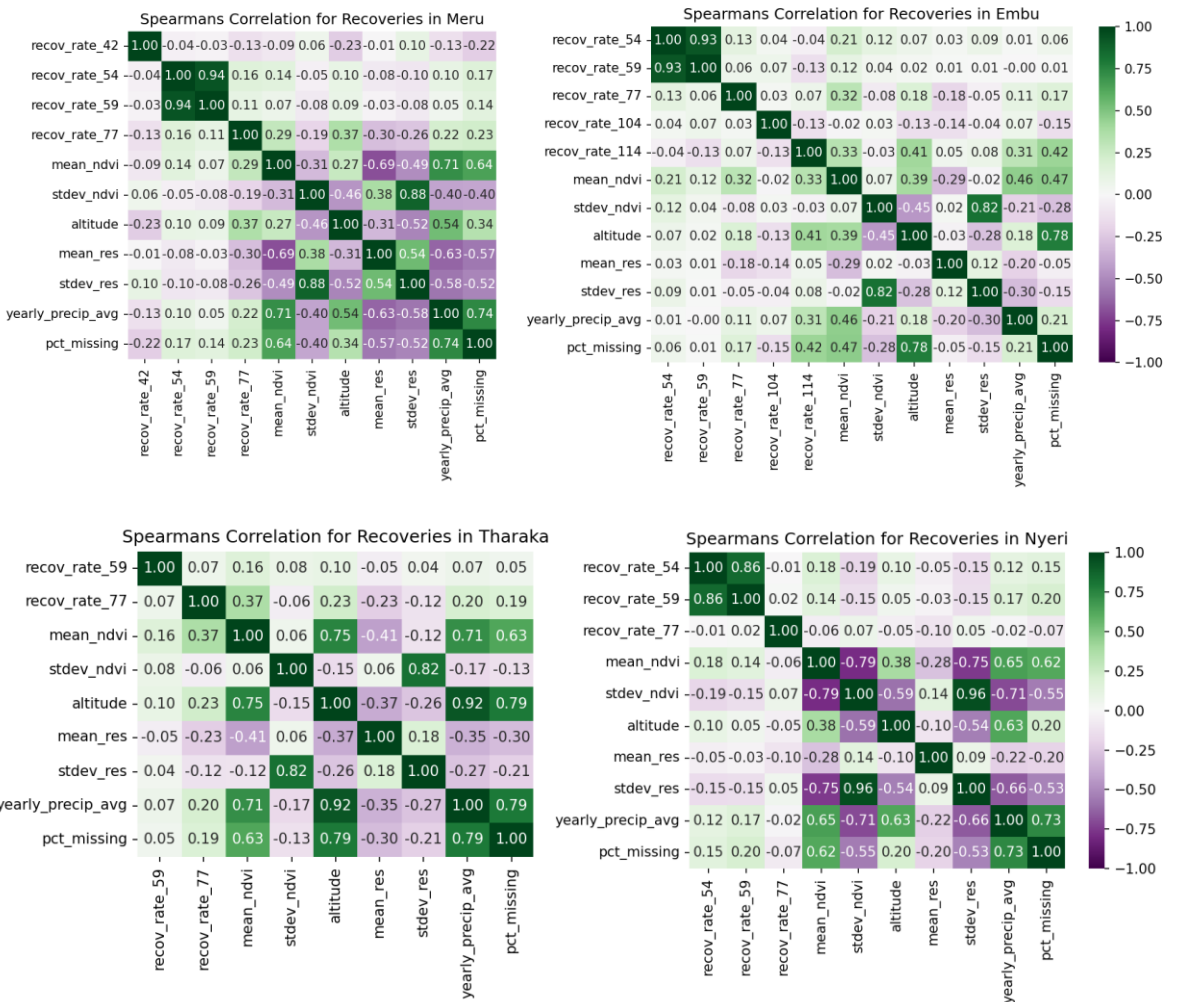


Figure 37: Spearman's rank correlations for recoveries and other characteristics across counties. All correlations are significant, $p < 0.001$.

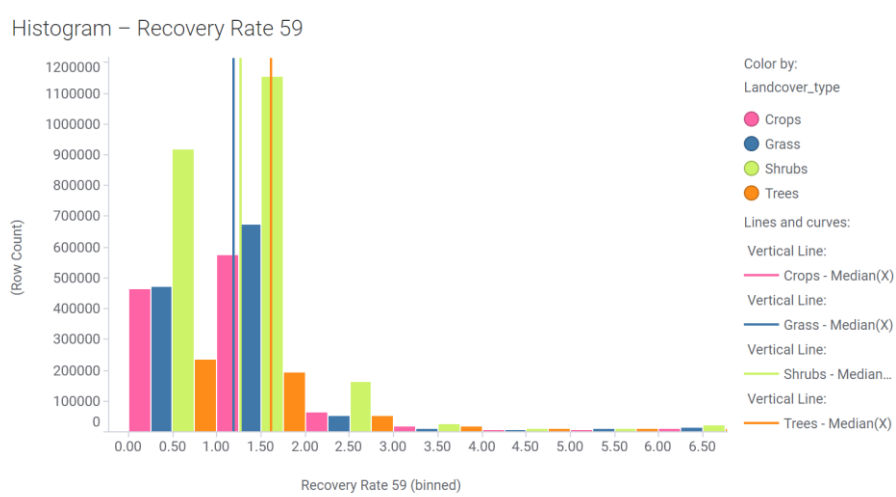
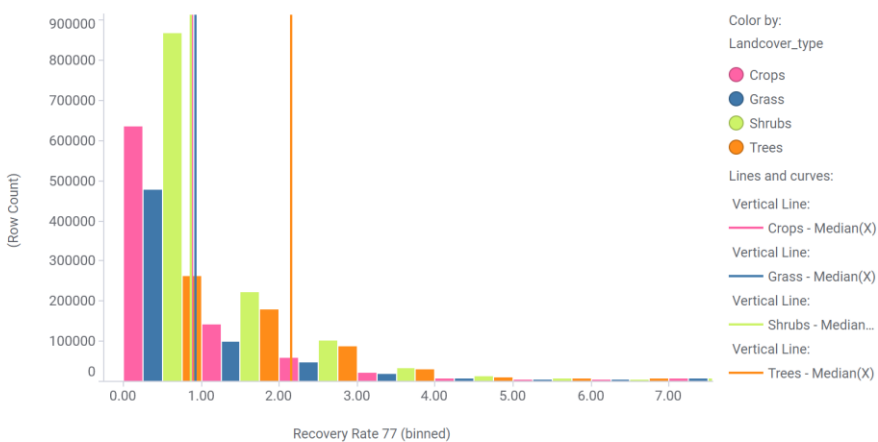


Figure 38a: Recovery rates for 59 by landcover type. Trees have the highest median recovery rates.

Histogram – Recovery Rate 77



38b: Recovery rates for 77 by landcover type.
Trees have the highest median recovery rates.

Histogram – Recovery Rate 59

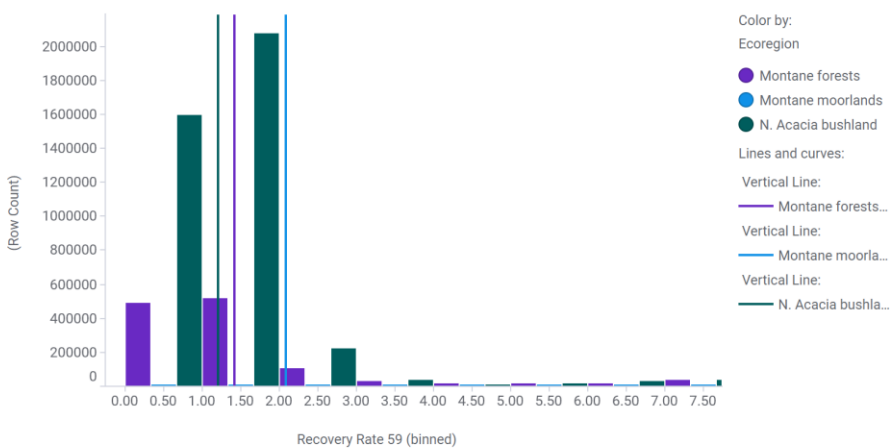
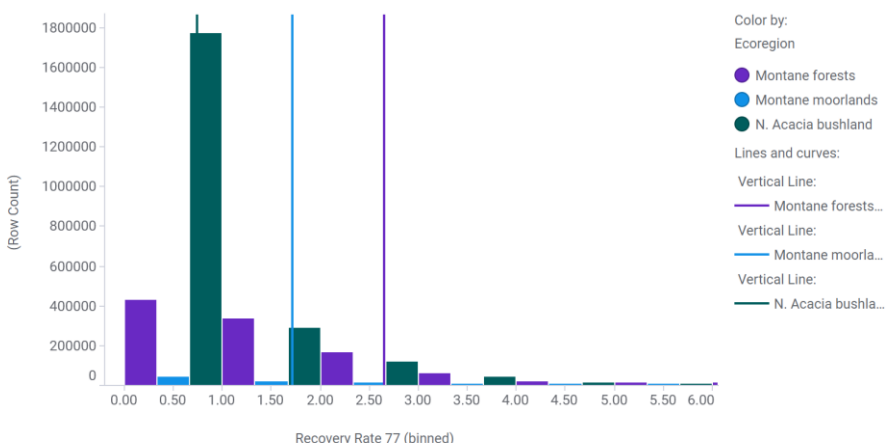


Figure 39a: Recovery rates for 59 by ecoregion.
Forests have the highest median recovery rates after montane moorlands, which are mostly ignored in this study due to their low numbers and irrelevance to agricultural areas.

Histogram – Recovery Rate 77



39b: Recovery rates for 77 by ecoregion.
Forests have the highest median recovery rates.

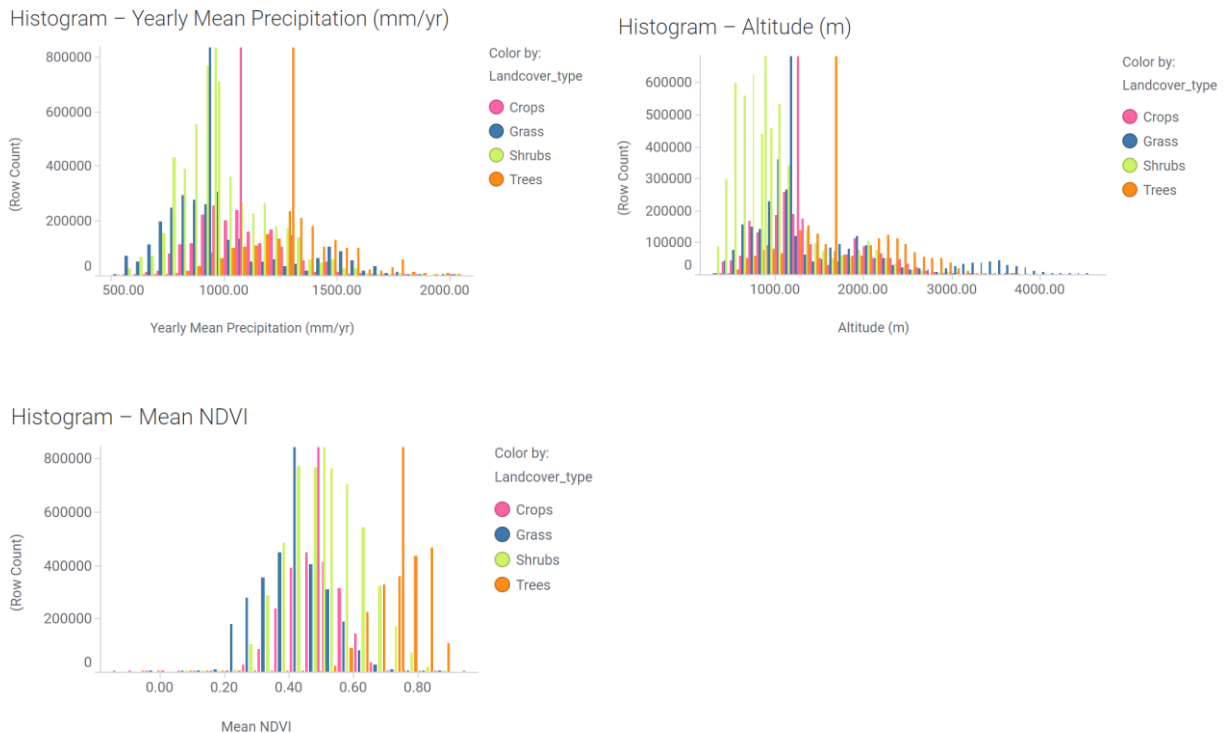


Figure 40 : Characteristics of each landcover type with medians marked. Medians are significantly different between each landcover type (KWH with PHD, $p < 0.001$).

Table 5: Sample size corresponding to recovery rates compared by county, recovery and landcover classification.

Landcover class		Tree cover		Shrubland		Grassland		Cropland	
Recovery Period		59	77	59	77	59	77	59	77
Tharaka	TIST	10,725	7,718	5,339	3,874	1,246	875	6,027	5,699
	Nbr.	11,318	6,794	6,463	4,270	1,267	887	6,973	6,415
	Oth.	127,264	100,611	1,028,514	563,916	187,604	143,671	263,324	251,687
Meru	TIST	31,274	22,429	13,391	11,262	3,239	2,816	31,745	28,323
	Nbr.	26,329	17,400	13,240	11,495	4,060	3,634	35,318	32,431
	Oth.	342,315	449,632	935,687	568,550	837,093	493,271	674,186	594,334
Nyeri	TIST	2,798	2,511	6,805	6,244	5,286	5,054	4,779	3,967
	Nbr.	2,525	2,102	6,599	5,272	7,786	6,834	7,055	5,535
	Oth.	159,404	246,757	146,113	134,820	228,587	182,764	161,299	118,147
Embu	TIST	35	31	756	581	318	288	796	583
	Nbr.	29	22	851	544	400	300	666	450
	Oth.	39,797	54,247	605,307	220,931	121,445	67,085	117,255	107,694

Table 6: Sample size for percent change in recovery rate from Recovery 59 to Recovery 77, compared by landcover.

Sample size		Tree cover	Shrubland	Grassland	Cropland
Tharaka	TIST	3,411	2,438	635	3,873
	Neighbor	2,872	2,541	652	4,239
	Other	40,367	419,856	108,961	174,820
Meru	TIST	12,149	5,868	1,809	20,276
	Neighbor	9,361	5,700	2,195	22,237
	Other	121,546	283,643	246,299	349,124
Nyeri	TIST	1,285	3,414	2,892	2,225
	Neighbor	1,176	3,028	4,051	3,200
	Other	72,158	75,673	114,309	71,624
Embu	TIST	7	264	88	256
	Neighbor	3	227	65	189
	Other	6,777	85,098	29,641	34,719

10. References

- Ben Abbes, A., Bounouh, O., Farah, I.R., de Jong, R. and Martínez, B. (2018) 'Comparative study of three satellite image time-series decomposition methods for vegetation change detection', *European Journal of Remote Sensing*, 51(1), pp. 607–615. Available at: <https://doi.org/10.1080/22797254.2018.1465360>.
- Abera, T.A., Heiskanen, J., Pellikka, P. and Maeda, E.E. (2018) 'Rainfall–vegetation interaction regulates temperature anomalies during extreme dry events in the Horn of Africa', *Global and Planetary Change*, 167, pp. 35–45. Available at: <https://doi.org/10.1016/j.gloplacha.2018.05.002>.
- Abera, T.A., Heiskanen, J., Pellikka, P.K.E., Adhikari, H. and Maeda, E.E. (2020) 'Climatic impacts of bushland to cropland conversion in Eastern Africa', *Science of The Total Environment*, 717, p. 137255. Available at: <https://doi.org/10.1016/j.scitotenv.2020.137255>.
- Anderegg, W.R.L., Trugman, A.T., Badgley, G., Konings, A.G. and Shaw, J. (2020) 'Divergent forest sensitivity to repeated extreme droughts', *Nature Climate Change* 2020 10:12, 10(12), pp. 1091–1095. Available at: <https://doi.org/10.1038/s41558-020-00919-1>.
- Arekhi, M., Goksel, C., Balik Sanli, F. and Senel, G. (2019) 'Comparative Evaluation of the Spectral and Spatial Consistency of Sentinel-2 and Landsat-8 OLI Data for Igneada Longos Forest', *ISPRS International Journal of Geo-Information*, 8(2), p. 56. Available at: <https://doi.org/10.3390/ijgi8020056>.
- Armstrong McKay, D.I., Staal, A., Abrams, J.F., Winkelmann, R., Sakschewski, B., Loriani, S., Fetzer, I., Cornell, S.E., Rockström, J. and Lenton, T.M. (2022) 'Exceeding 1.5°C global warming could trigger multiple climate tipping points', *Science*, 377(6611). Available at: <https://doi.org/10.1126/science.abn7950>.
- Beare, D J *et al.* (2017) 'Agriculture production as a major driver of the Earth system exceeding planetary boundaries', *Ecology and Society*, 22(4). Available at: <https://doi.org/10.5751/ES-09595-220408>.
- van Belzen, J., van de Koppel, J., Kirwan, M.L., van der Wal, D., Herman, P.M.J., Dakos, V., Kéfi, S., Scheffer, M., Guntenspergen, G.R. and Bouma, T.J. (2017) 'Vegetation recovery in tidal marshes reveals critical slowing down under increased inundation', *Nature Communications* 2017 8:1, 8(1), pp. 1–7. Available at: <https://doi.org/10.1038/ncomms15811>.
- Boillat, S., Jew, E.K.K., Steward, P.R., Speranza, C.I., Whitfield, S., Mkwambisi, D., Kiteme, B., Wambugu, G., Burdekin, O.J. and Dougill, A.J. (2019) 'Can smallholder farmers buffer rainfall variability through conservation agriculture? On-farm practices and maize yields in Kenya and Malawi', *Environmental Research Letters*, 14(11), p. 115007. Available at: <https://doi.org/10.1088/1748-9326/AB45AD>.
- Boulton, C.A., Lenton, T.M. and Boers, N. (2022) 'Pronounced loss of Amazon rainforest resilience since the early 2000s', *Nature Climate Change* 2022 12:3, 12(3), pp. 271–278. Available at: <https://doi.org/10.1038/s41558-022-01287-8>.

- Bowell, A., Salakpi, E.E., Guigma, K., Muthoka, J.M., Mwangi, J. and Rowhani, P. (2021) 'Validating commonly used drought indicators in Kenya', *Environmental Research Letters*, 16(8), p. 084066. Available at: <https://doi.org/10.1088/1748-9326/ac16a2>.
- Buxton, J., Abrams, J., Boulton, C., Barlow, N., Rangel Smith, C., Van Stroud, S., Lees, K. and Lenton, T. (2022) 'Quantitatively monitoring the resilience of patterned vegetation in the Sahel', *Global Change Biology*, 28(2), pp. 571–587. Available at: <https://doi.org/10.1111/gcb.15939>.
- Buxton, J., Powell, T., Ambler, J., Boulton, C., Nicholson, A., Arthur, R., Lees, K., Williams, H. and Lenton, T.M. (2021) 'Community-driven tree planting greens the neighbouring landscape', *Scientific reports*, 11(1). Available at: <https://doi.org/10.1038/S41598-021-96973-6>.
- Camberlin, P., Boyard-Micheau, J., Philippon, N., Baron, C., Leclerc, C. and Mwongera, C. (2014) 'Climatic gradients along the windward slopes of Mount Kenya and their implication for crop risks. Part 1: climate variability', *International Journal of Climatology*, 34(7), pp. 2136–2152. Available at: <https://doi.org/10.1002/joc.3427>.
- Campbell, A.D. and Wang, Y. (2020) 'Salt marsh monitoring along the mid-Atlantic coast by Google Earth Engine enabled time series', *PLOS ONE*, 15(2), p. e0229605. Available at: <https://doi.org/10.1371/journal.pone.0229605>.
- Cao, R., Chen, Y., Shen, M., Chen, J., Zhou, J., Wang, C. and Yang, W. (2018) 'A simple method to improve the quality of NDVI time-series data by integrating spatiotemporal information with the Savitzky-Golay filter', *Remote Sensing of Environment*, 217, pp. 244–257. Available at: <https://doi.org/10.1016/j.rse.2018.08.022>.
- Cavender-Bares, J., Schneider, F.D., Santos, M.J., Armstrong, A., Carnaval, A., Dahlin, K.M., Fatoyinbo, L., Hurtt, G.C., Schimel, D., Townsend, P.A., Ustin, S.L., Wang, Z. and Wilson, A.M. (2022) 'Integrating remote sensing with ecology and evolution to advance biodiversity conservation', *Nature Ecology & Evolution*, 6(5), pp. 506–519. Available at: <https://doi.org/10.1038/s41559-022-01702-5>.
- Chaves, M.M., Maroco, J.P. and Pereira, J.S. (2003) 'Understanding plant responses to drought — from genes to the whole plant', *Functional Plant Biology*, 30(3), p. 239. Available at: <https://doi.org/10.1071/FP02076>.
- Chen, J., Jönsson, Per., Tamura, M., Gu, Z., Matsushita, B. and Eklundh, L. (2004) 'A simple method for reconstructing a high-quality NDVI time-series data set based on the Savitzky–Golay filter', *Remote Sensing of Environment*, 91(3–4), pp. 332–344. Available at: <https://doi.org/10.1016/j.rse.2004.03.014>.
- Chen, Y., Cao, R., Chen, J., Liu, L. and Matsushita, B. (2021) 'A practical approach to reconstruct high-quality Landsat NDVI time-series data by gap filling and the Savitzky–Golay filter', *ISPRS Journal of Photogrammetry and Remote Sensing*, 180, pp. 174–190. Available at: <https://doi.org/10.1016/j.isprsjprs.2021.08.015>.
- Cleveland, R.B., Cleveland, W.S., McRae, J.E. and Terpenning, I. (1990) 'STL: A Seasonal-Trend Decomposition Procedure Based on Loess', *Journal of Official Statistics*, 6(1), pp. 3–73.

- Dakos, V., Carpenter, S.R., van Nes, E.H. and Scheffer, M. (2015) 'Resilience indicators: prospects and limitations for early warnings of regime shifts', *Philosophical Transactions of the Royal Society B: Biological Sciences*, 370(1659), p. 20130263. Available at: <https://doi.org/10.1098/rstb.2013.0263>.
- Dinerstein, E. et al. (2017) 'An Ecoregion-Based Approach to Protecting Half the Terrestrial Realm', *BioScience*, 67(6), pp. 534–545. Available at: <https://doi.org/10.1093/BIOSCI/BIX014>.
- Dollinger, J. and Jose, S. (2018) 'Agroforestry for soil health', *Agroforestry Systems*, 92(2), pp. 213–219. Available at: <https://link.springer.com/article/10.1007/s10457-018-0223-9> (Accessed: 17 June 2023).
- Donovan, M., Orwin, K., Roudier, P., Belliss, S., Phillips, C. and Research, W.-L. (2021) *Quantifying resilience to drought and flooding in agricultural systems*.
- Drake, J.M. and Griffen, B.D. (2010) 'Early warning signals of extinction in deteriorating environments', *Nature*, 467(7314), pp. 456–459. Available at: <https://doi.org/10.1038/nature09389>.
- Dunn, O.J. (1964) 'Multiple Comparisons Using Rank Sums', *Technometrics*, 6(3), pp. 241–252. Available at: <https://doi.org/10.1080/00401706.1964.10490181>.
- Eckert, S., Kiteme, B., Njuguna, E. and Zaehringer, J.G. (2017) 'Agricultural Expansion and Intensification in the Foothills of Mount Kenya: A Landscape Perspective', *Remote Sensing 2017, Vol. 9, Page 784*, 9(8), p. 784. Available at: <https://doi.org/10.3390/RS9080784>.
- Eriksen, S.H. and O'Brien, K. (2007) 'Vulnerability, poverty and the need for sustainable adaptation measures', *Climate Policy*, 7(4), pp. 337–352. Available at: <https://doi.org/10.1080/14693062.2007.9685660>.
- ESA (2023) *Sentinel-2, European Space Agency*. Available at: https://www.esa.int/Applications/Observing_the_Earth/Copernicus/Sentinel-2 (Accessed: 28 March 2023).
- Farr, T.G. et al. (2007) 'The Shuttle Radar Topography Mission', *Reviews of Geophysics*, 45(2), p. RG2004. Available at: <https://doi.org/10.1029/2005RG000183>.
- Fernandez-Manso, A., Quintano, C. and Roberts, D.A. (2016) 'Burn severity influence on post-fire vegetation cover resilience from Landsat MESMA fraction images time series in Mediterranean forest ecosystems', *Remote Sensing of Environment*, 184, pp. 112–123. Available at: <https://doi.org/10.1016/j.rse.2016.06.015>.
- Fischer, B.M.C., Mul, M.L. and Savenije, H.H.G. (2013) 'Determining spatial variability of dry spells: a Markov-based method, applied to the Makanya catchment, Tanzania', *Hydrology and Earth System Sciences*, 17(6), pp. 2161–2170. Available at: <https://doi.org/10.5194/hess-17-2161-2013>.
- Folke, C. (2006) 'Resilience: The emergence of a perspective for social–ecological systems analyses', *Global Environmental Change*, 16(3), pp. 253–267. Available at: <https://doi.org/10.1016/j.gloenvcha.2006.04.002>.

- Forzieri, G., Dakos, V., McDowell, N.G., Ramdane, A. and Cescatti, A. (2022) 'Emerging signals of declining forest resilience under climate change', *Nature* 2022 608:7923, 608(7923), pp. 534–539. Available at: <https://doi.org/10.1038/s41586-022-04959-9>.
- Franke, T.M., Ho, T. and Christie, C.A. (2012) 'The Chi-Square Test', *American Journal of Evaluation*, 33(3), pp. 448–458. Available at: <https://doi.org/10.1177/1098214011426594>.
- Funk, C., Peterson, P., Landsfeld, M., Pedreros, D., Verdin, J., Shukla, S., Husak, G., Rowland, J., Harrison, L., Hoell, A. and Michaelsen, J. (2015) 'The climate hazards infrared precipitation with stations—a new environmental record for monitoring extremes', *Scientific Data*, 2(1), p. 150066. Available at: <https://doi.org/10.1038/sdata.2015.66>.
- Gao, S., Zhou, T., Yi, C., Shi, P., Fang, W., Liu, R., Liang, E. and Julio Camarero, J. (2020) 'Asymmetric impacts of dryness and wetness on tree growth and forest coverage', *Agricultural and Forest Meteorology*, 288–289, p. 107980. Available at: <https://doi.org/10.1016/j.agrformet.2020.107980>.
- Gebremeskel Haile, G., Tang, Q., Leng, G., Jia, G., Wang, J., Cai, D., Sun, S., Baniya, B. and Zhang, Q. (2020) 'Long-term spatiotemporal variation of drought patterns over the Greater Horn of Africa', *Science of The Total Environment*, 704, p. 135299. Available at: <https://doi.org/10.1016/j.scitotenv.2019.135299>.
- Gebremeskel Haile, G., Tang, Q., Sun, S., Huang, Z., Zhang, X. and Liu, X. (2019) 'Droughts in East Africa: Causes, impacts and resilience', *Earth-Science Reviews*, 193, pp. 146–161. Available at: <https://doi.org/10.1016/j.earscirev.2019.04.015>.
- Gichenje, H. and Godinho, S. (2018) 'Establishing a land degradation neutrality national baseline through trend analysis of GIMMS NDVI Time-series', *Land Degradation & Development*, 29(9), pp. 2985–2997. Available at: <https://doi.org/10.1002/ldr.3067>.
- Gorelick, N., Hancher, M., Dixon, M., Ilyushchenko, S., Thau, D. and Moore, R. (2017) 'Google Earth Engine: Planetary-scale geospatial analysis for everyone', *Remote Sensing of Environment*, 202, pp. 18–27. Available at: <https://doi.org/10.1016/J.RSE.2017.06.031>.
- Hayes, M., Wilhite, D.A., Svoboda, M. and Trnka, M. (2011) 'Investigating the connections between climate change, drought and agricultural production', in *Handbook on Climate Change and Agriculture*. Edward Elgar Publishing Ltd., pp. 73–86. Available at: <https://doi.org/10.4337/9780857939869.00011>.
- Henry, M.C., Maingi, J.K. and McCarty, J. (2019) 'Fire on the Water Towers: Mapping Burn Scars on Mount Kenya Using Satellite Data to Reconstruct Recent Fire History', *Remote Sensing 2019, Vol. 11, Page 104*, 11(2), p. 104. Available at: <https://doi.org/10.3390/RS11020104>.
- Hishe, H., Oosterlynck, L., Giday, K., De Keersmaecker, W., Somers, B. and Muys, B. (2021) 'A combination of climate, tree diversity and local human disturbance determine the stability of dry Afromontane forests', *Forest Ecosystems*, 8(1), pp. 1–16. Available at: <https://link.springer.com/article/10.1186/s40663-021-00288-x> (Accessed: 14 July 2023).

- Hodgson, D., McDonald, J.L. and Hosken, D.J. (2015) 'What do you mean, "resilient"?' , *Trends in Ecology & Evolution*, 30(9), pp. 503–506. Available at: <https://doi.org/10.1016/j.tree.2015.06.010>.
- Holl, K.D. and Brancalion, P.H.S. (2020) 'Tree planting is not a simple solution', *Science*, 368(6491), pp. 580–581. Available at: https://doi.org/10.1126/SCIENCE.ABA8232/SUPPL_FILE/ABA8232_HOLL_SM.PDF.
- Holling, C.S. (1996) 'Engineering resilience versus ecological resilience', in P. Schulze (ed.) *Engineering within Ecological Constraints*, p. 32.
- Huang, S., Tang, L., Hupy, J.P., Wang, Y. and Shao, G. (2021) 'A commentary review on the use of normalized difference vegetation index (NDVI) in the era of popular remote sensing', *Journal of Forestry Research*, 32(1), pp. 1–6. Available at: <https://link.springer.com/article/10.1007/s11676-020-01155-1> (Accessed: 8 May 2023).
- Ingrisch, J. and Bahn, M. (2018) 'Towards a Comparable Quantification of Resilience', *Trends in Ecology & Evolution*, 33(4), pp. 251–259. Available at: <https://doi.org/10.1016/j.tree.2018.01.013>.
- Jing, L., Weng, B., Yan, D., Yuan, F., Zhang, S., Bi, W. and Yan, S. (2023) 'Assessment of resilience in maize suitable planting areas under drought stress', *Agricultural Water Management*, 277, p. 108096. Available at: <https://doi.org/10.1016/j.agwat.2022.108096>.
- Jose, S. (2009) 'Agroforestry for ecosystem services and environmental benefits: An overview', *Agroforestry Systems*, 76(1), pp. 1–10. Available at: <https://doi.org/10.1007/S10457-009-9229-7/TABLES/2>.
- De Keersmaecker, W., Lhermitte, S., Tits, L., Honnay, O., Somers, B. and Coppin, P. (2015) 'A model quantifying global vegetation resistance and resilience to short-term climate anomalies and their relationship with vegetation cover', *Global Ecology and Biogeography*, 24(5), pp. 539–548. Available at: <https://doi.org/10.1111/GEB.12279/SUPPINFO>.
- De Keersmaecker, W., van Rooijen, N., Lhermitte, S., Tits, L., Schaminée, J., Coppin, P., Honnay, O. and Somers, B. (2016) 'Species-rich semi-natural grasslands have a higher resistance but a lower resilience than intensively managed agricultural grasslands in response to climate anomalies', *Journal of Applied Ecology*. Edited by S. Diamond, 53(2), pp. 430–439. Available at: <https://doi.org/10.1111/1365-2664.12595>.
- Kennedy, C.M., Oakleaf, J.R., Theobald, D.M., Baruch-Mordo, S. and Kiesecker, J. (2019) 'Managing the middle: A shift in conservation priorities based on the global human modification gradient', *Global Change Biology*, 25(3), pp. 811–826. Available at: <https://doi.org/10.1111/GCB.14549>.
- Kennedy, R.E. et al. (2014) 'Bringing an ecological view of change to Landsat-based remote sensing', *Frontiers in Ecology and the Environment*, 12(6), pp. 339–346. Available at: <https://doi.org/10.1890/130066>.
- Kenya Meteorological Department (2020) *Extreme Weather Events in Kenya between 2011 and 2020*. Available at:

https://meteo.go.ke/sites/default/files/downloads/Extreme%20Climate%20Events_Kenya%202011_to_2020.pdf (Accessed: 17 August 2023).

Van De Kerchove, R., Zanaga, D., De Keersmaecker, W., Li, L., Tsendbazar, N. and Lesiv, M. (2020) *Product User Manual: WorldCover v1.0*. Available at: https://esa-worldcover.s3.eu-central-1.amazonaws.com/v100/2020/docs/WorldCover_PUM_V1.0.pdf (Accessed: 10 August 2023).

von Keyserlingk, J., de Hoop, M., Mayor, A.G., Dekker, S.C., Rietkerk, M. and Foerster, S. (2021) ‘Resilience of vegetation to drought: Studying the effect of grazing in a Mediterranean rangeland using satellite time series’, *Remote Sensing of Environment*, 255, p. 112270. Available at: <https://doi.org/10.1016/J.RSE.2020.112270>.

Kimutai, J. et al. (2023) ‘Human-induced climate change increased drought severity in Horn of Africa’, *Julie Arrighi*, 16. Available at: <https://doi.org/10.25561/103482>.

Kowalski, K., Senf, C., Hostert, P. and Pflugmacher, D. (2020) ‘Characterizing spring phenology of temperate broadleaf forests using Landsat and Sentinel-2 time series’, *International Journal of Applied Earth Observation and Geoinformation*, 92, p. 102172. Available at: <https://doi.org/10.1016/j.jag.2020.102172>.

Kruskal, W.H. and Wallis, W.A. (1952) ‘Use of Ranks in One-Criterion Variance Analysis’, *Journal of the American Statistical Association*, 47(260), pp. 583–621. Available at: <https://doi.org/10.1080/01621459.1952.10483441>.

Lasco, R.D., Delfino, R.J.P., Catacutan, D.C., Simelton, E.S. and Wilson, D.M. (2014) ‘Climate risk adaptation by smallholder farmers: the roles of trees and agroforestry’, *Current Opinion in Environmental Sustainability*, 6(1), pp. 83–88. Available at: <https://doi.org/10.1016/J.COSUST.2013.11.013>.

Lees, K.J., Artz, R.R.E., Chandler, D., Aspinall, T., Boulton, C.A., Buxton, J., Cowie, N.R. and Lenton, T.M. (2021) ‘Using remote sensing to assess peatland resilience by estimating soil surface moisture and drought recovery’, *Science of The Total Environment*, 761, p. 143312. Available at: <https://doi.org/10.1016/j.scitotenv.2020.143312>.

Lees, K. J., Buxton, J., Boulton, C.A., Abrams, J.F. and Lenton, T.M. (2021) ‘Using satellite data to assess management frequency and rate of regeneration on heather moorlands in England as a resilience indicator’, *Environmental Research Communications*, 3(8), p. 085003. Available at: <https://doi.org/10.1088/2515-7620/AC1A5F>.

Lenton, T.M. (2020) ‘Tipping positive change’, *Philosophical Transactions of the Royal Society B: Biological Sciences*, 375(1794), p. 20190123. Available at: <https://doi.org/10.1098/rstb.2019.0123>.

Lenton, T.M., Buxton, J.E., Armstrong McKay, D.I., Abrams, J.F., Boulton, C.A., Lees, K., Powell, T.W.R., Boers, N., Cunliffe, A.M. and Dakos, V. (2022) ‘A resilience sensing system for the biosphere’, *Philosophical Transactions of the Royal Society B*, 377(1857). Available at: <https://doi.org/10.1098/RSTB.2021.0383>.

Lenton, T.M., Held, H., Kriegler, E., Hall, J.W., Lucht, W., Rahmstorf, S. and Schellnhuber, H.J. (2008) 'Tipping elements in the Earth's climate system', *Proceedings of the National Academy of Sciences of the United States of America*, 105(6), pp. 1786–1793. Available at: <https://doi.org/10.1073/PNAS.0705414105>.

Lenton, T.M. and Latour, B. (2018) 'Gaia 2.0 Could humans add some level of self-awareness to Earth's self-regulation?', *Science*, 361(6407), pp. 1066–1068. Available at: https://doi.org/10.1126/SCIENCE.AAU0427/ASSET/426623BA-34B8-409A-B2AF-08CA8EEBC329/ASSETS/GRAFIC/361_1066_F1.JPG.

Linke, A.M., Witmer, F.D.W. and O'Loughlin, J. (2020) 'Do people accurately report droughts? Comparison of instrument-measured and national survey data in Kenya', *Climatic Change*, 162(3), pp. 1143–1160. Available at: <https://link.springer.com/article/10.1007/s10584-020-02724-3> (Accessed: 9 May 2023).

Liu, L., Zhang, Y., Wu, S., Li, S. and Qin, D. (2018) 'Water memory effects and their impacts on global vegetation productivity and resilience', *Scientific Reports*, 8(1), p. 2962. Available at: <https://doi.org/10.1038/s41598-018-21339-4>.

Liu, R., Shang, R., Liu, Y. and Lu, X. (2017) 'Global evaluation of gap-filling approaches for seasonal NDVI with considering vegetation growth trajectory, protection of key point, noise resistance and curve stability', *Remote Sensing of Environment*, 189, pp. 164–179. Available at: <https://doi.org/10.1016/j.rse.2016.11.023>.

Liu, W.T.H., Massambani, O. and Nobre, C.A. (1994) 'Satellite recorded vegetation response to drought in Brazil', *International Journal of Climatology*, 14(3), pp. 343–354. Available at: <https://doi.org/10.1002/joc.3370140307>.

Liu, X., Zhu, X., Pan, Y., Li, S., Liu, Y. and Ma, Y. (2016) 'Agricultural drought monitoring: Progress, challenges, and prospects', *Journal of Geographical Sciences*, 26(6), pp. 750–767. Available at: <https://doi.org/10.1007/S11442-016-1297-9/METRICS>.

Liu, Y., Kumar, M., Katul, G.G. and Porporato, A. (2019) 'Reduced resilience as an early warning signal of forest mortality', *Nature Climate Change*, 9(11), pp. 880–885. Available at: <https://doi.org/10.1038/s41558-019-0583-9>.

Ludwig, J.A., Wilcox, B.P., Breshears, D.D., Tongway, D.J. and Imeson, A.C. (2005) 'Vegetation Patches and Runoff-Erosion as Interacting Ecohydrological Processes in Semiarid Landscapes', *Ecology*, 86(2), pp. 288–297. Available at: <https://doi.org/10.1890/03-0569>.

Marshall, J. (2022) *Analysing the dynamics of 'positive tipping points' in The International Small Group and Tree Planting Program (TIST) from a systems thinking perspective*. University of Exeter.

Martin, E. and Burgess, N. (2023a) *East African Montane Forests, One Earth*. Available at: <https://www.oneearth.org/ecoregions/east-african-montane-forests/> (Accessed: 31 August 2023).

Martin, E. and Burgess, N. (2023b) *Northern Acacia-Commiphora Bushlands and Thickets, One Earth*. Available at: <https://www.oneearth.org/ecoregions/northern-acacia-commiphora-bushlands-and-thickets/> (Accessed: 31 August 2023).

Masiga, M., Yankel, C. and Iberre, C. (2012) *Institutional innovations in African smallholder carbon projects Case Study: The International Small Group Tree Planting Program (TIST)* . Available at: <https://assets.publishing.service.gov.uk/media/57a08a8e40f0b64974000662/AfricanAgCarbon-CaseStudy-Tist.pdf> (Accessed: 4 August 2023).

McKenna, P., Phinn, S. and Erskine, P. (2018) ‘Fire Severity and Vegetation Recovery on Mine Site Rehabilitation Using WorldView-3 Imagery’, *Fire*, 1(2), p. 22. Available at: <https://doi.org/10.3390/fire1020022>.

Mendelsohn, R. (2009) ‘The Impact of Climate Change on Agriculture in Developing Countries’, *Journal of Natural Resources Policy Research*, 1(1), pp. 5–19. Available at: <https://doi.org/10.1080/19390450802495882>.

Micheni, A.N., Kanampiu, F., Kitonyo, O., Mburu, D.M., Mugai, E.N., Makumbi, D. and Kassie, M. (2016) ‘On-farm experimentation on conservation agriculture in maize-legume based cropping systems in Kenya: Water use efficiency and economic impacts’, *Experimental Agriculture*, 52(1), pp. 51–68. Available at: <https://doi.org/10.1017/S0014479714000556>.

Miralles, D.G., Gentine, P., Seneviratne, S.I. and Teuling, A.J. (2019) ‘Land-atmospheric feedbacks during droughts and heatwaves: state of the science and current challenges’, *Annals of the New York Academy of Sciences*, 1436(1), pp. 19–35. Available at: <https://doi.org/10.1111/nyas.13912>.

Mishra, A.K. and Singh, V.P. (2010) ‘A review of drought concepts’, *Journal of Hydrology*, 391(1–2), pp. 202–216. Available at: <https://doi.org/10.1016/j.jhydrol.2010.07.012>.

Muchui, D. (2019) *Landslide blocks road in Meru*, *ReliefWeb*. Available at: <https://reliefweb.int/report/kenya/landslide-blocks-road-meru> (Accessed: 17 August 2023).

Myneni, R.B., Hall, F.G., Sellers, P.J. and Marshak, A.L. (1995) ‘The interpretation of spectral vegetation indexes’, *IEEE Transactions on Geoscience and Remote Sensing*, 33(2), pp. 481–486. Available at: <https://doi.org/10.1109/TGRS.1995.8746029>.

NASA Landsat Science (no date) *Landsat 8*. Available at: <https://landsat.gsfc.nasa.gov/satellites/landsat-8/> (Accessed: 30 July 2023).

Nash, D. (2022) *Is eastern Africa’s drought the worst in recent history? And are worse yet to come?* - *Climate Champions, UNFCCC Race to Resilience*. Available at: <https://climatechampions.unfccc.int/is-eastern-africas-drought-the-worst-in-recent-history-and-are-worse-yet-to-come/> (Accessed: 28 March 2023).

NDMA (2017) *National Drought Early Warning Bulletin (July 2017)*, *ReliefWeb*. Available at: <https://reliefweb.int/report/kenya/national-drought-early-warning-bulletin-july-2017> (Accessed: 11 August 2023).

NDMA (2022a) *Short Rains Assessment*. Available at: <https://www.ndma.go.ke/index.php/resource-center/send/87-2022/6833-2022-short-rains-assessment-national-report> (Accessed: 20 May 2023).

NDMA (2022b) *Short Rains Assessment*. Available at: <https://www.ndma.go.ke/index.php/resource-center/send/87-2022/6833-2022-short-rains-assessment-national-report> (Accessed: 20 May 2023).

NDMA (2023) *National drought bulletin, National Drought Management Authority Kenya*. Available at: <https://www.ndma.go.ke/index.php/resource-center/national-drought-bulletin/category/39-drought-updates?start=0> (Accessed: 20 June 2023).

NDMA (no date) *About NDMA, National Drought Management Authority Kenya*. Available at: <https://www.ndma.go.ke/index.php/features/about-ndma> (Accessed: 30 July 2023).

Van Nes, E.H. and Scheffer, M. (2007) 'Slow recovery from perturbations as a generic indicator of a nearby catastrophic shift', *American Naturalist*, 169(6), pp. 738–747. Available at: <https://doi.org/10.1086/516845> SUPPL_FILE/41794APA.PDF.

Nicholson, S.E. (2017) 'Climate and climatic variability of rainfall over eastern Africa', *Reviews of Geophysics*, 55(3), pp. 590–635. Available at: <https://doi.org/10.1002/2016RG000544>.

Nolè, A., Rita, A., Spatola, M.F. and Borghetti, M. (2022) 'Biogeographic variability in wildfire severity and post-fire vegetation recovery across the European forests via remote sensing-derived spectral metrics', *Science of The Total Environment*, 823, p. 153807. Available at: <https://doi.org/10.1016/J.SCITOTENV.2022.153807>.

Nyong, A.P., Ngankam, T.M. and Felicite, T.L. (2020) 'Enhancement of resilience to climate variability and change through agroforestry practices in smallholder farming systems in Cameroon', *Agroforestry Systems*, 94(3), pp. 687–705. Available at: <https://doi.org/10.1007/S10457-019-00435-Y/TABLES/10>.

Ochieng, J., Kirimi, L. and Mathenge, M. (2016) 'Effects of climate variability and change on agricultural production: The case of small scale farmers in Kenya', *NJAS: Wageningen Journal of Life Sciences*, 77(1), pp. 71–78. Available at: <https://doi.org/10.1016/j.njas.2016.03.005>.

Oppenheimer, S. (2011) *Impact Evaluation of the TIST Program in Kenya*. Available at: https://efdafrica.org/site/assets/files/1026/tist_ccb_community_survey_result.pdf (Accessed: 4 August 2023).

Pantera, Mosquera-Losada, M.R., Herzog, F. and den Herder, M. (2021) 'Agroforestry and the environment', *Agroforestry Systems*, 95(5), pp. 767–774. Available at: <https://link.springer.com/article/10.1007/s10457-021-00640-8> (Accessed: 17 June 2023).

Pellikka, P.K.E., Heikinheimo, V., Hietanen, J., Schäfer, E., Siljander, M. and Heiskanen, J. (2018) 'Impact of land cover change on aboveground carbon stocks in Afromontane landscape in Kenya', *Applied Geography*, 94, pp. 178–189. Available at: <https://doi.org/10.1016/j.apgeog.2018.03.017>.

Petropoulos, G. and Kalaitzidis, C. (2012) 'Multispectral Vegetation Indices in Remote Sensing: An Overview', in W. Zhang (ed.) *Ecological Modeling*. New York City: Nova Science Publishers, Inc.

Pettorelli, N., Vik, J.O., Mysterud, A., Gaillard, J.-M., Tucker, C.J. and Stenseth, N.Chr. (2005) 'Using the satellite-derived NDVI to assess ecological responses to environmental change', *Trends in Ecology & Evolution*, 20(9), pp. 503–510. Available at: <https://doi.org/10.1016/j.tree.2005.05.011>.

Pimm, S.L. (1984) 'The complexity and stability of ecosystems', *Nature*, 307(5949), pp. 321–326. Available at: <https://doi.org/10.1038/307321a0>.

QGIS.org (2023) 'QGIS Geographic Information System'. QGIS Association.

Quandt, A., Neufeldt, H. and McCabe, J.T. (2017) 'The role of agroforestry in building livelihood resilience to floods and drought in semiarid Kenya', *Ecology and Society*, 22(3), p. art10. Available at: <https://doi.org/10.5751/ES-09461-220310>.

Recha, C.W. (2018) 'Local and regional variations in conditions for agriculture and food security in Kenya', in. Available at: www.slu.se/agrifose (Accessed: 27 August 2023).

Rivest, D., Lorente, M., Olivier, A. and Messier, C. (2013) 'Soil biochemical properties and microbial resilience in agroforestry systems: Effects on wheat growth under controlled drought and flooding conditions', *Science of The Total Environment*, 463–464, pp. 51–60. Available at: <https://doi.org/10.1016/j.scitotenv.2013.05.071>.

RMCMD Africa GeoPortal (2020) *Kenya County Boundaries*. Available at: https://rcmrd.africageoportal.com/datasets/d2f2df2a08ef42e88cb6bdc00e41dcc9_0/explore?location=0.611650%2C37.976045%2C7.91 (Accessed: 31 July 2023).

Scheffer, M. et al. (2018) 'Quantifying resilience of humans and other animals.', *Proceedings of the National Academy of Sciences of the United States of America*, 115(47), pp. 11883–11890. Available at: <https://doi.org/10.1073/pnas.1810630115>.

Scheffer, M., Bascompte, J., Brock, W.A., Brovkin, V., Carpenter, S.R., Dakos, V., Held, H., Van Nes, E.H., Rietkerk, M. and Sugihara, G. (2009) 'Early-warning signals for critical transitions', *Nature 2009* 461:7260, 461(7260), pp. 53–59. Available at: <https://doi.org/10.1038/nature08227>.

Schwalm, C.R. et al. (2017) 'Global patterns of drought recovery', *Nature*, 548(7666), pp. 202–205. Available at: <https://doi.org/10.1038/nature23021>.

Sherwood, A. (2013) 'Community adaptation to climate change: exploring drought and poverty traps in Gituamba location, Kenya', *Journal of Natural Resources Policy Research*, 5(2–3), pp. 147–161. Available at: <https://doi.org/10.1080/19390459.2013.811857>.

Shisanya, C.A., Recha, C. and Anyamba, A. (2011) 'Rainfall Variability and Its Impact on Normalized Difference Vegetation Index in Arid and Semi-Arid Lands of Kenya', *International Journal of Geosciences*, 02(01), pp. 36–47. Available at: <https://doi.org/10.4236/ijg.2011.21004>.

Silleos, N.G., Alexandridis, T.K., Gitas, I.Z. and Perakis, K. (2006) 'Vegetation Indices: Advances Made in Biomass Estimation and Vegetation Monitoring in the Last 30 Years', *Geocarto International*, 21(4), pp. 21–28. Available at: <https://doi.org/10.1080/10106040608542399>.

- Sims, D., Luo, H., Hastings, S., Oechel, W. and Rahman, A. (2006) 'Parallel adjustments in vegetation greenness and ecosystem CO₂ exchange in response to drought in a Southern California chaparral ecosystem', *Remote Sensing of Environment*, 103(3), pp. 289–303. Available at: <https://doi.org/10.1016/j.rse.2005.01.020>.
- Smith, T. and Boers, N. (2023) 'Global vegetation resilience linked to water availability and variability', *Nature Communications*, 14(1), p. 498. Available at: <https://doi.org/10.1038/s41467-023-36207-7>.
- Smith, T., Traxl, D. and Boers, N. (2022) 'Empirical evidence for recent global shifts in vegetation resilience', *Nature Climate Change* 2022 12:5, 12(5), pp. 477–484. Available at: <https://doi.org/10.1038/s41558-022-01352-2>.
- Suir, G.M., Sasser, C.E. and Harris, J.M. (2020) 'Use of Remote Sensing and Field Data to Quantify the Performance and Resilience of Restored Louisiana Wetlands', *Wetlands*, 40(6), pp. 2643–2658. Available at: <https://link.springer.com/article/10.1007/s13157-020-01344-y> (Accessed: 17 June 2023).
- Tai, X., Trugman, A.T. and Anderegg, W.R.L. (2023) 'Linking remotely sensed ecosystem resilience with forest mortality across the continental United States', *Global Change Biology*, 29(4), pp. 1096–1105. Available at: <https://doi.org/10.1111/GCB.16529>.
- Thackway, R., Lymburner, L. and Guerschman, J.P. (2013) 'Dynamic land cover information bridging the gap between remote sensing and natural resource management on JSTOR', *Ecology and Society*, 18(1). Available at: <https://www.jstor.org/stable/26269254> (Accessed: 17 June 2023).
- TIST (2023) *TIST Farmers*. Available at: <https://program.tist.org/farmers> (Accessed: 9 March 2023).
- TIST (no date) *TIST Courses*. Available at: <https://learn.tist.org/1/offset/0,24> (Accessed: 20 August 2023).
- Tommasino, A., Lezama, F., Gallego, F., Camba Sans, G. and Paruelo, J.M. (2023) 'Rangeland resilience to droughts: Changes across an intensification gradient', *Applied Vegetation Science*, 26(2), p. e12722. Available at: <https://doi.org/10.1111/avsc.12722>.
- Trisos, C.H., Adelekan, I.O., Totin, E., Ayanlade, A., Eftre, J., Gemedo, A., Kalaba, K., Lennard, C., Masao, C., Mgaya, Y., Ngaruuya, G., Olago, D., Simpson, N.P. and Zakieldeen, S. (2023) 'Africa', in H.-O. Pörtner, D.C. Roberts, M. Tignor, E.S. Poloczanska, K. Mintenbeck, A. Alegría, M. Craig, S. Langsdorf, S. Löschke, V. Möller, A. Okem, and B. Rama (eds) *Climate Change 2022 – Impacts, Adaptation and Vulnerability*. Cambridge, UK and New York, NY, USA: Cambridge University Press, pp. 1285–1456. Available at: <https://doi.org/10.1017/9781009325844.011>.
- Tsendbazar, N., Li, L., Koopman, M., Carter, S., Herold, M., Georgieva, I. and Lesiv, M. (2021) *WorldCover Product Validation Report (D12-PVR)*. Available at: https://esa-worldcover.s3.eu-central-1.amazonaws.com/v100/2020/docs/WorldCover_PVR_V1.1.pdf (Accessed: 31 July 2023).
- Von Uexkull, N., Croicu, M., Fjelde, H. and Buhaug, H. (2016) 'Civil conflict sensitivity to growing-season drought', *Proceedings of the National Academy of Sciences of the United States of America*, 113(44), pp. 12391–12396. Available at: https://doi.org/10.1073/PNAS.1607542113/SUPPL_FILE/PNAS.201607542SI.PDF.

Uhe, P., Philip, S., Kew, S., Shah, K., Kimutai, J., Mwangi, E., van Oldenborgh, G.J., Singh, R., Arrighi, J., Jjemba, E., Cullen, H. and Otto, F. (2018) 'Attributing drivers of the 2016 Kenyan drought', *International Journal of Climatology*, 38, pp. e554–e568. Available at: <https://doi.org/10.1002/joc.5389>.

UNICEF (2018) *Kenya Floods Response Update*, ReliefWeb. Available at: <https://reliefweb.int/report/kenya/kenya-floods-response-update-15-june-2018-flash-update> (Accessed: 17 August 2023).

USAID (2020) *East Africa: USAID Response to the Desert Locust Crisis*, ReliefWeb. Available at: <https://reliefweb.int/map/kenya/east-africa-usaid-response-desert-locust-crisis-093020> (Accessed: 17 August 2023).

Venter, Z.S., Barton, D.N., Chakraborty, T., Simensen, T. and Singh, G. (2022) 'Global 10 m Land Use Land Cover Datasets: A Comparison of Dynamic World, World Cover and Esri Land Cover', *Remote Sensing*, 14(16), p. 4101. Available at: <https://doi.org/10.3390/RS14164101/S1>.

Veraart, A.J., Faassen, E.J., Dakos, V., Van Nes, E.H., Lürling, M. and Scheffer, M. (2011) 'Recovery rates reflect distance to a tipping point in a living system', *Nature* 2011 481:7381, 481(7381), pp. 357–359. Available at: <https://doi.org/10.1038/nature10723>.

Verbesselt, J., Umlauf, N., Hirota, M., Holmgren, M., Van Nes, E.H., Herold, M., Zeileis, A. and Scheffer, M. (2016) 'Remotely sensed resilience of tropical forests', *Nature Climate Change*, 6(11), pp. 1028–1031. Available at: <https://doi.org/10.1038/nclimate3108>.

Vicente-Serrano, S.M., Gouveia, C., Camarero, J.J., Beguería, S., Trigo, R., López-Moreno, J.I., Azorín-Molina, C., Pasho, E., Lorenzo-Lacruz, J., Revuelto, J., Morán-Tejeda, E. and Sanchez-Lorenzo, A. (2013) 'Response of vegetation to drought time-scales across global land biomes.', *Proceedings of the National Academy of Sciences of the United States of America*, 110(1), pp. 52–7. Available at: <https://doi.org/10.1073/pnas.1207068110>.

Wallace, J.S. (2000) 'Increasing agricultural water use efficiency to meet future food production', *Agriculture, Ecosystems & Environment*, 82(1–3), pp. 105–119. Available at: [https://doi.org/10.1016/S0167-8809\(00\)00220-6](https://doi.org/10.1016/S0167-8809(00)00220-6).

Wang, J., Rich, P.M., Price, K.P. and Kettle, W.D. (2004) 'Relations between NDVI and tree productivity in the central Great Plains', *International Journal of Remote Sensing*, 25(16), pp. 3127–3138. Available at: <https://doi.org/10.1080/0143116032000160499>.

Wessels, K.J., Prince, S.D., Zambatis, N., MacFadyen, S., Frost, P.E. and Van Zyl, D. (2006) 'Relationship between herbaceous biomass and 1-km² Advanced Very High Resolution Radiometer (AVHRR) NDVI in Kruger National Park, South Africa', *International Journal of Remote Sensing*, 27(5), pp. 951–973. Available at: <https://doi.org/10.1080/01431160500169098>.

White, H.J., Gaul, W., Sadykova, D., León-Sánchez, L., Caplat, P., Emmerson, M.C. and Yearsley, J.M. (2020) 'Quantifying large-scale ecosystem stability with remote sensing data', *Remote Sensing in Ecology*

and Conservation. Edited by N. Pettorelli and A. Zlinszky, 6(3), pp. 354–365. Available at: <https://doi.org/10.1002/rse2.148>.

Wissel, C. (1984) ‘A universal law of the characteristic return time near thresholds’, *Oecologia*, 65(1), pp. 101–107. Available at: <https://doi.org/10.1007/BF00384470>/METRICS.

Zanaga, D. *et al.* (2021) ‘ESA WorldCover 10 m 2020 v100’. Available at: <https://doi.org/10.5281/ZENODO.5571936>.

Zeng, Y., Hao, D., Huete, A., Dechant, B., Berry, J., Chen, J.M., Joiner, J., Frankenberg, C., Bond-Lamberty, B., Ryu, Y., Xiao, J., Asrar, G.R. and Chen, M. (2022) ‘Optical vegetation indices for monitoring terrestrial ecosystems globally’, *Nature Reviews Earth & Environment*, 3(7), pp. 477–493. Available at: <https://doi.org/10.1038/s43017-022-00298-5>.

Zhong, Z., He, B., Chen, Y., Yuan, W., Huang, L., Guo, L., Zhang, Y. and Xie, X. (2021) ‘Higher Sensitivity of Planted Forests’ Productivity Than Natural Forests to Droughts in China’, *Journal of Geophysical Research: Biogeosciences*, 126(10), p. e2021JG006306. Available at: <https://doi.org/10.1029/2021JG006306>.